



DIPLOMARBEIT

Reanalysis of the 2019 $B^0 \rightarrow D^{*-} \ell^+ \nu_\ell$ data from Belle and extraction of the Cabibbo-Kobayashi-Maskawa matrix element $|V_{cb}|$

Ausgeführt am Atominstitut der Technischen Universität Wien

in Zusammenarbeit mit dem Institut für Hochenergiephysik
der Österreichischen Akademie der Wissenschaften

zur Erlangung des akademischen Grades

Diplom-Ingenieur

im Rahmen des Studiums

066 461 Technische Physik

unter der Anleitung von

Privatdoz. Dipl.-Ing. Dr.techn. Christoph Schwanda

Institut für Hochenergiephysik

eingereicht an der Technischen Universität Wien

Fakultät für Physik

von

Hannes Kößl, BSc

Unterschrift des Verfassers

Unterschrift des Betreuers

Wien, am 20. Oktober 2022

Zusammenfassung

Das Standardmodell der Teilchenphysik beschreibt die schwache, elektromagnetische und starke Wechselwirkung zwischen den Elementarteilchen. Im Standardmodell wird die Häufigkeit von Übergängen zwischen den drei Flavour-Generationen der Quarks bei einer Wechselwirkung mit einem W-Boson durch die Cabibbo-Kobayashi-Maskawa-Matrix (CKM-Matrix) angegeben. Sie ist wichtig um die CP-Verletzung zu verstehen. Die CKM-Matrix ist eine 3x3-Matrix und besitzt wegen der Unitarität nur vier unabhängige Parameter. Diese vier Parameter werden nicht vom Standardmodell der Teilchenphysik vorhergesagt und müssen experimentell bestimmt werden. Die Bestimmung des Matrixelement $|V_{cb}|$ der CKM-Matrix ist von besonderem Interesse, da es seit langem eine Abweichung zwischen den Resultaten bei Verwendung von exklusiven und inklusiven semileptonischen Zerfällen besteht.

In dieser Arbeit wird der exklusive semileptonische Zerfall $B^0 \rightarrow D^{*-} \ell^+ \nu_\ell$ ($\ell = e, \mu$) betrachtet und eine Neuanalyse der von Belle 2019 veröffentlichten Daten durchgeführt. Es werden Daten verwendet, die mit dem Belle Detektor am KEKB Elektron-Positron Beschleuniger aufgezeichnet wurden. Die Belle Analyse umfasste einen Datensatz von 711fb^{-1} bei der $\Upsilon(4S)$ Resonanz, das entspricht $(772 \pm 11) \times 10^6 B\bar{B}$ Paare. Dabei wurde die differentielle Zerfallsrate als Funktion des hadronischen Rückstoßes w und der Winkel θ_l , θ_ν und χ gemessen. Die Caprini Lellouch Neubert (CLN) Parametrisierung wird verwendet um die differenzielle Zerfallsrate mit den vier Parametern ρ^2 , $R_1(1)$, $R_1(2)$ und $\mathcal{F}(1)|V_{cb}|\eta_{EW}$ zu beschreiben. Mit einem vierdimensionaler Fit werden aus den Messdaten das Matrixelement $|V_{cb}|$ und die vier Parameter der CLN Parametrisierung bestimmt. Es wird geprüft ob die Fit-Ergebnisse stabil bleiben unter verschiedenen Annahmen wie unterschiedliche Anzahl der gefiteten Bins oder Berücksichtigung des D'Agostini Bias.

Die Parameter der CLN Parametrisierung bei Berücksichtigung des D'Agostini Bias werden mit $\rho^2 = 1.166 \pm 0.034$, $R_1(1) = 1.184 \pm 0.028$, $R_2(1) = 0.848 \pm 0.022$ und $\mathcal{F}(1)|V_{cb}|\eta_{EW} = (36.49 \pm 0.46) \times 10^{-3}$ bestimmt und gezeigt, dass sich die Ergebnisse nur geringfügig ändern in Bezug auf verschiedene Annahmen.

Die approbierte gedruckte Originalversion dieser Diplomarbeit ist an der TU Wien Bibliothek verfügbar.
The approved original version of this thesis is available in print at TU Wien Bibliothek.

Abstract

The Standard Model of Particle Physics describes the weak, electromagnetic and strong interaction between the elementary particles. In the Standard Model, the Cabibbo-Kobayashi-Maskawa matrix (CKM matrix) describes the strength of transitions between the three flavor generations of quarks when interacting with a W boson. It is important to understand the CP violation. The CKM matrix is a 3x3 matrix and has only four independent parameters because of its unitarity. These four parameters are not predicted by the Standard Model of Particle Physics and must be determined experimentally. The determination of the matrix element $|V_{cb}|$ of the CKM matrix is of particular interest because there is a discrepancy between the results when using exclusive and inclusive semileptonic decays.

In this work, the exclusive semileptonic decay $B^0 \rightarrow D^{*-} \ell^+ \nu_\ell$ ($\ell = e, \mu$) is analyzed and a reanalysis of the data published by Belle 2019 is done. The data were recorded with the detector at the KEKB electron-positron collider. The Belle analysis contains a data set of 711fb^{-1} at the $\Upsilon(4S)$ resonance, which corresponds to $(772 \pm 11) \times 10^6 B\bar{B}$ pairs. The differential decay rate was measured as a function of the hadronic recoil w and the angles θ_ℓ , θ_ν and χ . The Caprini Lellouch Neubert (CLN) parametrization is used to describe the differential decay rate with the four parameters ρ^2 , $R_1(1)$, $R_1(2)$ and $\mathcal{F}(1)|V_{cb}|\eta_{EW}$. The matrix element $|V_{cb}|$ and the four parameters of the CLN parametrization are determined from the measured data with a four-dimensional fit. The fit results are checked for their stability under various assumptions such as different numbers of fitted bins or consideration of the D'Agostini bias.

The parameters of the CLN parametrization are determined with $\rho^2 = 1.166 \pm 0.034$, $R_1(1) = 1.184 \pm 0.028$, $R_2(1) = 0.848 \pm 0.022$ and $\mathcal{F}(1)|V_{cb}|\eta_{EW} = (36.49 \pm 0.46) \times 10^{-3}$ taking into account the D'Agostini bias and the results are stable with respect to various assumptions.

Die approbierte gedruckte Originalversion dieser Diplomarbeit ist an der TU Wien Bibliothek verfügbar.
The approved original version of this thesis is available in print at TU Wien Bibliothek.

Contents

1	Introduction	1
2	Theoretical Overview	3
2.1	Standard Model of particle physics	3
2.2	Charged current interactions	4
2.3	Measurement of $ V_{cb} $	6
2.3.1	Exclusive semileptonic decay	6
2.3.2	Inclusive semileptonic decay	10
3	The Belle experiment	13
3.1	The KEKB accelerator	13
3.2	The Belle detector	14
3.2.1	Silicon Vertex Detector (SVD)	15
3.2.2	Central Drift Chamber (CDC)	16
3.2.3	Aerogel Cerenkov counters (ACC)	17
3.2.4	Time-of-flight counters (TOF)	18
3.2.5	Electromagnetic calorimeter (ECL)	18
3.2.6	K_L and muon detection system (KLM)	19
3.2.7	Trigger	19
4	Det. of the CKM matrix element V_{cb}	21
4.1	Belle 2019 analysis of $B^0 \rightarrow D^{*-} \ell^+ \nu_\ell$	21
4.1.1	Event selection and candidate reconstruction	21
4.1.2	Signal extraction	22
4.1.3	Differential data	22
4.1.4	Results	24
4.2	Expected number of signal events	24
4.3	Comparison of different integration methods	27
4.4	Binned χ^2 fit	29
4.5	Numeric methods	29
4.5.1	scipy.integrate.quad	30
4.5.2	iminuit	30

5 Results	35
5.1 40 bin Fit	35
5.2 37 bin Fit	36
5.3 40 Bin Fit using only the statistical uncertainties	36
5.4 40 bin Fit considering the d'Agostini bias	37
6 Conclusions	41
A Data	43
B Fit Results	59
B.1 40 bin Fit	59
B.2 37 bin Fit	60
B.3 40 Bin Fit using only the statistical uncertainties	61
Bibliography	69

Chapter 1

Introduction

The standard model of particle physics is the theory that describes the weak, electromagnetic and strong interaction, i.e. three of the four known interactions that act on the fundamental fermions. Fermions are particles that follow Fermi-Dirac statistics and include all quarks and leptons. The second type of particles included in the standard model are bosons, which obey Bose-Einstein statistics. Bosons include gauge bosons associated with the interaction fields and a scalar boson (Higgs boson) [1].

The violation of the CP-symmetry (charge conjugation parity symmetry) is an important part of understanding particle physics. In the Standard Model, the only place where CP violation effects come into play is in the weak interaction of quarks and leptons [1]. CP violation was discovered by studying rare kaon decays by Christenson, Cronin, Fitch and Turlay in 1964. This led Kobayashi and Maskawa postulating a third quark generation in 1973. The quark mixing matrix has been expanded from the 2×2 Cabibbo matrix to the 3×3 Cabibbo-Kobayashi-Maskawa (CKM) matrix [2]. The CKM-matrix couples all up-type quarks (u, c, t) with all down-type quarks (d, s, b). The coefficients of the CKM matrix are not determined by the standard model but have to be measured experimentally.

There are two different ways to measure the CKM matrix element $|V_{cb}|$ using semileptonic decays. Either inclusive or exclusive decays are used. Both variants should deliver the same result. However, that is not the case. There is a discrepancy of the order of 3σ between using exclusive decays $B \rightarrow D^* \ell^+ \nu_\ell$ or $B \rightarrow D \ell^+ \nu_\ell$ and inclusive decays $\bar{B} \rightarrow X \ell^- \bar{\nu}_\ell$. In this thesis the exclusive decay $B^0 \rightarrow D^{*-} \ell^+ \nu_\ell$ ($\ell = e, \mu$) is analyzed and a reanalysis of the Belle publication from 2019 is done. The data used were recorded with the Belle detector at the electron-positron collider KEKB from 1999 to 2010. To determine the product $\mathcal{F}(1)|V_{cb}|\eta_{EW}$, the form factor parametrization of Caprini Lellouch Neubert (CLN) is used, where $\mathcal{F}(1)$ is a normalization factor and η_{EW} is a small electroweak correction.

This thesis is divided in six chapters and starts with an introduction to the theoretical background and the Standard Model in Chapter 2. Chapter 3 describes the particle accelerator KEKB and the components of the Belle detector. Chapter 4 is about the determination of the CKM matrix element $|V_{cb}|$. First, a summary of the Belle 2019 publication is given. Furthermore, the implementation of the CLN fit is explained in detail. In Chapter 5 the fit results are presented and in Chapter 6 a comparison of the results from this thesis with the results of the Belle 2019 publication is given. Appendix A lists all the data necessary to perform the CLN-fit. Appendix B shows all fit results with different settings.

Natural units are used in this thesis. The natural system of units is based on universal physical constants. The speed of light c and the reduced Planck constant \hbar are set to 1. As a result, all quantities in particle physics can be expressed in powers of GeV.

Chapter 2

Theoretical Overview

2.1 Standard Model of particle physics

The Standard Model of Particle Physics (SM) is a quantum field theory. It is based on the symmetry group $SU(3)_C \times SU(2)_L \times U(1)_Y$ [3]. The basic particles of the SM are twelve fermions interacting through the electromagnetic, weak and strong interaction fields (Table 2.1) [1]. The fermions are the sources of these interacting fields and the gauge bosons are the particles associated with those fields. The gauge bosons are the massless photon, three massive bosons, W^\pm and Z and eight massless gluons (Table 2.2). The Higgs mechanism is necessary to explain the mass of the massive gauge bosons W^\pm and Z . For this purpose, a quantum field, the Higgs field is added to the standard model. The Higgs boson is the quantum excitation of the Higgs field.

There are two types of fermions: leptons and quarks. Leptons interact through the electromagnetic and weak interaction. Quarks interact through electromagnetic, weak and strong interaction. The fermions are divided into three families or generations of four particles each. The three families have the same characteristics, they differ only in their mass. The fermionic fields are divided into right-handed and left-handed components [3]. The left-handed components transform as doublets

$$\begin{pmatrix} \nu_\ell \\ \ell^- \end{pmatrix}_L, \begin{pmatrix} q_u \\ q_d \end{pmatrix}_L \quad (2.1)$$

and the right-handed components transform as singlets

$$l_R^-, \quad q_{uR}, \quad q_{dR} \quad (2.2)$$

under $SU(2)_L$. Here ℓ stands for the leptons (e, μ, τ) and ν_ℓ is the corresponding neutrino. q_u stands for the up-type quarks (u, c, t) and q_d for the down-type quarks (d, s, b).

Family	Leptons			Quarks		
	Particle	Q	Mass/GeV	Particle	Q	Mass/GeV
First	electron (e^-)	-1	0.0005	up (u)	+2/3	0.002
	neutrino (ν_e)	0	$< 2 \times 10^{-9}$	down (d)	-1/3	0.005
Second	muon (μ^-)	-1	0.106	charm (c)	+2/3	1.3
	neutrino (ν_μ)	0	< 0.0002	strange (s)	-1/3	0.1
Third	tau (τ^-)	-1	1.78	top (t)	+2/3	173
	neutrino (ν_τ)	0	< 0.02	bottom (b)	-1/3	4.2

Table 2.1: The twelve fundamental fermions of the Standard Model are divided into leptons and quarks.

Boson	Mass/GeV	Force
Gluon	g	Strong
Photon	γ	Electromagnetism
W boson	W^\pm	Weak
Z boson	Z	Weak

Table 2.2: The gauge bosons in the standard model.

2.2 Charged current interactions

The Cabibbo-Kobayashi-Maskawa (CKM) matrix occurs in the charged-current part of the electroweak Lagrangian density

$$\mathcal{L}_{CC} = -\frac{g}{2\sqrt{2}} \left\{ W_\mu^\dagger \left[\sum_{ij} \bar{u}_i \gamma^\mu (1 - \gamma^5) \mathbf{V}_{ij} d_j + \sum_l \bar{\nu}_l \gamma^\mu (1 - \gamma^5) l \right] + h.c. \right\} \quad (2.3)$$

for quarks [3]. The CKM-matrix

$$\mathbf{V} = \begin{pmatrix} V_{ud} & V_{us} & V_{ub} \\ V_{cd} & V_{cs} & V_{cb} \\ V_{td} & V_{ts} & V_{tb} \end{pmatrix} \quad (2.4)$$

couples all up-type quarks (electrical charge +2/3e) with all down-type quarks (electrical charge -1/3e). Figure 2.1 shows a schematic representation of these flavour-changing transitions. The coefficients of the quark mixing matrix \mathbf{V} are not known and must be determined by measurements. A unitary $N_G \times N_G$ matrix is determined by N_G^2 real parameters. $N_G(N_G - 1)/2$ of the

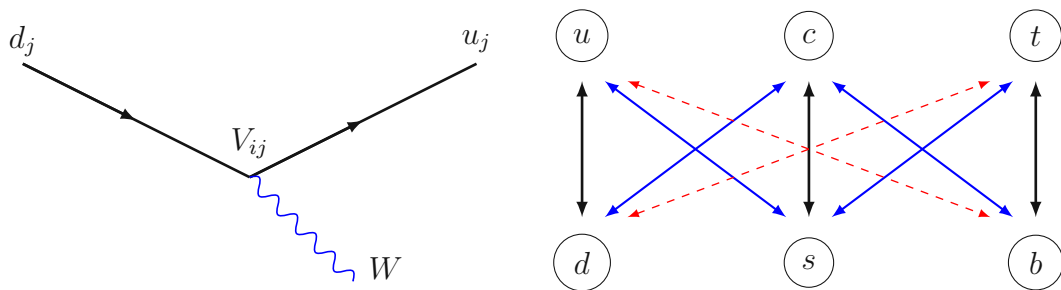


Figure 2.1: Flavour-changing transitions.

parameters can be written as angles and $N_G(N_G+1)/2$ as phases. Many of these parameters are irrelevant for the CKM-matrix \mathbf{V} because the quark phases can be chosen arbitrarily. In the standard model, $N_G = 3$ and the CKM matrix is parameterized by three angles and a phase. The standard parametrization is

$$\mathbf{V} = \begin{pmatrix} c_{12}c_{13} & c_{13}s_{12} & e^{-i\delta_{13}}s_{13} \\ -c_{23}s_{12} - e^{i\delta_{13}}c_{12}s_{13}s_{23} & c_{12}c_{23} - e^{i\delta_{13}}s_{12}s_{13}s_{23} & c_{13}s_{23} \\ s_{12}s_{23} - e^{i\delta_{13}}c_{12}c_{23}s_{13} & -e^{i\delta_{13}}c_{23}s_{12}s_{13} - c_{12}s_{23} & c_{13}c_{23} \end{pmatrix} \quad (2.5)$$

with $c_{ij} = \cos\theta_{ij}$, $s_{ij} = \sin\theta_{ij}$ [3]. Here i and j are the generation labels (i,j = 1,2,3). The phase δ is the reason for all CP violation phenomena. The parametrization by Wolfenstein is an approximate parametrization of the CKM matrix [3]:

$$\mathbf{V} = \begin{pmatrix} 1 - \frac{\lambda^2}{2} & \lambda & A\lambda^3(\rho - i\eta) \\ -\lambda & 1 - \frac{\lambda^2}{2} & A\lambda^2 \\ A\lambda^3(-\rho - i\eta + 1) & -A\lambda^2 & 1 \end{pmatrix} + \mathcal{O}(\lambda^4), \quad (2.6)$$

with

$$A \approx \frac{\mathbf{V}_{cb}}{\lambda^2} = 0.831 \pm 0.014, \quad (2.7)$$

$$\sqrt{\rho^2 + \eta^2} \approx \left| \frac{\mathbf{V}_{ub}}{\lambda \mathbf{V}_{cb}} \right| = 0.478 \pm 0.033. \quad (2.8)$$

It shows a hierarchical pattern of the matrix elements. The diagonal elements are very close to one. The elements that connect the first and second generations are in the order of $\lambda \approx |V_{us}| = 0.2230 \pm 0.0015$. The elements that connect the second with the third generation have the order of λ^2 and those that connect the first with the third have the order of λ^3 [4]. The unity condition $\mathbf{V}\mathbf{V}^\dagger = \mathbf{1}$ leads to the expressions

$$\mathbf{V}_{ud}^* \mathbf{V}_{us} + \mathbf{V}_{cd}^* \mathbf{V}_{cs} + \mathbf{V}_{td}^* \mathbf{V}_{ts} = 0, \quad (2.9)$$

$$\mathbf{V}_{us}^* \mathbf{V}_{ub} + \mathbf{V}_{cs}^* \mathbf{V}_{cb} + \mathbf{V}_{ts}^* \mathbf{V}_{tb} = 0, \quad (2.10)$$

$$\mathbf{V}_{ub}^* \mathbf{V}_{ud} + \mathbf{V}_{cb}^* \mathbf{V}_{cd} + \mathbf{V}_{tb}^* \mathbf{V}_{td} = 0. \quad (2.11)$$

All three expressions can be visualized as triangles in the complex plane and have the same area. Usually equation (2.11) is used to draw the unitarity triangle (Figure 2.2) [4]. The equation is divided by $\mathbf{V}_{cb}^* \mathbf{V}_{cd}$ to align one side of the triangle with the real axis. The length CA is given by

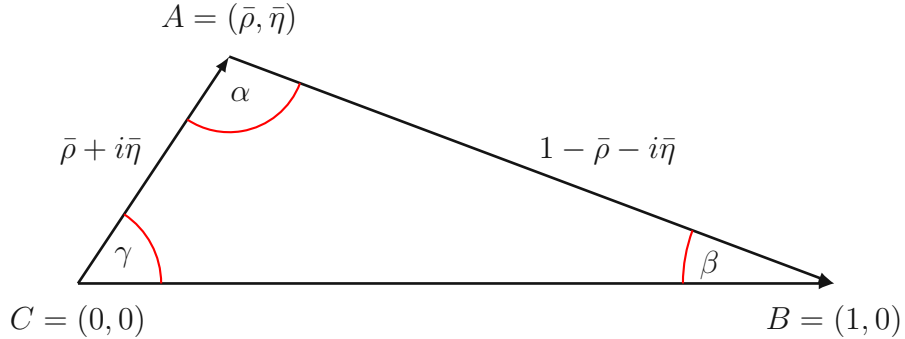


Figure 2.2: Unitarity Triangle.

$$R_b = \frac{|V_{ud}V_{ub}^*|}{|V_{cd}V_{cb}^*|} = \sqrt{\bar{\rho}^2 + \bar{\eta}^2} \quad (2.12)$$

and the length BA is given by

$$R_t = \frac{|V_{td}V_{tb}^*|}{|V_{cd}V_{cb}^*|} = \sqrt{(1 - \bar{\rho})^2 + \bar{\eta}^2}. \quad (2.13)$$

2.3 Measurement of $|V_{cb}|$

There are two different ways of measuring $|V_{cb}|$ using semileptonic decays. When using exclusive semileptonic decays, only a specific final state such as $D^*\ell\nu$ is evaluated [5]. Or when using inclusive semileptonic decays, all possible final states such as $X_c\ell\nu$ are used. X_c is any hadronic system with charm quarks. Exclusive and inclusive analysis use different theoretical approaches to describe the QCD contribution [5]. The results for $|V_{cb}|$ using exclusive decays and using inclusive decays are given in table 2.3 and a comparison of the results is shown in Figure 2.3. There is a discrepancy in the value of $|V_{cb}|$ between measurements with exclusive and inclusive decays of about 3σ .

	$ V_{cb} \times 10^3$
exclusive	39.10 ± 0.50
inclusive	42.19 ± 0.78

Table 2.3: Values for $|V_{cb}|$ using exclusive and inclusive decays [9].

2.3.1 Exclusive semileptonic decay

For the exclusive determination of $|V_{cb}|$ a specific decay mode is used such as $B^0 \rightarrow D^{*-}\ell^+\nu_\ell$ or $B^0 \rightarrow D^-\ell^+\nu_\ell$. The decay is described as a function of the three angles θ_l , θ_ν , χ and the hadronic recoil w [6]. Figure 2.4 shows the tree level Feynman diagram of the $B^0 \rightarrow D^{*-}\ell^+\nu_\ell$ decay. The hadronic recoil

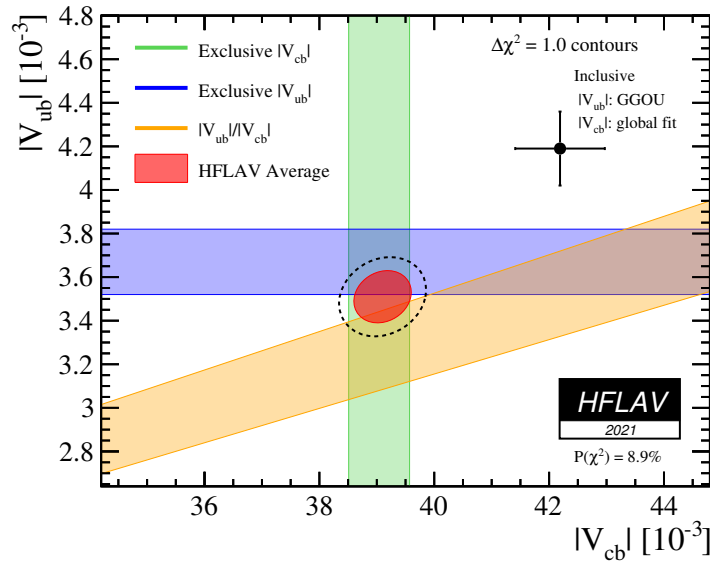


Figure 2.3: The colored bands show the results of the exclusive measurement of $|V_{cb}|$ and $|V_{ub}|$ and the LHCb measurement of $|V_{ub}|/|V_{cb}|$. The red ellipse shows the combined average of the exclusive measurements. The point with the error bars shows the combined result of the inclusive measurements [9].

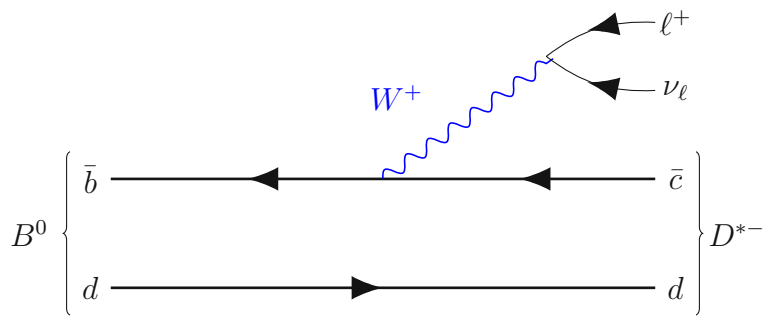


Figure 2.4: Feynman diagram for $B^0 \rightarrow D^{*-} \ell^+ \nu_\ell$ [6].

is given by

$$w = \frac{P_B \cdot P_{D^*}}{m_B m_{D^*}} = \frac{m_B^2 + m_{D^*}^2 - q^2}{2m_B m_{D^*}}, \quad (2.14)$$

where P_B and P_{D^*} are the four momenta and m_B and m_{D^*} are the masses of the B and D^* mesons, respectively. q^2 is the invariant mass squared of the lepton-neutrino system [5, 6]. The maximum value of w is reached at $q_{min}^2 = m_\ell^2 \approx 0$ GeV^2 with

$$w_{max} = \frac{P_B \cdot P_{D^*}}{m_B m_{D^*}} \approx \frac{m_B^2 + m_{D^*}^2}{2m_B m_{D^*}} = 1.504. \quad (2.15)$$

The three angles are shown in Figure 2.5 and are defined as follows [2, 6]:

- θ_l is the angle between the direction of the lepton and the direction opposite the B meson in the rest frame of the virtual W .
- θ_ν is the angle between the direction of the D meson and the direction opposite the B meson in the D^* rest frame.
- χ : is the angle between the decay planes of the D^* and W , defined in the B meson rest frame.

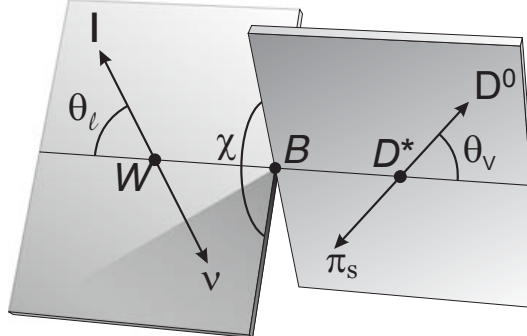


Figure 2.5: Definition of the angles θ_l , θ_ν and χ for the decay $B^0 \rightarrow D^{*-} l^+ \nu_\ell$ [6].

The differential decay rate of $B^0 \rightarrow D^{*-} l^+ \nu_\ell$ with neglected lepton mass is given by [7]

$$\begin{aligned} \frac{d\Gamma(B^0 \rightarrow D^{*-} l^+ \nu_\ell)}{dw d\cos\theta_l d\cos\theta_\nu d\chi} &= \frac{\eta_{EW}^2 3m_B m_{D^*}^2}{4(4\pi)^4} G_F^2 |V_{cb}|^2 \sqrt{w^2 - 1} (1 - 2wr + r^2) \{(1 - \cos\theta_l)^2 \sin^2\theta_\nu H_+^2(w) \\ &+ (1 + \cos\theta_l)^2 \sin^2\theta_\nu H_-^2(w) + 4\sin^2\theta_l \cos^2\theta_\nu H_0^2(w) \\ &- 2\sin^2\theta_l \sin^2\theta_\nu \cos 2\chi H_+(w) H_-(w) \\ &- 4\sin\theta_l (1 - \cos\theta_l) \sin\theta_\nu \cos\theta_\nu \cos\chi H_+(w) H_0(w) \\ &+ 4\sin\theta_l (1 + \cos\theta_l) \sin\theta_\nu \cos\theta_\nu \cos\chi H_-(w) H_0(w)\}, \end{aligned} \quad (2.16)$$

where G_F is the Fermi constant equal to $(1.16637 \pm 0.00001) \times 10^{-5} \text{GeV}^{-2}$, $r = m_{D^*}/m_B$ and η_{EW} is a small electroweak correction. The helicity amplitudes

H_{\pm} and H_0 are defined in terms of the form factor $h_{A_1}(w)$ and the form factor ratios $R_1(w)$ and $R_2(w)$. They are given by [6, 8]

$$H_i(w) = m_B \frac{R^* (1 - r^2) (w + 1)}{2\sqrt{1 - 2wr + r^2}} h_{A_1}(w) |\tilde{H}_i(w)| \quad (2.17)$$

where

$$\tilde{H}_{\pm}(w) = \frac{\sqrt{1 - 2wr + r^2} (1 \mp \sqrt{\frac{w-1}{w+1}} R_1(w))}{(1 - r)}, \quad (2.18)$$

$$\tilde{H}_0(w) = 1 + \frac{(w - 1)(1 - R_2(w))}{(1 - r)}, \quad (2.19)$$

$$R^* = \frac{2\sqrt{m_B m_{D^*}}}{m_B + m_{D^*}}. \quad (2.20)$$

The form factor $h_{A_1}(w)$ and the form factor ratios $R_1(w)$ and $R_2(w)$ are defined differently depending on the parametrization. In the Caprini Lellouch Neubert (CLN) parametrization they are given by

$$\begin{aligned} h_{A_1}(w) &= h_{A_1}(1) \left[1 - 8\rho^2 z + (53\rho^2 - 15)z^2 - (231\rho^2 - 91)z^3 \right], \\ R_1(w) &= R_1(1) - 0.12(w - 1) + 0.05(w - 1)^2, \\ R_2(w) &= R_2(1) + 0.11(w - 1) - 0.06(w - 1)^2, \end{aligned} \quad (2.21)$$

where $z(w) = \frac{\sqrt{w+1}-\sqrt{2}}{\sqrt{w+1}+\sqrt{2}}$ [8]. The CLN parametrization has three independent parameters ρ^2 , $R_1(1)$ and $R_2(1)$ in addition to the normalization. $h_{A_1}(1)$ is set to $\mathcal{F}(1)$ and the product $\mathcal{F}(1)|V_{cb}|\eta_{EW}$ is used as the normalization factor. The differential decay rate of $B^0 \rightarrow D^{*-} \ell^+ \nu_\ell$ becomes [9]

$$\frac{d\Gamma(B^0 \rightarrow D^{*-} \ell^+ \nu_\ell)}{dw} = \frac{G_F^2 m_{D^*}^3}{48\pi^3} (m_B - m_{D^*})^2 \chi(w) \eta_{EW}^2 \mathcal{F}^2(w) |V_{cb}|^2 \quad (2.22)$$

by integration over $d(\cos\theta_l)$, $d(\cos\theta_\nu)$ and χ . $\chi(w)$ is the phase space factor and $\mathcal{F}(w)$ the form factor for the $\bar{B} \rightarrow D^* \ell \bar{\nu}_\ell$ decay given by [9]

$$\begin{aligned} \chi(w)\mathcal{F}^2(w) &= \\ h_{A_1}^2(w) \sqrt{w^2 - 1} (w + 1)^2 &\left\{ 2 \left[\frac{1 - 2wr + r^2}{(1 - r)^2} \right] \left[1 + R_1^2(w) \frac{w - 1}{w + 1} \right] + \right. \\ &\left. \left[1 + (1 - R_2(w)) \frac{w - 1}{1 - r} \right]^2 \right\}. \end{aligned} \quad (2.23)$$

The value of the form factor at $w = 1$ is

$$\mathcal{F}(1) = 0.906 \pm 0.013 \quad (2.24)$$

and is determined by Lattice QCD [10]. For the decay $B^0 \rightarrow D^- \ell^+ \nu_\ell$, the differential decay rate is given by [9]

$$\frac{d\Gamma(B^0 \rightarrow D^- \ell^+ \nu_\ell)}{dw} = \frac{G_F^2 m_D^3}{48\pi^3} (m_B + m_D)^2 (w^2 - 1)^{3/2} \eta_{EW}^2 \mathcal{G}^2(w) |V_{cb}|^2, \quad (2.25)$$

where m_D is the mass of the D meson. In the CLN parametrization the form factor $\mathcal{G}(w)$ can be parametrized by the normalization $\mathcal{G}(1)|V_{cb}|\eta_{EW}^2$ and the slope ρ_D^2 and is given by

$$\mathcal{G}(w) = \mathcal{G}(1)[1 - 8\rho_D^2 z + (51\rho_D^2 - 10)z^2 - (252\rho_D^2 - 84)z^3], \quad (2.26)$$

where $z(w) = \frac{\sqrt{w+1}-\sqrt{2}}{\sqrt{w+1}+\sqrt{2}}$ [9]. The value of the form factor at $w = 1$ is determined by Lattice QCD with [11]

$$\mathcal{G}(1) = 1.074 \pm 0.024. \quad (2.27)$$

2.3.2 Inclusive semileptonic decay

The inclusive semileptonic decay width $\Gamma(B \rightarrow X_c \ell \nu)$ is described using the Operator Product Expansion (OPE). The semileptonic width is given by [5]

$$\Gamma(B \rightarrow X_c \ell \nu) = \frac{G_F^2 m_b^5}{192\pi^3} |V_{cb}|^2 \left(1 + \frac{c_5(\mu) \langle O_5 \rangle(\mu)}{m_b^2} + \frac{c_6(\mu) \langle O_6 \rangle(\mu)}{m_b^3} + \mathcal{O}\left(\frac{1}{m_b^4}\right) \right). \quad (2.28)$$

c_5 and c_6 are the Wilson coefficients that can be calculated by perturbative QCD. $\langle O_5 \rangle$ and $\langle O_6 \rangle$ are the expectation values of local operators. They describe basic hadronic properties of the B meson and cannot be calculated by perturbative QCD [5]. The moments of the lepton energy E_ℓ and the hadronic mass squared m_X^2 spectra in $B \rightarrow X \ell \nu$ are observables containing the same non-perturbative parameters as the local operators and can be expanded similarly to the semileptonic width in equation (2.28). The lepton energy moments are defined as [5]

$$\langle E_\ell^n \rangle_{E_{cut}} = \frac{R_n(E_{cut})}{R_0(E_{cut})}, \quad (2.29)$$

with

$$R_n(E_{cut}) = \int_{E_\ell > E_{cut}} E_\ell^n \frac{d\Gamma}{dE_\ell} dE_\ell. \quad (2.30)$$

E_{cut} is the lower lepton energy threshold. The hadronic mass moments are [5]

$$\langle m_X^{2n} \rangle_{E_{cut}} = \frac{S_n(E_{cut})}{S_0(E_{cut})}, \quad (2.31)$$

with

$$S_n(E_{cut}) = \int_{E_\ell > E_{cut}} m_X^{2n} \frac{d\Gamma}{dm_X^2} dm_X^2. \quad (2.32)$$

There are two theoretical frameworks used to calculate the semileptonic width and moments in $B \rightarrow X_c \ell \nu$: The kinetic scheme and the 1S scheme. In the kinematic scheme, the non-perturbative parameters of the $1/m_b$ expansion are μ_π^2 and μ_G^2 at order $\mathcal{O}(1/m_b^2)$ and ρ_D^3 and ρ_{LS}^3 at order $\mathcal{O}(1/m_b^3)$. In the 1S scheme, the non-perturbative parameters are λ_1 and λ_2 at order $\mathcal{O}(1/m_b^2)$ and ρ_1 and τ_{1-3} at order $\mathcal{O}(1/m_b^3)$. By measuring the energy moment E_ℓ and the hadronic mass squared m_X^2 , the non-perturbative OPE parameters can be determined and thus also $|V_{cb}|$ [5].

Chapter 3

The Belle experiment

3.1 The KEKB accelerator

KEKB was an e^+e^- asymmetric energy accelerator used for the Belle experiment. It was located at KEK (High Energy Accelerator Research Organization) in Tsukuba, Japan and ran from 1999 to 2010. Figure 3.1 shows a schematic view of the KEKB particle accelerator. The accelerator has two rings. The low-energy ring (LER) works at an energy of 3.5 GeV and accelerates the positrons and the high-energy ring (HER) works at 8 GeV and accelerates electrons [2, 12]. Table 3.1 shows the basic parameters of the KEKB accelerator. The center-of-

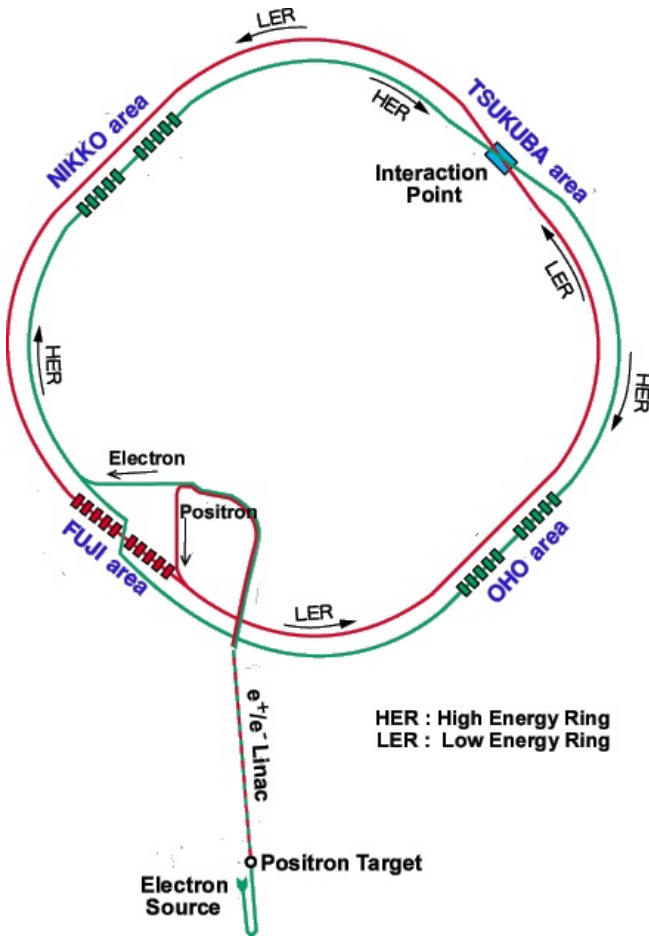


Figure 3.1: A schematic view of the KEKB particle accelerator [13].

\sqrt{s}	10.6 GeV at $\Upsilon(4S)$
Type	e^+e^-
Date	1999-2010
Luminosity	$2.1 \times 10^{34} cm^{-2}s^{-1}$

Table 3.1: The basic parameters of the KEKB accelerator.

mass \sqrt{s} energy is the energy available to produce massive particles. It is given by the root of the Lorentz invariant quantity s and is calculated by [1]

$$s = \left(\sum_{i=1}^2 E_i \right)^2 - \left(\sum_{i=1}^2 \mathbf{p}_i \right)^2. \quad (3.1)$$

The luminosity is an important parameter of an accelerator. It indicates the ability of an accelerator to generate a sufficient number of events. It is defined by

$$\mathcal{L} = \frac{1}{\sigma} \frac{dN}{dt}, \quad (3.2)$$

where σ is the cross section and $\frac{dN}{dt}$ is the number of scattering events per time. The unit of luminosity is therefore $cm^{-2}s^{-1}$. For an e^+e^- particle accelerator, the luminosity can be calculated by

$$\mathcal{L} = \frac{N_b n_{e-} n_{e+} f}{A_{eff}}, \quad (3.3)$$

where N_b is the number of brunches, n_{e-} and n_{e+} are the number of electrons and positrons in each brunch, f is the circulation frequency and A_{eff} is the effective cross-sectional overlapping transverse area [2]. KEKB reached a peak luminosity of $2.1 \times 10^{34} cm^{-2}s^{-1}$. The integrated luminosity

$$\mathcal{L}_{int} = \int \mathcal{L}(t) dt \quad (3.4)$$

is calculated by integrating the luminosity over time. The Belle Experiment was able to record more than $1000 fb^{-1}$ of data during its runtime. Figure 3.2 shows the integrated luminosity. Most of the data was recorded at the $\Upsilon(4S)$ resonance because that is the optimal energy to produce $B\bar{B}$ pairs. However, data were also recorded at the $\Upsilon(1S)$, $\Upsilon(2S)$ and $\Upsilon(5S)$ resonance [2, 12].

3.2 The Belle detector

Figure 3.3 shows the configuration of the Belle detector. The Belle Detector consists of the following components [15]:

- Silicon Vertex Detector (SVD)
- Central Drift Chamber (CDC)

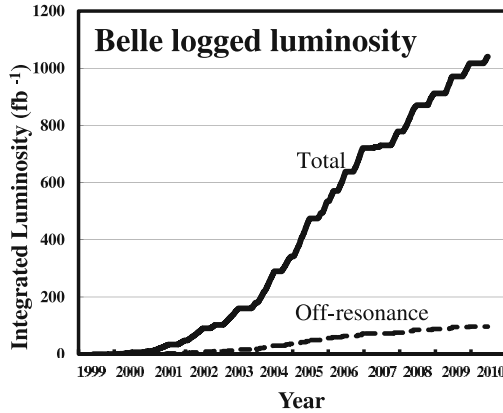


Figure 3.2: The Integrated Luminosity of the Belle Experiment [12].

- Aerogel Cerenkov counters (ACC)
- Time-of-flight counters (TOF)
- Electromagnetic calorimeter (ECL)
- K_L and muon detection system (KLM)

The components of the detector are described individually below.

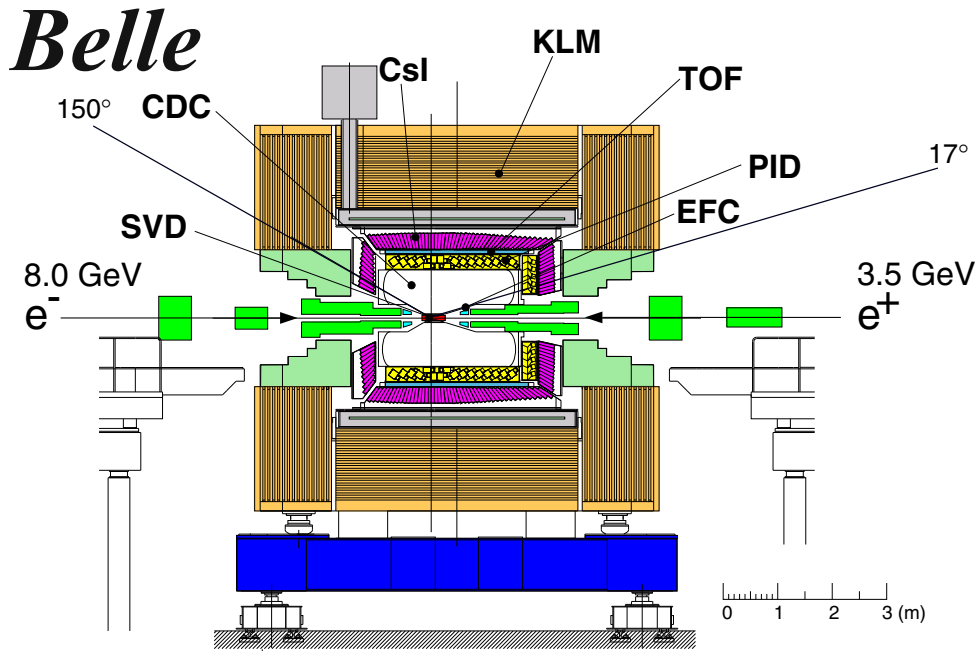


Figure 3.3: The Belle detector [15].

3.2.1 Silicon Vertex Detector (SVD)

The Silicon Vertex Detector (SVD) is used to reconstruct vertices, measure the momentum of low-energy charged particles and provide information to the Central Drift Chamber (CDC) [2]. The Belle silicon vertex detector SVD1 has worked since 1999 and was replaced by the SVD2 in 2003 [14]. Figure 3.4

shows the structure of the SVD2. The SVD2 consists of 246 double-sided silicon detectors (DSSD) [12]. The DSSD are arranged in four layers around the beam pipe. The beam pipe has a radius of 15 mm and the four layers of the DSSD are arranged with radii of 20, 43.5, 70 and 88 mm [14]. The layers consist of ladders. Two different types of DSSDs are used. Layers 1 to 3 have DSSDs with a size of 79.2 x 28.4 mm and layer four have DSSDs with a size of 76.4 x 34.9 mm [14]. The DSSDs are read out by VA1 integrated circuits. The analog signal from the VA1 integrated circuit is digitized by flash analog-to-digital converters (FADCs) and is further processed using field programmable gate arrays (FPGAs) [12].

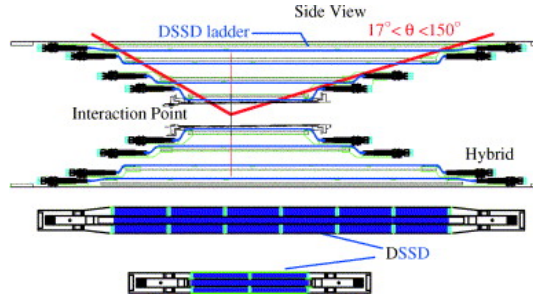


Figure 3.4: Longitudinal cross section of the updated Silicon Vertex Detector SVD2 and ladder configuration of the 1st and 4th layer [14].

3.2.2 Central Drift Chamber (CDC)

The Central Drift Chamber (CDC) reconstructs charged particle tracks and measures their momentum [2]. By measuring the energy loss in the gas volume, information about the particle type can also be provided. Particles with low momentum can therefore also be determined. It also provides trigger signals for charged particles [2]. The CDC is filled with a gas mixture of He (50%) and C₂H₆ (50%). A low-Z gas is used to minimize multiple scattering [12]. Figure 3.5 shows the structure of the CDC. The CDC is asymmetrical in the z-direction for optimal angle coverage. The inner radius of the CDC is 80mm and the outer radius is 880mm. It has an angular coverage of $17^\circ \leq \theta \leq 150^\circ$ [2]. The CDC consists of 8400 drift cells [12]. Figure 3.6 shows a plot of the

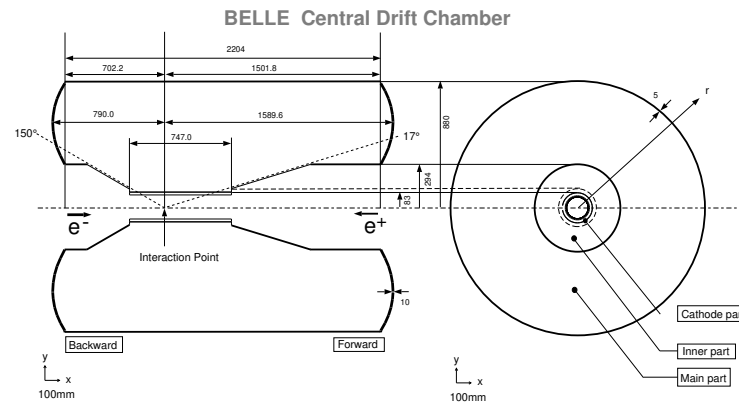


Figure 3.5: Structure of the The Central Drift Chamber (CDC) [15].

measured energy loss (dE/dx) as a function of the momentum. Kaons, pions, protons and electrons can be recognized [15].

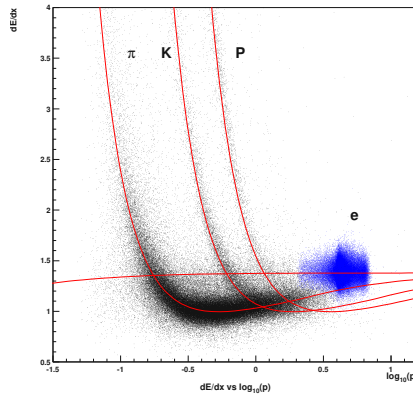


Figure 3.6: Energy loss (dE/dx) as a function of the momentum [15].

3.2.3 Aerogel Cerenkov counters (ACC)

The Aerogel Cerenkov counters (ACC) is mainly used to distinguish charged pions and kaons [15]. Cherenkov radiation occurs when charged particles move faster than light in a dielectric medium. The atoms in the dielectric material get polarized by the charged particles and emit light. The light emitted by the atoms along the trajectory forms a combined conical wave front. 3.7 shows the arrangement of the ACC. The ACC at Belle consists of 960 counter modules in the barrel section and 228 modules for the forward end-cap part of the detector [12]. Aerogel is used as the dielectric material. The refractive index of the aerogel blocks is between 1.01 and 1.03 depending on the position [12]. Fine mesh-type photomultiplier are used to detect the Cherenkov radiation [2].

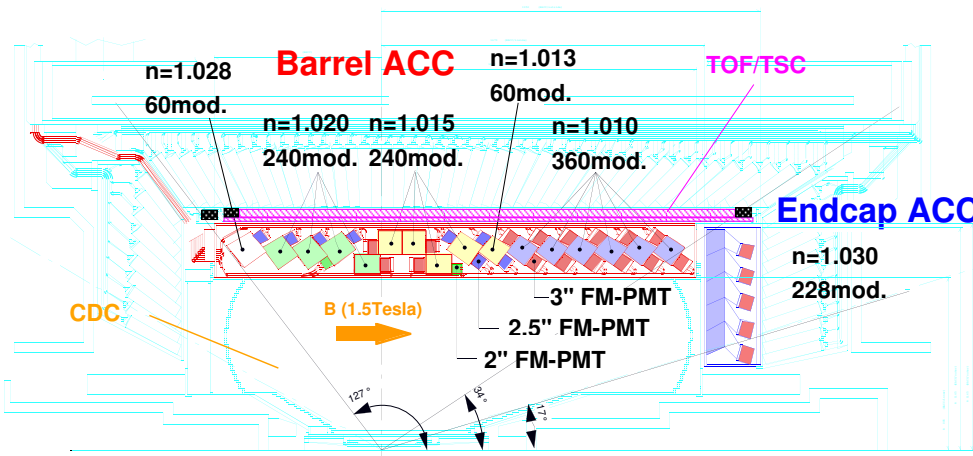


Figure 3.7: Arrangement of the Aerogel Cerenkov counters (ACC) [15].

3.2.4 Time-of-flight counters (TOF)

Time-of-flight counters (TOF) are used for particle identification. In addition, tiny trigger scintillation counters (TSC) provide timing signals for the trigger system. Two TOF counters and one TSC counter form one module [12]. 64 modules are arranged at a distance of 1.2 m from the interaction point and measures the time it takes for a charged particle to get to the detector. The time resolution is 100pm and thus particles with a momentum of less than 1.2 GeV/c can be detected [2]. This covers 90% of the particles produced at the $\Upsilon(4S)$ resonance. Plastic scintillators are used for the TOF detector system. The angle covered by the TOF ranges from 34° to 120° [15].

3.2.5 Electromagnetic calorimeter (ECL)

The Electromagnetic calorimeter (ECL) is mainly used to measure the energy of photons. It is also used to identify electrons by comparing the energy measured by the electromagnetic calorimeter with the charged particle impulse. The ECL contains 8736 CsI(Tl) counters [12]. The arrangement is shown in Figure 3.8. The Belle calorimeter system consists of a 3m long barrel section and ring-shaped end-caps [15]. Particles falling into the calorimeter create a particle shower. Electrons and positrons produce photons through bremsstrahlung and photons create an electron-positron pair through pair production. This process continues until the energy has fallen below a critical value. Then the energy of the particles is emitted by ionization. Two silicon photodiodes are attached to each CsI(Tl) crystal to detect the scintillation light [2].

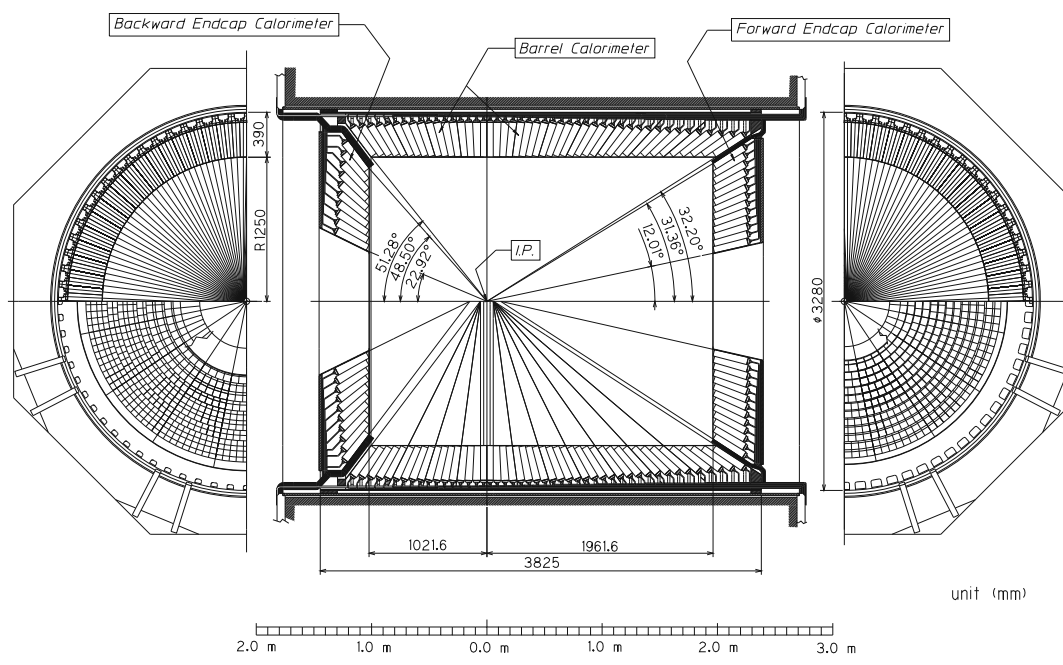


Figure 3.8: Configuration of the Electromagnetic calorimeter (ECL) [15].

3.2.6 K_L and muon detection system (KLM)

The K_L and muon detection system (KLM) identifies K_L mesons and muons. The KLM consists of alternating layers of two types. Namely layers with detectors for charged particles and a layer of 4.7 cm thick iron plates [12]. The iron layers also serve as a return path for the magnetic flux generated by the superconducting solenoid magnet. Glass-electrode-resistive plate counters (RPCs) are used to detect the charged particles [12]. RPCs have two parallel plate electrodes. The gap between the plates is filled with gas. Charged particles create a streamer in the gas which leads to a discharge on the plates [2].

3.2.7 Trigger

Triggers are needed to handle the large amount of data coming from the detector since only a small part of the data can be recorded. The total cross section at a luminosity of $10^{34} \text{ cm}^{-2}\text{s}^{-1}$ is very different for various physical processes. $\Upsilon(4S) \rightarrow B\bar{B}$ has a cross section of 1.2 nanobarn (nb) while Bhabha events have a cross section of 44nb and $\gamma\gamma$ events have a cross section of 2.4nb [15]. Because the trigger rates of the Bhabha and $\gamma\gamma$ events are so large, they must be prescaled by a factor of ~ 100 [15]. The Belle Experiment has a level 1 hardware trigger and a level 3 software trigger:

- Level 1 Hardware Trigger: It is formed by a sub-detector trigger system and the Global Decision Logic (GDL). The sub-detector trigger system uses signals from the CDC, ECL, TOF and KLM. The global decision logic (GDL) combines information from the sub-detector trigger system [12].
- Level 3 Software Trigger: It runs on the online computer farm. The Level 3 software trigger is used to check charged track candidates to reduce the amount of data recorded [12].

Chapter 4

Determination of the CKM matrix element $|V_{cb}|$ from Belle data

4.1 Belle 2019 analysis of $B^0 \rightarrow D^{*-} \ell^+ \nu_\ell$

In 2019 the Belle Collaboration presented a new measurement of the CKM matrix element $|V_{cb}|$ from the semileptonic decay $B^0 \rightarrow D^{*-} \ell^+ \nu_\ell$ ($\ell = e, \mu$) [6]. This analysis is based on the full data set of 711fb^{-1} at the $\Upsilon(4S)$ resonance recorded with the Belle detector. 711fb^{-1} of integrated luminosity corresponds to $(772 \pm 11) \times 10^6 B\bar{B}$ pairs. $152 \times 10^6 B\bar{B}$ pairs were recorded with a 2.0 cm radius beam pipe and a 3-layer silicon vertex detector (SVD1) and $620 \times 10^6 B\bar{B}$ pairs were recorded with a 1.5 cm radius beam pipe and a 4-layer silicon vertex detector (SVD2). A dataset with additional 88 fb^{-1} of data recorded 60 MeV below the $\Upsilon(4S)$ resonance is used to estimate the $q\bar{q}$ continuum background. In addition, events generated by a Monte Carlo simulation are used.

4.1.1 Event selection and candidate reconstruction

After selecting hadronic events, charged particles tracks are selected by the track impact parameters dr and dz . A charged particle can be parameterized as a helix. dr is the distance in the x-y plane from the pivotal point to the helix of the charged particle. dz is the distance along the z-axis from the pivotal point to the helix [2]. The criteria are $dr < 2\text{cm}$ and $|dz| < 4\text{cm}$ [6]. The $\bar{D}^0 \rightarrow K^+ \pi^-$ channel is used to reconstruct the neutral \bar{D}^0 meson. The invariant mass of a particle is the mass of the particle in its rest frame. The invariant mass of the reconstructed \bar{D}^0 meson, i.e. the mass in its rest frame, must be within $\pm 13\text{MeV}/c^2$ of the D^0 mass [6]. Next, the D^{*-} candidates are reconstructed. For this, the \bar{D}^0 candidates are combined with an additional pion. This pion must have the opposite charge of the kaon. They are called slow pions π_s^- because they have a mean momentum of approximately $100\text{MeV}/c$.

Furthermore, ΔM is restricted. ΔM is the difference of the invariant masses of D^{*-} and \bar{D}^0 candidates. ΔM is required to be below $165\text{MeV}/c^2$ for the background fit. It must be further restricted for the signal yield determination [6]. To suppress the continuum, an upper limit for the momentum of the D^* of $2.45\text{GeV}/c$ in the center-of-mass frame is used. The center-of-mass frame is defined as the reference system in which the center of mass remains at the origin. The D^* candidates are combined with oppositely charged electrons or muons to form a B meson candidate [6].

4.1.2 Signal extraction

The variable $\cos\theta_{B,D^*\ell}$ is used to select the exclusive semileptonic decay $B \rightarrow D^* l \nu$. It is defined as [6]

$$\cos\theta_{B,D^*\ell} = \frac{2E_B^* E_{D^*\ell}^* - m_B^2 - m_{D^*\ell}^2}{2|\mathbf{p}_B^*||\mathbf{p}_{D^*\ell}^*|}, \quad (4.1)$$

where E_B^* is half of the centre of mass energy and \mathbf{p}_B^* is $\sqrt{E_B^{*2} - m_B^2}$. $m_{D^*\ell}$ is the invariant mass and $\mathbf{p}_{D^*\ell}$ is the momentum sum of the hadron D^* and the charged lepton ℓ . $\theta_{B,D^*\ell}$ represents the angle between the momentum vectors \mathbf{p}_B^* and $\mathbf{p}_{D^*\ell}$. With the condition $|\cos\theta_{B,D^*\ell}| \leq 1$, background events and incompletely reconstructed events can be separated [6]. These events are way out of this range. In addition, the off-resonance data is used to estimate the remaining continuum background. However, an irreducible background remains. To estimate the background a binned maximum log likelihood fit is performed to the $D^*\ell$ candidates [6]. The fit is done in the three variables ΔM , $\cos\theta_{B,D^*\ell}$ and the lepton momentum p_l . The remaining background is modeled with a Monte Carlo simulation. Figure 4.1 shows the result of the fits. A total of 90738 $B^0 \rightarrow D^{*-} e^+ \nu_e$ signal decays and 89082 $B^0 \rightarrow D^{*-} \mu^+ \nu_\mu$ signal decays were found [6].

4.1.3 Differential data

The three angles $\cos\theta_l$, $\cos\theta_\ell$ and χ are defined in Chapter 2.3.1. To perform the form factor fits the events are divided into bins in the variables w , $\cos\theta_l$, $\cos\theta_\ell$ and χ . Each distributions is divided into 10 bins [6]. Table 4.1 shows the binning used. Each distribution is divided into equal steps respectively. For example, bins of the distribution in w are labeled by the index 1...10. The range in w is from $w = 1.00$ to $w = 1.50$ and each bin has a width of 0.05. Figure 4.2 show plots of the background subtracted signal yield for the electron and muon mode.

Each event is included once in each of the four distributions. This results in a correlation of the signal yields among the four distributions. The Belle collaboration provides all the information needed to perform fits to any form

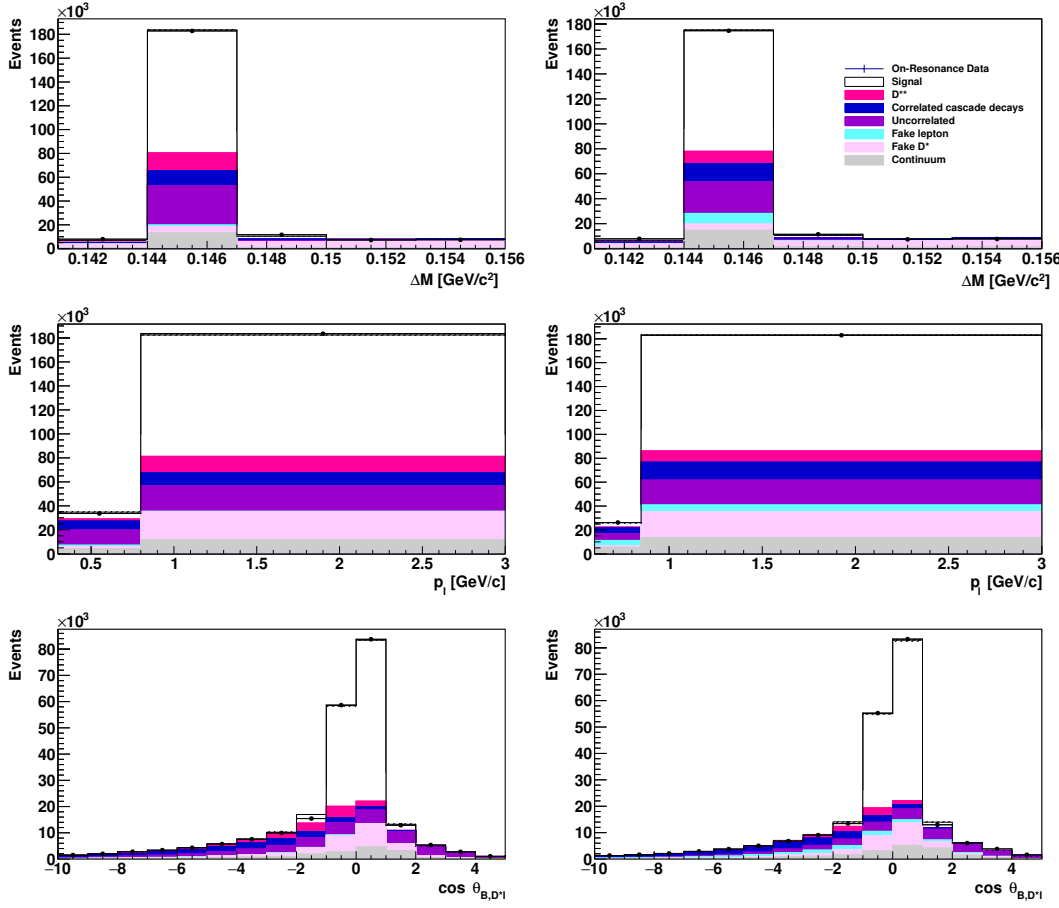


Figure 4.1: Fit to the $(\Delta M, \cos\theta_{B,D^*\ell})$ distributions. The e mode is shown on the left and the μ mode on the right[6].

bin index	variable	range	width
1...10	w	1.00 ... 1.50	0.05
11...20	$\cos\theta_l$	-1.0 ... +1.0	0.2
21...30	$\cos\theta_\nu$	-1.0 ... +1.0	0.2
31...40	χ	$-\pi \dots +\pi$	$2\pi/10$

Table 4.1: Classification of the bins.

factor parametrization [6]. All data are listed in the appendix:

- Background subtracted differential yields N_{obs} with statistical uncertainties σ_{sys} (table A.1)
- Signal efficiency ϵ (table A.1)
- Systematic uncertainties σ_{stat} (table A.2)
- Detector response matrices R for electrons and muons (table A.6 - A.10)
- Statistical uncertainty correlation ρ_{stat} for electrons and muons (table A.11 - A.18)
- Systematic uncertainty correlation ρ_{stat} (table A.19 - A.22)

4.1.4 Results

Two different form factor parametrizations are used in the Belle analysis [6], namely the Caprini Lellouch Neubert (CLN) and the Boyd, Grinstein and Lebed (BGL) parametrization. The CLN parameterization has the parameters ρ^2 , $R_1(1)$, $R_1(2)$ and $\mathcal{F}(1)|V_{cb}|\eta_{\text{EW}}$ and was introduced in Chapter 2.3.1. The results of the fit to the CLN parameterization from the Belle 2019 publication [6] are given below:

$$\begin{aligned}\rho^2 &= 1.106 \pm 0.031 \pm 0.007, \\ R_1(1) &= 1.229 \pm 0.028 \pm 0.009, \\ R_2(1) &= 0.852 \pm 0.021 \pm 0.006, \\ \mathcal{F}(1)|V_{cb}|\eta_{\text{EW}} \times 10^3 &= 35.06 \pm 0.15 \pm 0.56.\end{aligned}\tag{4.2}$$

The first uncertainty is statistical and the second is systematic.

4.2 Expected number of signal events

In order to calculate the events for a bin, it is necessary to integrate formula 2.16. The integral can be written as

$$\begin{aligned}\Gamma = & \int_a^b \int_c^d \int_e^f \int_g^h \frac{d\Gamma(B^0 \rightarrow D^{*-} \ell^+ \nu_\ell)}{dw d(\cos \theta_l) d(\cos \theta_\nu) d\chi} dw d(\cos \theta_l) d(\cos \theta_\nu) d\chi = \\ & = \int_a^b \int_c^d \int_e^f \int_g^h \frac{\eta_{\text{EW}}^2 3m_B m_{D^*}^2}{4(4\pi)^4} G_F^2 |V_{cb}|^2 \{a_1 + a_2 + 4a_3 - 2a_4 - 4a_5 + 4a_6\} dw d(\cos \theta_l) d(\cos \theta_\nu) d\chi\end{aligned}\tag{4.3}$$

with

$$\begin{aligned}a_1 &= (1 - \cos \theta_l)^2 \sin^2 \theta_\nu \sqrt{w^2 - 1} (1 - 2wr + r^2) H_+^2(w), \\ a_2 &= (1 + \cos \theta_l)^2 \sin^2 \theta_\nu \sqrt{w^2 - 1} (1 - 2wr + r^2) H_-^2(w), \\ a_3 &= \sin^2 \theta_l \cos^2 \theta_\nu \sqrt{w^2 - 1} (1 - 2wr + r^2) H_0^2(w), \\ a_4 &= \sin^2 \theta_l \sin^2 \theta_\nu \cos 2\chi \sqrt{w^2 - 1} (1 - 2wr + r^2) H_+(w) H_-(w), \\ a_5 &= \sin \theta_l (1 - \cos \theta_l) \sin \theta_\nu \cos \theta_\nu \cos \chi \sqrt{w^2 - 1} (1 - 2wr + r^2) H_+(w) H_0(w), \\ a_6 &= \sin \theta_l (1 + \cos \theta_l) \sin \theta_\nu \cos \theta_\nu \cos \chi \sqrt{w^2 - 1} (1 - 2wr + r^2) H_-(w) H_0(w).\end{aligned}\tag{4.4}$$

The integrals of the terms a_1 to a_4 can be partially solved analytically using the integral tables 4.4 - 4.7. For example, the result for the term a_1 is given by

$$\begin{aligned}& \int_a^b \int_c^d \int_e^f \int_g^h a_1 dw d\chi d(\cos \theta_\nu) d(\cos \theta_l) \\ &= \int_a^b (1 - \cos \theta_l)^2 d(\cos \theta_l) \int_c^d \sin^2 \theta_\nu d(\cos \theta_\nu) \int_e^f d\chi \int_g^h \sqrt{w^2 - 1} (1 - 2wr + r^2) H_+^2(w) dw \\ &= (\cos \theta_l - \cos^2 \theta_l + \frac{\cos^3 \theta_l}{3}) \Big|_a^b (\cos \theta_\nu - \frac{\cos^3 \theta_\nu}{3}) \Big|_c^d \chi \Big|_e^f \int_g^h \sqrt{w^2 - 1} (1 - 2wr + r^2) H_+^2(w) dw\end{aligned}\tag{4.5}$$

Only the integration over w is done numerically. The limits of integration a - h result from the definition of the bins in table 4.1. A one-dimensional projection of the distributions in w , $\cos \theta_l$, $\cos \theta_\nu$ and χ is calculated. The terms a_5 and a_6 are always zero for the limits of integration used because the integrals

$\int_{-\pi}^{\pi} \cos \chi d\chi$ and $\int_{-1}^1 \sin(\theta_\nu) \cos(\theta_\nu) d(\cos \theta_\nu)$ are zero. The differential decay rate in formula 2.16 is given in natural units ($\hbar = c = 1$). It has the unit GeV/\hbar . To get the result in SI units, the differential decay rate must be multiplied by $GeV/\hbar = 1.519 * 10^{24} s^{-1}$. For example, the integral over the differential decay rate with the integration limits for bin 1 is calculated as follows:

$$\begin{aligned}
 \Gamma_1 &= \int_{-\pi}^{\pi} \int_{-1}^1 \int_{-1}^1 \int_{1.00}^{1.05} \frac{d\Gamma(B^0 \rightarrow D^{*-} \ell^+ \nu_\ell)}{dw d(\cos \theta_l) d(\cos \theta_\nu) d\chi} dw d(\cos \theta_l) d(\cos \theta_\nu) d\chi = \\
 &= \frac{\eta_{EW}^2 3m_B m_{D^*}^2 G_F^2 |V_{cb}|^2}{4(4\pi)^4} \int_{-\pi}^{\pi} \int_{-1}^1 \int_{-1}^1 \int_{1.00}^{1.05} \{a_1 + a_2 + 4a_3 - 2a_4\} dw d(\cos \theta_l) d(\cos \theta_\nu) d\chi = \\
 &= \frac{\eta_{EW}^2 3m_B m_{D^*}^2 G_F^2 |V_{cb}|^2}{4(4\pi)^4} * \\
 &\quad \left\{ \int_{-1}^1 (1 - \cos \theta_l)^2 d(\cos \theta_l) \int_{-1}^1 \sin^2 \theta_\nu d(\cos \theta_\nu) \int_{-\pi}^{\pi} d\chi \int_{1.00}^{1.05} \sqrt{w^2 - 1} (1 - 2wr + r^2) H_+^2(w) dw \right. \\
 &\quad + \int_{-1}^1 (1 + \cos \theta_l)^2 d(\cos \theta_l) \int_{-1}^1 \sin^2 \theta_\nu d(\cos \theta_\nu) \int_{-\pi}^{\pi} d\chi \int_{1.00}^{1.05} \sqrt{w^2 - 1} (1 - 2wr + r^2) H_-^2(w) dw \\
 &\quad + 4 \int_{-1}^1 \sin^2 \theta_l d(\cos \theta_l) \int_{-1}^1 \cos^2 \theta_\nu d(\cos \theta_\nu) \int_{-\pi}^{\pi} d\chi \int_{1.00}^{1.05} \sqrt{w^2 - 1} (1 - 2wr + r^2) H_0^2(w) dw \\
 &\quad \left. - 2 \int_{-1}^1 \sin^2 \theta_l d(\cos \theta_l) \int_{-1}^1 \sin^2 \theta_\nu d(\cos \theta_\nu) \int_{-\pi}^{\pi} \cos 2\chi d\chi \int_{1.00}^{1.05} \sqrt{w^2 - 1} (1 - 2wr + r^2) H_+(w) H_-(w) dw \right\} \tag{4.6}
 \end{aligned}$$

For all other bins the calculation is the same only with different limits of integration. Table 4.2 shows the limits of integration for each bin. For the first bin, the integral becomes

$$\begin{aligned}
 \Gamma_1 &= \frac{\eta_{EW}^2 3m_B m_{D^*}^2 G_F^2 |V_{cb}|^2}{4(4\pi)^4} \left\{ 105.28 \int_{1.00}^{1.05} \sqrt{w^2 - 1} (1 - 2wr + r^2) H_+^2(w) dw \right. \\
 &\quad + 4.74 \int_{1.00}^{1.05} \sqrt{w^2 - 1} (1 - 2wr + r^2) H_-^2(w) dw \\
 &\quad + 2.37 \int_{1.00}^{1.05} \sqrt{w^2 - 1} (1 - 2wr + r^2) H_0^2(w) dw \\
 &\quad \left. - 4.74 \int_{1.00}^{1.05} \sqrt{w^2 - 1} (1 - 2wr + r^2) H_+(w) H_-(w) dw \right\}. \tag{4.7}
 \end{aligned}$$

The number of expected signal events produced in a bin i is calculated by

$$N_i^{prod} = N_{B^0} \mathcal{B}(D^{*+} \rightarrow D^0 \pi^+) \mathcal{B}(D^0 \rightarrow K^- \pi^+) \tau_{B^0} \Gamma_i, \tag{4.8}$$

where N_{B^0} is the number of B^0 mesons [6]. $\mathcal{B}(D^{*+} \rightarrow D^0 \pi^+)$ and $\mathcal{B}(D^0 \rightarrow K^- \pi^+)$ are the branching ratios for the decay $D^{*+} \rightarrow D^0 \pi^+$ and $D^0 \rightarrow K^- \pi^+$. τ_{B^0} is the B^0 lifetime. Γ_i is the integral over the differential decay rate in formula 4.3 within the corresponding limits of integration. N_{B^0} is calculated

<i>bin index</i>	<i>w</i>	$\cos\theta_l$	$\cos\theta_\nu$	χ
1	1.00 ... 1.05	-1.0 ... 1.0	-1.0 ... 1.0	$-\pi \dots \pi$
2	1.05 ... 1.10	-1.0 ... 1.0	-1.0 ... 1.0	$-\pi \dots \pi$
3	1.10 ... 1.15	-1.0 ... 1.0	-1.0 ... 1.0	$-\pi \dots \pi$
4	1.15 ... 1.20	-1.0 ... 1.0	-1.0 ... 1.0	$-\pi \dots \pi$
5	1.20 ... 1.25	-1.0 ... 1.0	-1.0 ... 1.0	$-\pi \dots \pi$
6	1.25 ... 1.30	-1.0 ... 1.0	-1.0 ... 1.0	$-\pi \dots \pi$
7	1.30 ... 1.35	-1.0 ... 1.0	-1.0 ... 1.0	$-\pi \dots \pi$
8	1.35 ... 1.40	-1.0 ... 1.0	-1.0 ... 1.0	$-\pi \dots \pi$
9	1.40 ... 1.45	-1.0 ... 1.0	-1.0 ... 1.0	$-\pi \dots \pi$
10	1.45 ... 1.50	-1.0 ... 1.0	-1.0 ... 1.0	$-\pi \dots \pi$
11	1.00 ... 1.50	-1.0 ... -0.8	-1.0 ... 1.0	$-\pi \dots \pi$
12	1.00 ... 1.50	-0.8 ... -0.6	-1.0 ... 1.0	$-\pi \dots \pi$
13	1.00 ... 1.50	-0.6 ... -0.4	-1.0 ... 1.0	$-\pi \dots \pi$
14	1.00 ... 1.50	-0.4 ... -0.2	-1.0 ... 1.0	$-\pi \dots \pi$
15	1.00 ... 1.50	-0.2 ... 0.0	-1.0 ... 1.0	$-\pi \dots \pi$
16	1.00 ... 1.50	0.0 ... 0.2	-1.0 ... 1.0	$-\pi \dots \pi$
17	1.00 ... 1.50	0.2 ... 0.4	-1.0 ... 1.0	$-\pi \dots \pi$
18	1.00 ... 1.50	0.4 ... 0.6	-1.0 ... 1.0	$-\pi \dots \pi$
19	1.00 ... 1.50	0.6 ... 0.8	-1.0 ... 1.0	$-\pi \dots \pi$
20	1.00 ... 1.50	0.8 ... 1.0	-1.0 ... 1.0	$-\pi \dots \pi$
21	1.00 ... 1.50	-1.0 ... 1.0	-1.0 ... -0.8	$-\pi \dots \pi$
22	1.00 ... 1.50	-1.0 ... 1.0	-0.8 ... -0.6	$-\pi \dots \pi$
23	1.00 ... 1.50	-1.0 ... 1.0	-0.6 ... -0.4	$-\pi \dots \pi$
24	1.00 ... 1.50	-1.0 ... 1.0	-0.4 ... -0.2	$-\pi \dots \pi$
25	1.00 ... 1.50	-1.0 ... 1.0	-0.2 ... 0.0	$-\pi \dots \pi$
26	1.00 ... 1.50	-1.0 ... 1.0	0.0 ... 0.2	$-\pi \dots \pi$
27	1.00 ... 1.50	-1.0 ... 1.0	0.2 ... 0.4	$-\pi \dots \pi$
28	1.00 ... 1.50	-1.0 ... 1.0	0.4 ... 0.6	$-\pi \dots \pi$
29	1.00 ... 1.50	-1.0 ... 1.0	0.6 ... 0.8	$-\pi \dots \pi$
30	1.00 ... 1.50	-1.0 ... 1.0	0.8 ... 1.0	$-\pi \dots \pi$
31	1.00 ... 1.50	-1.0 ... 1.0	-1.0 ... 1.0	$-\pi \dots -0.8\pi$
32	1.00 ... 1.50	-1.0 ... 1.0	-1.0 ... 1.0	$-0.8\pi \dots -0.6\pi$
33	1.00 ... 1.50	-1.0 ... 1.0	-1.0 ... 1.0	$-0.6\pi \dots -0.4\pi$
34	1.00 ... 1.50	-1.0 ... 1.0	-1.0 ... 1.0	$-0.4\pi \dots -0.2\pi$
35	1.00 ... 1.50	-1.0 ... 1.0	-1.0 ... 1.0	$-0.2\pi \dots 0$
36	1.00 ... 1.50	-1.0 ... 1.0	-1.0 ... 1.0	$0 \dots 0.2\pi$
37	1.00 ... 1.50	-1.0 ... 1.0	-1.0 ... 1.0	$0.2\pi \dots 0.4\pi$
38	1.00 ... 1.50	-1.0 ... 1.0	-1.0 ... 1.0	$0.4\pi \dots 0.6\pi$
39	1.00 ... 1.50	-1.0 ... 1.0	-1.0 ... 1.0	$0.6\pi \dots 0.8\pi$
40	1.00 ... 1.50	-1.0 ... 1.0	-1.0 ... 1.0	$0.8\pi \dots \pi$

Table 4.2: Limits of integration for the individual bins to calculate the integral over the differential decay rate.

by

$$N_{B^0} = 2f_{00}N_{BB}, \quad (4.9)$$

where f_{00} is the branching fraction of $e^+e^- \rightarrow B^0\bar{B}^0$ and N_{BB} is the integrated luminosity recorded by the Belle detector [6]. The input values are all listed in Table 4.3. In order to get the number of expected events N_i^{exp} , the finite detector resolution and the signal efficiency must be considered. N_i^{exp} is calculated by

$$N_i^{exp} = \sum_{j=1}^{40} (R_{ij}\epsilon_j N_j^{\text{prod}}), \quad (4.10)$$

where ϵ_j is the signal efficiency of bin j which was determined using a Monte Carlo simulation [6]. R_{ij} is the detector response matrix. It gives the probability of an event generated in bin j is observed in bin i [6]. Figure 4.3 shows a plot of N_i^{exp} for the parameters $\rho^2 = 1.106$, $R_1(1) = 1.229$, $R_2(1) = 0.852$ and $\mathcal{F}(1)|V_{cb}|\eta_{EW} \times 10^3 = 35.06$.

N_{BB}	771.6×10^6
f_{00}	0.486
$\mathcal{B}(D^{*+} \rightarrow D^0\pi^+)$	0.677
$\mathcal{B}(D^0 \rightarrow K^-\pi^+)$	0.0393
τ_{B^0}	1519×10^{-15} s
G_F	1.16637×10^{-5} GeV $^{-2}$
$m_{D^{*+}}$	2.01 GeV
m_{B^0}	5.279 GeV
η_{EW}	1.0066
$\mathcal{F}(1)$	0.904

Table 4.3: Numerical inputs used for the CLN Fit.

4.3 Comparison of different integration methods to calculate the expected number of signal events

To verify the integration procedure, a comparison with other integration methods is done. Two methods are used for checking, in which the differential decay rate in formula 2.16 is numerically integrated in all four dimensions. Figure 4.4 shows the result for the following settings:

- Trapezoidal rule: Formula 2.16 is integrated numerically using the Trapezoidal rule with n=8 subintervals in all four dimensions.

Function	Variable	Integral
$(1 - \cos \theta_l)^2$	$\cos \theta_l$	$\frac{\cos^3 \theta_l}{3} - \cos^2 \theta_l + \cos \theta_l + C$
$\sin^2 \theta_\nu$	$\cos \theta_\nu$	$-\frac{\cos^3 \theta_\nu}{3} + \cos \theta_\nu + C$
1	χ	$\chi + C$
$\sqrt{w^2 - 1}(1 - 2wr + r^2)H_+^2(w)$	w	is solved numerically

Table 4.4: Solved integrals for the term a_1 .

Function	Variable	Integral
$(1 + \cos \theta_l)^2$	$\cos \theta_l$	$\frac{\cos^3 \theta_l}{3} + \cos^2 \theta_l + \cos \theta_l + C$
$\sin^2 \theta_\nu$	$\cos \theta_\nu$	$-\frac{\cos^3 \theta_\nu}{3} + \cos \theta_\nu + C$
1	χ	$\chi + C$
$\sqrt{w^2 - 1}(1 - 2wr + r^2)H_-^2(w)$	w	is solved numerically

Table 4.5: Solved integrals for the term a_2 .

Function	Variable	Integral
$\sin^2 \theta_l$	$\cos \theta_l$	$-\frac{\cos^3 \theta_l}{3} + \cos \theta_l + C$
$\cos^2 \theta_\nu$	$\cos \theta_\nu$	$\frac{\cos^3 \theta_\nu}{3} + C$
1	χ	$\chi + C$
$\sqrt{w^2 - 1}(1 - 2wr + r^2)H_0^2(w)$	w	is solved numerically

Table 4.6: Solved integrals for the term a_3 .

Function	Variable	Integral
$\sin^2 \theta_l$	$\cos \theta_l$	$-\frac{\cos^3 \theta_l}{3} + \cos \theta_l + C$
$\sin^2 \theta_\nu$	$\cos \theta_\nu$	$-\frac{\cos^3 \theta_\nu}{3} + \cos \theta_\nu + C$
$\cos 2\chi$	χ	$\frac{1}{2} \sin 2\chi + C$
$\sqrt{w^2 - 1}(1 - 2wr + r^2)H_+(w)H_-(w)$	w	is solved numerically

Table 4.7: Solved integrals for the term a_4 .

- Simpson's rule: Formula 2.16 is integrated numerically using the Simpson's rule with n=8 subintervals in all four dimensions.
- Analytical: The method being verified and described in Chapter 4.2. Formula 4.3 is partially solved analytically. The integration over the variables $\cos\theta_l$, $\cos\theta_\nu$ and χ are done analytically. Only the integration over w is performed numerically. The Python function `scipy.integrate.quad` is used for the numerical integration.

The results are consistent for Simpson's rule and the partially analytical method. The result with the trapezoidal rule differs because few subintervals were used here.

4.4 Binned χ^2 fit

A binned χ^2 fit is performed to determine the parameters ρ^2 , $R_1(1)$, $R_2(1)$ and the product $\mathcal{F}(1)|V_{cb}|\eta_{EW}$ of the CLN parameterization. To reduce the complexity, a one-dimensional projection of the distributions in w, $\cos\theta_l$, $\cos\theta_\nu$ and χ is fitted. The function

$$\chi^2 = \sum_{i,j} (N_i^{obs} - N_i^{exp}) C_{ij}^{-1} (N_j^{obs} - N_j^{exp}) \quad (4.11)$$

is used to perform the fit [6]. N_i^{obs} is the number of events observed in bin i and is given in Table A.1. N_i^{exp} is the number of expected signal events and is calculated as described in Chapter 4.2. C_{ij}^{-1} is the inverse of the covariance matrix C_{ij} . C_{ij} is defined by [6]

$$C_{ij} = \rho_{ij}^{stat} \sigma_i^{stat} \sigma_j^{stat} + \rho_{ij}^{sys} \sigma_i^{sys} \sigma_j^{sys}. \quad (4.12)$$

Here ρ_{ij}^{stat} and ρ_{ij}^{sys} are the statistical and systematic uncertainty correlation matrix and σ_{stat} and σ_{sys} the statistical and systematic uncertainties. The bins are classified as shown in Table 4.1. A fit is performed separately for the electron and muon mode. To fit the whole data sample, the χ^2 -functions of the electron and muon mode are added.

4.5 Numeric methods

A Python script was written to perform the fit and determine the matrix element $|V_{cb}|$. Several numerical functions are used. This section describes two of them:

- `scipy.integrate.quad`: Integrals can be calculated numerically with `scipy.integrate.quad`. It is used to calculate the integral of the differential decay rate.

- iminuit: Multidimensional functions can be minimized with iminuit. It is used to perform the fit by minimizing χ^2 .

4.5.1 scipy.integrate.quad

scipy.integrate.quad is a Python function to calculate an integral numerically. It is commonly used to calculate a one-dimensional integral of a function $f(x)$ between limits a and b [16]. For example, the integral over w from Table 4.4 can be calculated using

`scipy.integrate.quad(f,a,b,args=(para))`. Here $f = \sqrt{w^2 - 1}(1 - 2wr + r^2)H_+^2(w)$ and the limits of integration are $a = 1.00$ and $b = 1.05$ for bin 1. The argument `args=(para)` is used to pass the fit parameters ρ^2 , $R_1(1)$, $R_1(2)$ and $\mathcal{F}(1)|V_{cb}|\eta_{EW}$.

4.5.2 iminuit

iminuit is a tool to minimize functions with multiple variables [17]. It is a Python interface using the MINUIT2 C++ library developed and maintained by scientists at CERN. iminuit also calculates error estimates for the parameters. To test iminuit, a fit is performed to the CLN parameterization and the result is compared to the Python function `scipy.optimize.minimize`. Table 4.8 shows the results of the comparison.

	iminuit	minimize
ρ^2	1.177534	1.177548
$R_1(1)$	1.091527	1.091544
$R_2(1)$	0.844338	0.844371
$\mathcal{F}(1) V_{cb} \eta_{EW} \times 10^3$	36.22028	36.22056

Table 4.8: Fit results to the CLN parameterization to compare different minimization functions. The left column shows the result using iminuit and the right column shows the result using `scipy.optimize.minimize`. The fit was performed on the electron mode.

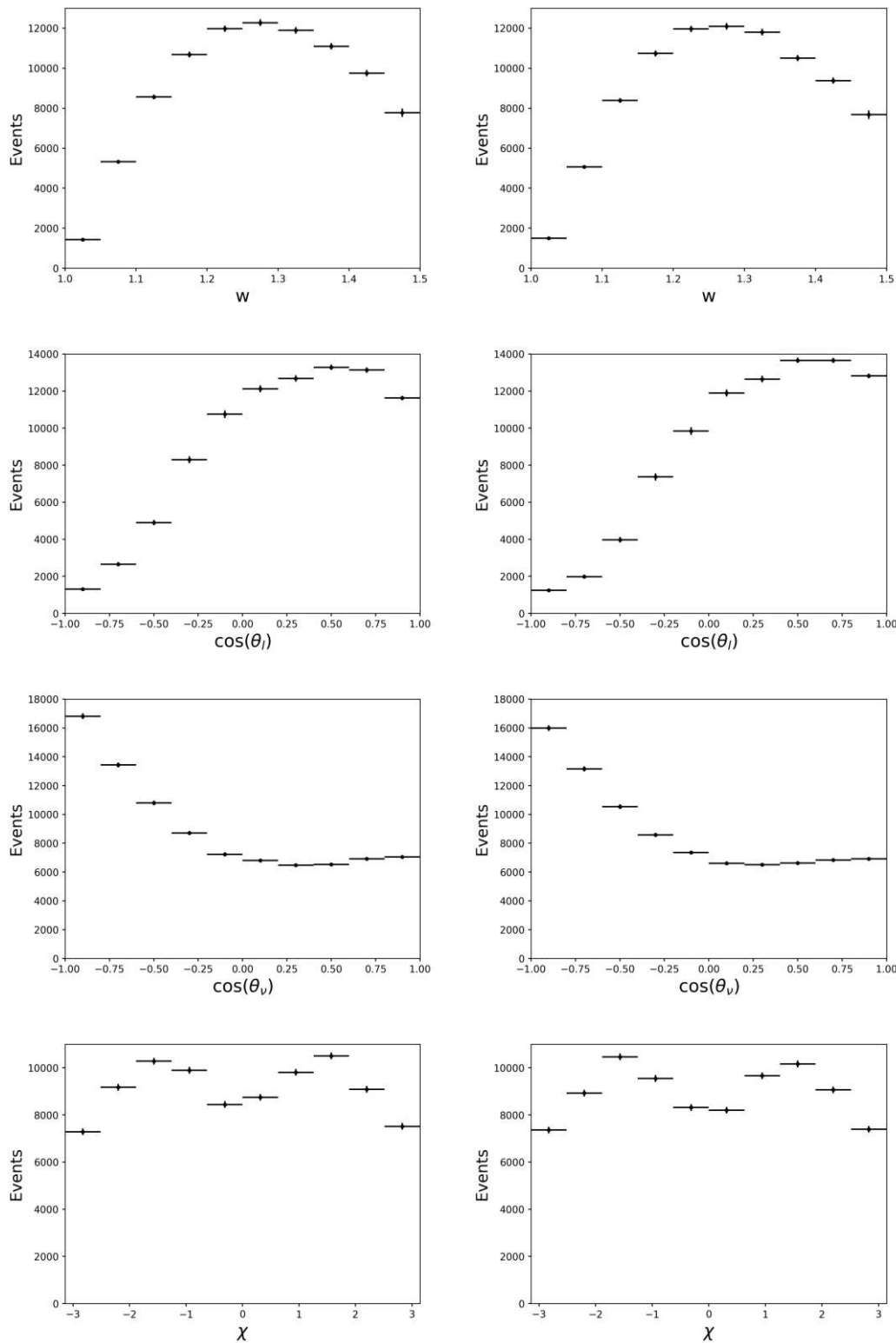


Figure 4.2: Background subtracted signal yields for the electron and muon modes. The e mode is shown on the left and the μ mode on the right. The figures show the distributions in w , $\cos\theta_l$, $\cos\theta_\nu$, and χ .

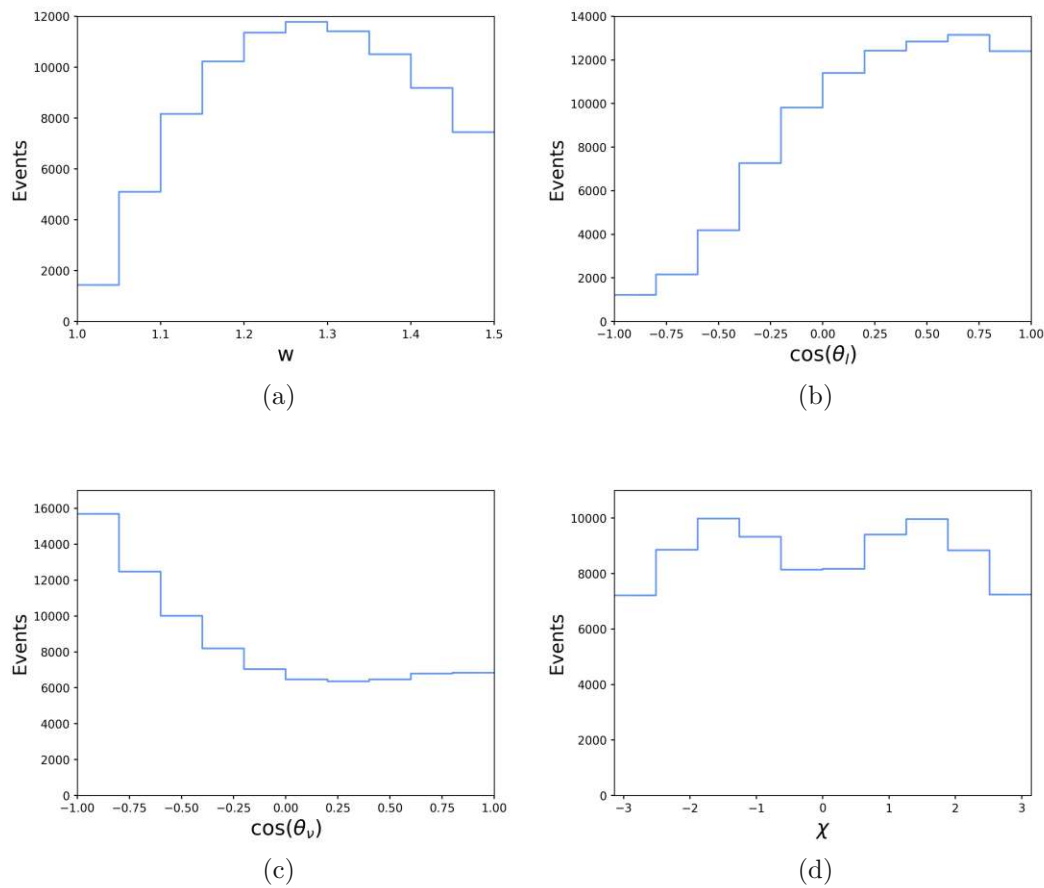


Figure 4.3: CLN parametrization $\rho^2 = 1.106$, $R_1(1) = 1.229$, $R_2(1) = 0.852$ and $\mathcal{F}(1)|V_{cb}|\eta_{EW} \times 10^3 = 35.06$. Distribution in (a) w , (b) $\cos\theta_l$, (c) $\cos\theta_v$ and (d) χ .

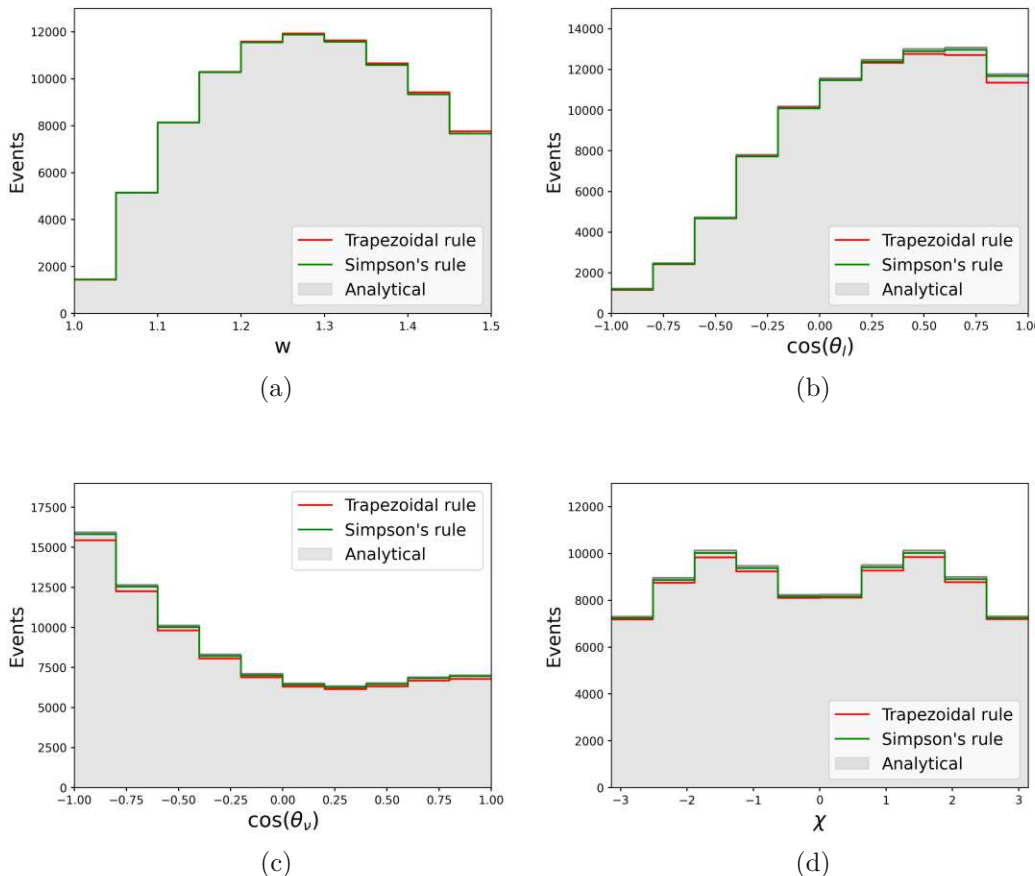


Figure 4.4: Calculation of the number of events with the CLN parameterization using different integration methods: Trapezoidal rule (red), Simpson's rule (green) and partially analytical (grey). Using the parameters $\rho^2 = 1.106$, $R_1(1) = 1.229$, $R_2(1) = 0.852$ and $\mathcal{F}(1)|V_{cb}|\eta_{EW} \times 10^3 = 35.06$. Distribution in (a) w , (b) $\cos\theta_l$, (c) $\cos\theta_\nu$ and (d) χ .

 **Bibliothek**, Your knowledge hub Die approbierte gedruckte Originalversion dieser Diplomarbeit ist an der TU Wien Bibliothek verfügbar.
The approved original version of this thesis is available in print at TU Wien Bibliothek.

Chapter 5

Results

In this chapter the fit results are presented. Fit results with different settings are shown and the results are compared to the Belle 2019 analysis. The fits were performed with the following settings:

- 40 bin Fit: The distributions in w , $\cos\theta_l$, $\cos\theta_t$ and χ are fitted.
- 37 bin Fit: 10 bins of the distributions in w and 9 bins each of the distributions in $\cos\theta_l$, $\cos\theta_t$ and χ are fitted.
- 40 Bin Fit using only the statistical uncertainties: Only the statistical uncertainties are taken into account when calculating the covariance matrix.
- 40 bin Fit considering the d'Agostini bias: The distributions in w , $\cos\theta_l$, $\cos\theta_t$ and χ are fitted and the d'Agostini bias is taken into account.

As a result, the fit parameters ρ^2 , $R_1(1)$, $R_1(2)$ and $\mathcal{F}(1)|V_{cb}|\eta_{EW}$ and their statistical correlation matrix are stated and a plot of the observed and expected number of signal events. The result is given separately for the electron and muon modes and for the full data sample. $\chi^2/n.d.f.$ is stated as a parameter for the quality of the fit [2]. It is calculated by

$$\frac{\chi^2}{n.d.f.} = \frac{1}{n.d.f.} \sum_{i,j} (N_i^{obs} - N_i^{exp}) C_{ij}^{-1} (N_j^{obs} - N_j^{exp}), \quad (5.1)$$

where n.d.f. is the number of degrees of freedom. It results from the number of fitted bins minus the number of parameters. For example, 40 bins are fitted to 4 parameters, resulting in a n.f.d. of $40 - 4 = 36$. $\chi^2/n.d.f. \approx 1$ means that there is a good fit result. $\chi^2/n.d.f. > 1$ means that the measurement results do not correlate well with each other. $\chi^2/n.d.f. < 1$ means that the errors of the measurement results are overestimated.

5.1 40 bin Fit

A 40 bin fit is performed separately for the electron and muon modes. The distributions in w , $\cos\theta_l$, $\cos\theta_t$ and χ are fitted and each distribution is divided

into 10 bins. An 80 bin fit is performed for the entire data sample. Here the χ^2 -function for electron and muon mode are added together. The fit results are given in Table B.1 and Figures B.1-B.2. The Statistical correlation matrices are given in Tables B.2-B.4.

5.2 37 bin Fit

The distributions in w , $\cos\theta_l$, $\cos\theta_\nu$ and χ are each divided into 10 bins. Each measured signal event is included once in each distribution. Table 5.1 shows the sum of the measured signal events for each of the four distributions. The events in 10 bins add up to the same number. There are 90743.4 events for the electrons and 89087.0 for the muons. That means all 40 bins are not independent of each other. The content of 3 bins can be calculated from the other bins. One would expect the statistical part of the 40x40 covariance matrix to be non-invertible. However, this is not the case and it is unclear why this is so [18]. To get independent bins, a 37 bin fit is done. The last bin from the distributions in $\cos\theta_l$, $\cos\theta_\nu$ and χ is omitted and a 37x37 covariance matrix is created. The fit results are given in Table B.5 and Figures B.3-B.4. The Statistical correlation matrices are given in Tables B.6-B.8.

$\sum_{i=1}^{10} N_{i,e}^{obs} = 90743.32$	$\sum_{i=1}^{10} N_{i,\mu}^{obs} = 89086.89$
$\sum_{i=11}^{20} N_{i,e}^{obs} = 90743.37$	$\sum_{i=11}^{20} N_{i,\mu}^{obs} = 89086.97$
$\sum_{i=21}^{30} N_{i,e}^{obs} = 90743.43$	$\sum_{i=21}^{30} N_{i,\mu}^{obs} = 89087.01$
$\sum_{i=31}^{40} N_{i,e}^{obs} = 90743.38$	$\sum_{i=31}^{40} N_{i,\mu}^{obs} = 89087.02$

Table 5.1: Sum of observed signal events calculated for each distribution. In the left column for the electron mode and in the right column for the muon mode.

5.3 40 Bin Fit using only the statistical uncertainties

The covariance matrix is calculated by

$$C_{ij} = \rho_{ij}^{stat} \sigma_i^{stat} \sigma_j^{stat}, \quad (5.2)$$

without systematic uncertainties, only with the statistical uncertainties. The fit results are given in Table B.9 and Figures B.5-B.6. The Statistical correlation matrices are given in Tables B.10-B.12.

5.4 40 bin Fit considering the d'Agostini bias

For this fit, the covariance matrix is calculated with the systematic uncertainties as in formula (4.12). This can lead to bias in the covariance matrix and the fit result when the systematic uncertainties are large [19, 20]. This effect is called d'Agostini bias. It results from the fact that the systematic uncertainties are calculated by multiplying the relative systematic uncertainties with the measurement data. However, since the measurement data is subject to uncertainties, this can lead to an incorrect covariance matrix. In order to take the d'Agostini bias into account, the systematic uncertainties are not calculated using the measured events N^{obs} , but are calculated using the expected events N^{exp} . This is calculated separately for the e-mode and for the μ -mode. The systematic uncertainties σ^{sys} are thus calculated with

$$\sigma^{sys} = \frac{\sigma^{sys}}{N} * N^{exp}. \quad (5.3)$$

Here $\frac{\sigma^{sys}}{N}$ are the relative statistical uncertainties from Table A.2. N^{exp} is the number of expected events calculated by the fit. In order to get a stable result, the fit is repeated several times, each time with the new value of N^{exp} . The fit results for the 40 bin Fit considering the d'Agostini bias are given in Table 5.2 and Figures 5.1-5.2. The Statistical correlation matrices are given in Tables 5.3-5.5.

	e-mode	μ -mode	full sample
ρ^2	1.177 ± 0.047	1.154 ± 0.050	1.166 ± 0.034
$R_1(1)$	1.085 ± 0.038	1.282 ± 0.042	1.184 ± 0.028
$R_2(1)$	0.846 ± 0.029	0.851 ± 0.032	0.848 ± 0.022
$\mathcal{F}(1) V_{cb} \eta_{EW} \times 10^3$	36.76 ± 0.65	36.20 ± 0.65	36.49 ± 0.46
$\chi^2/\text{n.d.f.}$	$29.9 / 36.0$	$40.2 / 36.0$	$93.7 / 76.0$

Table 5.2: Fit result of the 40 bin Fit considering the d'Agostini bias to the CLN parametrization. The first two columns show the results for the electron and muon modes and the third column shows the results for the full sample. The statistical uncertainties are stated.

	ρ^2	$R_1(1)$	$R_2(1)$	$\mathcal{F}(1) V_{cb} \eta_{EW}$
ρ^2	+1.000	+0.495	-0.812	+0.308
$R_1(1)$		+1.000	-0.650	-0.165
$R_2(1)$			+1.000	-0.039
$\mathcal{F}(1) V_{cb} \eta_{EW}$				+1.000

Table 5.3: Statistical correlation matrix of the 40 bin Fit considering the d'Agostini bias for the electron mode in the CLN parametrization.

	ρ^2	$R_1(1)$	$R_2(1)$	$\mathcal{F}(1) V_{cb} \eta_{\text{EW}}$
ρ^2	+1.000	+0.554	-0.820	+0.305
$R_1(1)$		+1.000	-0.719	-0.162
$R_2(1)$			+1.000	-0.030
$\mathcal{F}(1) V_{cb} \eta_{\text{EW}}$				+1.000

Table 5.4: Statistical correlation matrix of the 40 bin Fit considering the d'Agostini bias for the muon mode in the CLN parametrization.

	ρ^2	$R_1(1)$	$R_2(1)$	$\mathcal{F}(1) V_{cb} \eta_{\text{EW}}$
ρ^2	+1.000	+0.525	-0.815	+0.306
$R_1(1)$		+1.000	-0.686	-0.164
$R_2(1)$			+1.000	-0.035
$\mathcal{F}(1) V_{cb} \eta_{\text{EW}}$				+1.000

Table 5.5: Statistical correlation matrix of the 40 bin Fit considering the d'Agostini bias for the full sample in the CLN parametrization.

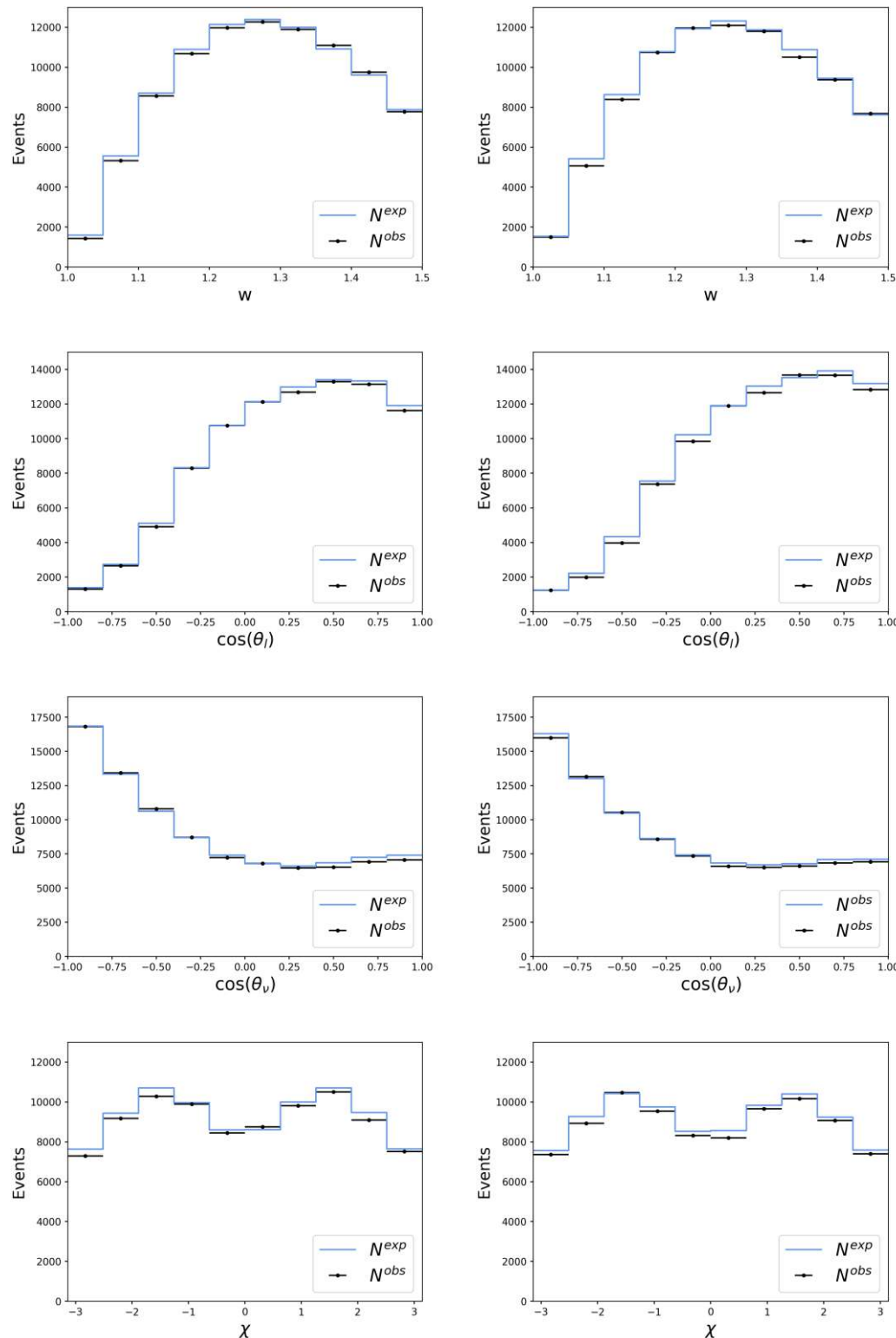


Figure 5.1: Result of the 40 bin Fit considering the d'Agostini bias to the CLN parametrization. The number of observed events N^{obs} and the number of expected events N^{exp} are plotted. The e mode is shown on the left and the μ mode on the right. The figures show the distributions in w , \cos_{θ_l} , \cos_{θ_v} and χ .

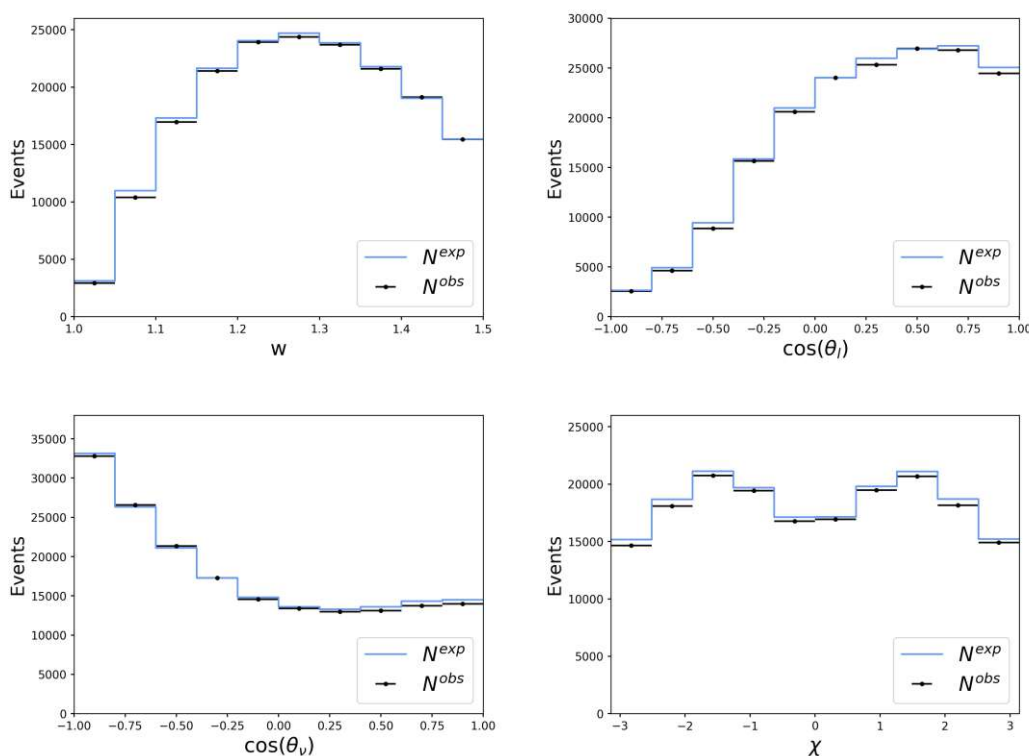


Figure 5.2: Result of the 40 bin Fit considering the d'Agostini bias to the CLN parametrization for the full sample. The figures show the distributions in w , $\cos\theta_l$, $\cos\theta_\nu$ and χ .

Chapter 6

Conclusions

In this thesis, the exclusive semileptonic decay $B^0 \rightarrow D^{*-} \ell^+ \nu_\ell$ ($\ell = e, \mu$) was analyzed and a reanalysis of the data published by Belle 2019 was done. The Caprini Lellouch Neubert (CLN) parametrization was used to describe the differential decay rate. The four parameters of the CLN parametrization ρ^2 , $R_1(1)$, $R_1(2)$ and $\mathcal{F}(1)|V_{cb}|\eta_{EW}$ were determined from the measured data with a four-dimensional fit. The fit results was done under various assumptions such as different numbers of fitted bins or consideration of the D'Agostini bias. Table 6.1 shows all the results obtained in this work and Figure 6.1 shows a comparison of the fit results with the result from the Belle publication from 2019. Although several fits were performed with different assumptions, the result of the 2019 Belle publication could not be reproduced.

	40 bin	37 bin	stat.	d'Agostini bias
ρ^2	1.167 ± 0.036	1.168 ± 0.036	1.087 ± 0.030	1.166 ± 0.034
$R_1(1)$	1.195 ± 0.030	1.234 ± 0.037	1.190 ± 0.027	1.184 ± 0.028
$R_2(1)$	0.845 ± 0.023	0.844 ± 0.024	0.863 ± 0.020	0.848 ± 0.022
$\mathcal{F}(1) V_{cb} \eta_{EW} \times 10^3$	35.63 ± 0.46	35.65 ± 0.47	35.57 ± 0.15	36.49 ± 0.46
$\chi^2/\text{n.d.f.}$	$93.2 / 76.0$	$80.3 / 70.0$	$126.7 / 76.0$	$93.7 / 76.0$

Table 6.1: Fit result for different settings. Results are given for the the 40 bin fit, the 37 bin fit, 40 bin fit using only the statistical part of the covariance matrix and the 40 bin fit considering the d'Agostini bias.

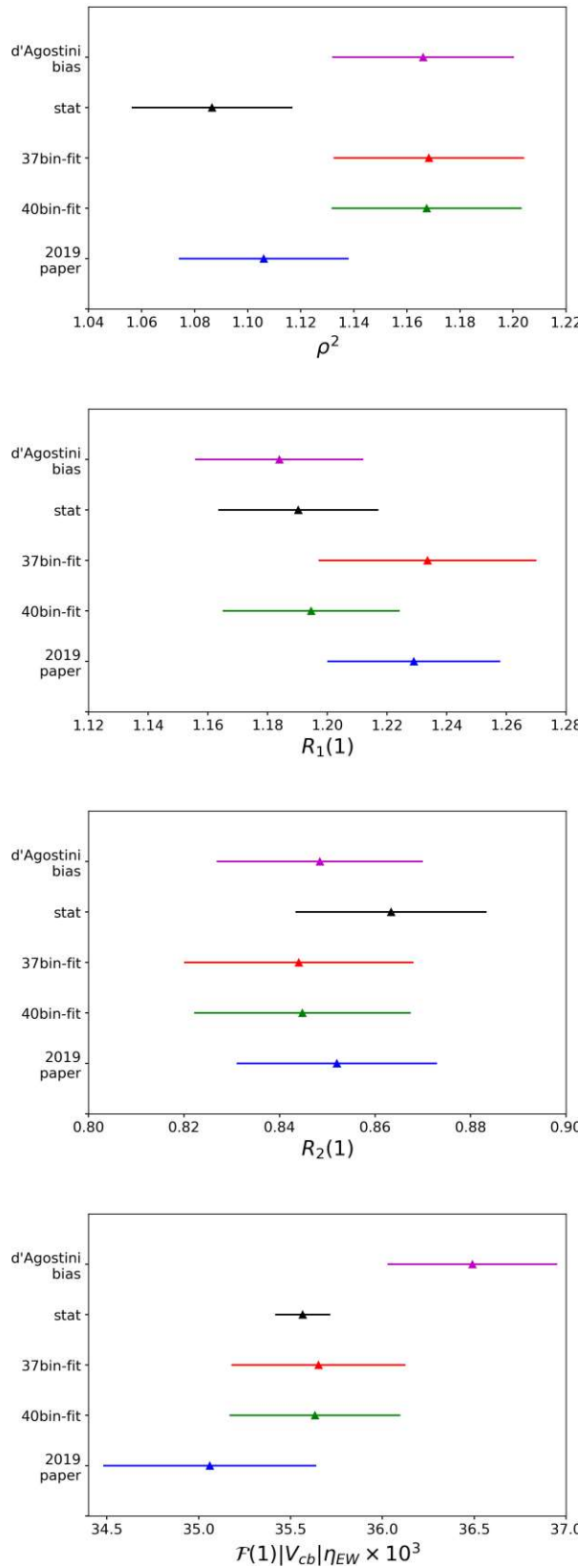


Figure 6.1: Comparison of the fit results with different settings and with the result from the Belle publication from 2019. Shown are the results from the Belle publication 2019 (blue), the 40 bin fit (green), the 37 bin fit (red), 40 bin fit using only the statistical part of the covariance matrix (black) and the 40 bin fit considering the d'Agostini bias (purple).

Appendix A

Data

Table A.1: Background subtracted differential yields N_{obs} with statistical uncertainties σ_{sys} and signal efficiency ϵ . The left part of the table shows the electron mode and the right part the muon mode [6].

Bin	Yield	Efficiency (%)	Yield	Efficiency (%)
1	1421 ± 42	2.72 ± 0.02	1494 ± 44	2.68 ± 0.02
2	5319 ± 86	5.72 ± 0.02	5063 ± 89	5.66 ± 0.02
3	8563 ± 113	7.70 ± 0.03	8385 ± 121	7.66 ± 0.03
4	10685 ± 129	9.10 ± 0.03	10734 ± 143	9.05 ± 0.03
5	11972 ± 156	10.03 ± 0.03	11962 ± 160	9.91 ± 0.03
6	12276 ± 167	10.61 ± 0.03	12091 ± 167	10.43 ± 0.03
7	11888 ± 167	10.74 ± 0.03	11803 ± 168	10.60 ± 0.03
8	11097 ± 151	10.67 ± 0.03	10502 ± 155	10.52 ± 0.03
9	9751 ± 159	10.23 ± 0.03	9378 ± 161	10.04 ± 0.03
10	7771 ± 216	9.10 ± 0.03	7674 ± 214	9.14 ± 0.03
11	1306 ± 79	3.12 ± 0.03	1240 ± 96	3.16 ± 0.03
12	2651 ± 143	3.97 ± 0.02	1984 ± 110	3.52 ± 0.02
13	4903 ± 154	5.73 ± 0.02	3972 ± 151	5.19 ± 0.02
14	8295 ± 173	7.96 ± 0.03	7366 ± 194	7.59 ± 0.03
15	10748 ± 187	9.31 ± 0.03	9841 ± 213	9.10 ± 0.03
16	12119 ± 183	9.85 ± 0.03	11894 ± 191	9.78 ± 0.03
17	12682 ± 220	10.23 ± 0.03	12647 ± 181	10.27 ± 0.03
18	13283 ± 158	10.59 ± 0.03	13664 ± 149	10.43 ± 0.03
19	13133 ± 153	11.06 ± 0.03	13659 ± 144	11.00 ± 0.03
20	11624 ± 120	11.21 ± 0.03	12821 ± 123	11.36 ± 0.03
21	16815 ± 196	11.72 ± 0.03	15992 ± 206	11.54 ± 0.03
22	13428 ± 180	11.53 ± 0.03	13157 ± 178	11.43 ± 0.03
23	10797 ± 152	11.35 ± 0.03	10533 ± 160	11.14 ± 0.03
24	8706 ± 140	10.88 ± 0.04	8574 ± 148	10.74 ± 0.04
25	7227 ± 134	10.20 ± 0.04	7353 ± 138	10.09 ± 0.04
26	6803 ± 128	9.34 ± 0.04	6600 ± 128	9.29 ± 0.04
27	6477 ± 122	8.29 ± 0.03	6516 ± 122	8.25 ± 0.03
28	6518 ± 123	7.16 ± 0.03	6615 ± 130	7.10 ± 0.03
29	6921 ± 122	6.05 ± 0.02	6833 ± 124	5.97 ± 0.02
30	7051 ± 115	4.82 ± 0.02	6915 ± 119	4.72 ± 0.02
31	7286 ± 143	8.60 ± 0.03	7361 ± 147	8.51 ± 0.03
32	9174 ± 140	8.74 ± 0.03	8923 ± 147	8.67 ± 0.03
33	10279 ± 146	8.96 ± 0.03	10466 ± 147	8.82 ± 0.03
34	9893 ± 144	9.30 ± 0.03	9541 ± 149	9.15 ± 0.03
35	8443 ± 143	9.81 ± 0.03	8319 ± 145	9.70 ± 0.03
36	8746 ± 133	9.82 ± 0.03	8198 ± 140	9.73 ± 0.03
37	9809 ± 145	9.33 ± 0.03	9662 ± 145	9.20 ± 0.03
38	10506 ± 144	9.00 ± 0.03	10162 ± 146	8.83 ± 0.03
39	9090 ± 142	8.77 ± 0.03	9063 ± 148	8.62 ± 0.03
40	7518 ± 138	8.59 ± 0.03	7392 ± 142	8.54 ± 0.03

Table A.2: Systematic uncertainty (%) [6].

<i>Bin</i>	σ_{sys}	<i>Bin</i>	σ_{sys}	<i>Bin</i>	σ_{sys}	<i>Bin</i>	σ_{sys}
1	6.42	11	4.39	21	3.09	31	3.21
2	4.12	12	3.90	22	3.12	32	3.20
3	3.55	13	3.61	23	3.16	33	3.21
4	3.35	14	3.30	24	3.19	34	3.16
5	3.26	15	3.17	25	3.23	35	3.15
6	3.22	16	3.07	26	3.30	36	3.16
7	3.20	17	3.09	27	3.40	37	3.20
8	3.23	18	3.11	28	3.49	38	3.23
9	3.14	19	3.14	29	3.62	39	3.22
10	3.16	20	3.16	30	3.90	40	3.21

Table A.3: Detector response matrix R_{ji} for observable w for the electron mode [6].

Bin	1	2	3	4	5	6	7	8	9	10
1	0.803	0.053	0.000	0.000	0.000	0.000	0.000	0.000	0.000	0.000
2	0.197	0.778	0.098	0.000	0.000	0.000	0.000	0.000	0.000	0.000
3	0.000	0.168	0.717	0.126	0.002	0.000	0.000	0.000	0.000	0.000
4	0.000	0.001	0.182	0.667	0.149	0.006	0.000	0.000	0.000	0.000
5	0.000	0.000	0.004	0.199	0.626	0.167	0.011	0.000	0.000	0.000
6	0.000	0.000	0.000	0.009	0.207	0.592	0.177	0.015	0.000	0.000
7	0.000	0.000	0.000	0.000	0.016	0.215	0.575	0.183	0.018	0.000
8	0.000	0.000	0.000	0.000	0.000	0.021	0.213	0.567	0.186	0.017
9	0.000	0.000	0.000	0.000	0.000	0.000	0.024	0.214	0.598	0.186
10	0.000	0.000	0.000	0.000	0.000	0.000	0.022	0.198	0.797	

Table A.4: Detector response matrix R_{ji} for observable $\cos\theta_l$ for the electron mode [6].

Bin	11	12	13	14	15	16	17	18	19	20
11	0.961	0.024	0.000	0.000	0.000	0.000	0.000	0.000	0.000	0.000
12	0.038	0.952	0.027	0.000	0.000	0.000	0.000	0.000	0.000	0.000
13	0.000	0.021	0.948	0.041	0.001	0.000	0.000	0.000	0.000	0.000
14	0.000	0.001	0.023	0.918	0.067	0.003	0.001	0.001	0.001	0.000
15	0.000	0.001	0.001	0.040	0.871	0.097	0.005	0.001	0.001	0.000
16	0.000	0.000	0.000	0.001	0.060	0.817	0.129	0.006	0.001	0.000
17	0.000	0.000	0.000	0.000	0.001	0.082	0.758	0.164	0.007	0.001
18	0.000	0.000	0.000	0.000	0.000	0.001	0.106	0.698	0.196	0.008
19	0.000	0.000	0.000	0.000	0.000	0.000	0.001	0.128	0.657	0.212
20	0.000	0.000	0.000	0.000	0.000	0.000	0.000	0.002	0.137	0.777

Table A.5: Detector response matrix R_{ji} for observable $\cos\theta_\nu$ for the electron mode [6].

Bin	21	22	23	24	25	26	27	28	29	30
21	0.918	0.077	0.000	0.000	0.000	0.000	0.000	0.000	0.000	0.000
22	0.082	0.806	0.095	0.001	0.000	0.000	0.000	0.000	0.000	0.000
23	0.000	0.115	0.761	0.101	0.002	0.000	0.000	0.000	0.000	0.000
24	0.000	0.001	0.141	0.735	0.105	0.002	0.000	0.000	0.000	0.000
25	0.000	0.000	0.002	0.160	0.719	0.100	0.001	0.000	0.000	0.000
26	0.000	0.000	0.000	0.003	0.170	0.722	0.093	0.001	0.000	0.000
27	0.000	0.000	0.000	0.000	0.003	0.173	0.738	0.080	0.001	0.000
28	0.000	0.000	0.000	0.000	0.000	0.002	0.166	0.771	0.072	0.000
29	0.000	0.000	0.000	0.000	0.000	0.000	0.001	0.147	0.819	0.064
30	0.000	0.000	0.000	0.000	0.000	0.000	0.000	0.001	0.108	0.936

Table A.6: Detector response matrix R_{ji} for observable χ for the electron mode [6].

Bin	31	32	33	34	35	36	37	38	39	40
31	0.659	0.129	0.011	0.003	0.002	0.002	0.002	0.004	0.013	0.144
32	0.151	0.691	0.132	0.012	0.004	0.002	0.002	0.002	0.004	0.016
33	0.015	0.141	0.697	0.147	0.016	0.005	0.002	0.002	0.002	0.005
34	0.005	0.012	0.134	0.671	0.162	0.018	0.005	0.002	0.002	0.002
35	0.002	0.004	0.013	0.140	0.634	0.155	0.016	0.004	0.002	0.002
36	0.002	0.002	0.004	0.015	0.155	0.633	0.141	0.013	0.004	0.003
37	0.002	0.002	0.002	0.004	0.018	0.163	0.670	0.136	0.012	0.004
38	0.005	0.002	0.002	0.002	0.005	0.015	0.147	0.695	0.140	0.015
39	0.016	0.004	0.002	0.002	0.002	0.004	0.013	0.132	0.691	0.150
40	0.142	0.013	0.003	0.002	0.002	0.002	0.003	0.012	0.130	0.659

Table A.7: Detector response matrix R_{ji} for observable w for the muon mode [6].

Bin	1	2	3	4	5	6	7	8	9	10
1	0.812	0.051	0.000	0.000	0.000	0.000	0.000	0.000	0.000	0.000
2	0.188	0.784	0.096	0.000	0.000	0.000	0.000	0.000	0.000	0.000
3	0.000	0.164	0.728	0.126	0.002	0.000	0.000	0.000	0.000	0.000
4	0.000	0.001	0.172	0.676	0.149	0.006	0.000	0.000	0.000	0.000
5	0.000	0.000	0.004	0.190	0.631	0.165	0.010	0.000	0.000	0.000
6	0.000	0.000	0.000	0.008	0.203	0.600	0.181	0.016	0.000	0.000
7	0.000	0.000	0.000	0.000	0.014	0.209	0.578	0.187	0.019	0.000
8	0.000	0.000	0.000	0.000	0.000	0.020	0.209	0.573	0.195	0.017
9	0.000	0.000	0.000	0.000	0.000	0.000	0.022	0.205	0.600	0.195
10	0.000	0.000	0.000	0.000	0.000	0.000	0.019	0.186	0.788	

Table A.8: Detector response matrix R_{ji} for observable for $\cos\theta_l$ the muon mode [6].

Bin	11	12	13	14	15	16	17	18	19	20
11	0.959	0.022	0.000	0.000	0.000	0.000	0.000	0.000	0.000	0.000
12	0.039	0.955	0.012	0.000	0.000	0.000	0.000	0.000	0.000	0.000
13	0.000	0.021	0.960	0.022	0.001	0.000	0.000	0.000	0.000	0.000
14	0.001	0.001	0.026	0.931	0.043	0.001	0.000	0.000	0.000	0.000
15	0.000	0.000	0.001	0.047	0.889	0.070	0.002	0.000	0.000	0.000
16	0.000	0.001	0.000	0.000	0.067	0.837	0.103	0.002	0.001	0.000
17	0.000	0.000	0.000	0.000	0.000	0.091	0.778	0.138	0.003	0.000
18	0.000	0.000	0.000	0.000	0.000	0.000	0.117	0.715	0.174	0.004
19	0.000	0.000	0.000	0.000	0.000	0.000	0.001	0.142	0.672	0.193
20	0.000	0.000	0.000	0.000	0.000	0.000	0.000	0.002	0.151	0.803

Table A.9: Detector response matrix R_{ji} for observable $\cos\theta_\nu$ for the muon mode [6].

Bin	21	22	23	24	25	26	27	28	29	30
21	0.918	0.077	0.000	0.000	0.000	0.000	0.000	0.000	0.000	0.000
22	0.082	0.805	0.091	0.001	0.000	0.000	0.000	0.000	0.000	0.000
23	0.000	0.117	0.763	0.101	0.002	0.000	0.000	0.000	0.000	0.000
24	0.000	0.001	0.142	0.735	0.103	0.002	0.000	0.000	0.000	0.000
25	0.000	0.000	0.003	0.159	0.723	0.098	0.001	0.000	0.000	0.000
26	0.000	0.000	0.000	0.004	0.169	0.726	0.091	0.001	0.000	0.000
27	0.000	0.000	0.000	0.000	0.004	0.172	0.745	0.082	0.001	0.000
28	0.000	0.000	0.000	0.000	0.000	0.002	0.161	0.771	0.074	0.000
29	0.000	0.000	0.000	0.000	0.000	0.000	0.001	0.145	0.817	0.066
30	0.000	0.000	0.000	0.000	0.000	0.000	0.000	0.000	0.107	0.934

Table A.10: Detector response matrix R_{ji} for observable χ for the muon mode [6].

Bin	31	32	33	34	35	36	37	38	39	40
31	0.653	0.129	0.012	0.004	0.003	0.002	0.002	0.004	0.014	0.144
32	0.152	0.686	0.130	0.013	0.004	0.003	0.002	0.002	0.005	0.017
33	0.016	0.143	0.693	0.147	0.016	0.006	0.003	0.002	0.003	0.005
34	0.005	0.013	0.138	0.667	0.160	0.018	0.005	0.002	0.002	0.003
35	0.003	0.004	0.013	0.142	0.630	0.156	0.015	0.004	0.002	0.002
36	0.002	0.002	0.004	0.015	0.158	0.629	0.142	0.013	0.004	0.003
37	0.003	0.002	0.002	0.005	0.018	0.164	0.667	0.138	0.013	0.005
38	0.005	0.003	0.002	0.003	0.006	0.016	0.148	0.692	0.141	0.016
39	0.017	0.004	0.002	0.002	0.003	0.005	0.013	0.131	0.686	0.152
40	0.144	0.014	0.004	0.002	0.002	0.002	0.004	0.012	0.129	0.654

Table A.11: Statistical uncertainty correlation matrix for the electron mode [6].

Bin	1	2	3	4	5	6	7	8	9	10	11	12	13	14	15	16	17	18	19	20
1	1.000	0.000	0.000	0.000	0.000	0.000	0.000	0.000	0.000	0.016	0.012	0.007	0.002	-0.003	-0.006	-0.004	-0.006	-0.003	0.007	
2	0.000	1.000	0.000	0.000	0.000	0.000	0.000	0.000	0.000	0.032	0.015	0.005	-0.005	-0.010	-0.009	-0.005	-0.002	0.003	0.019	
3	0.000	0.000	1.000	0.000	0.000	0.000	0.000	0.000	0.000	0.031	0.016	0.007	-0.005	-0.010	-0.010	-0.007	-0.003	0.004	0.028	
4	0.000	0.000	0.000	1.000	0.000	0.000	0.000	0.000	0.000	0.022	0.011	0.008	-0.005	-0.011	-0.008	-0.005	-0.001	0.008	0.030	
5	0.000	0.000	0.000	0.000	1.000	0.000	0.000	0.000	0.000	0.015	0.008	0.001	-0.005	-0.008	-0.006	-0.003	0.002	0.009	0.024	
6	0.000	0.000	0.000	0.000	0.000	1.000	0.000	0.000	0.000	0.005	0.002	-0.001	-0.001	-0.002	-0.000	0.000	0.002	0.003	0.010	
7	0.000	0.000	0.000	0.000	0.000	0.000	1.000	0.000	0.000	0.016	0.001	0.001	0.001	0.003	0.002	0.003	0.004	0.001		
8	0.000	0.000	0.000	0.000	0.000	0.000	0.000	1.000	0.000	0.000	-0.022	-0.009	0.001	0.003	0.006	0.006	0.003	0.009	-0.011	
9	0.000	0.000	0.000	0.000	0.000	0.000	0.000	0.000	1.000	0.000	-0.016	-0.015	-0.007	0.004	0.008	0.008	0.005	0.004	-0.005	-0.025
10	0.000	0.000	0.000	0.000	0.000	0.000	0.000	0.000	0.000	1.000	-0.011	-0.012	-0.015	-0.003	0.004	0.004	-0.001	-0.002	-0.009	-0.025
11	0.016	0.032	0.031	0.022	0.015	-0.001	-0.016	-0.022	-0.016	-0.011	1.000	0.000	0.000	0.000	0.000	0.000	0.000	0.000	0.000	
12	0.012	0.015	0.016	0.011	0.008	0.005	0.005	0.001	-0.009	-0.015	-0.012	1.000	0.000	0.000	0.000	0.000	0.000	0.000	0.000	
13	0.007	0.005	0.007	0.008	0.001	0.002	0.002	0.001	0.001	-0.007	-0.015	0.000	1.000	0.000	0.000	0.000	0.000	0.000	0.000	
14	0.002	-0.005	-0.005	-0.005	-0.005	-0.001	0.001	0.003	0.004	-0.003	0.000	0.000	1.000	0.000	0.000	0.000	0.000	0.000	0.000	
15	-0.003	-0.010	-0.010	-0.011	-0.008	-0.002	0.001	0.006	0.008	0.003	0.000	0.000	1.000	0.000	0.000	0.000	0.000	0.000	0.000	
16	-0.002	-0.009	-0.010	-0.008	-0.006	-0.000	0.003	0.006	0.008	0.004	0.000	0.000	1.000	0.000	0.000	0.000	0.000	0.000	0.000	
17	-0.004	-0.005	-0.007	-0.005	-0.003	0.000	0.002	0.003	0.005	-0.001	0.000	0.000	0.000	1.000	0.000	0.000	0.000	0.000	0.000	
18	-0.006	-0.002	-0.003	-0.001	0.002	0.002	0.003	0.009	0.004	-0.002	0.000	0.000	0.000	0.000	1.000	0.000	0.000	0.000	0.000	
19	-0.003	0.003	0.004	0.008	0.009	0.003	0.004	0.004	-0.005	-0.009	0.000	0.000	0.000	0.000	0.000	1.000	0.000	0.000	0.000	
20	0.007	0.019	0.028	0.030	0.024	0.010	0.001	-0.011	-0.025	-0.025	0.000	0.000	0.000	0.000	0.000	0.000	0.000	0.000	0.000	

Table A.12: Statistical uncertainty correlation matrix for the electron mode [6].

Bin	21	22	23	24	25	26	27	28	29	30	31	32	33	34	35	36	37	38	39	40	
1	0.022	0.019	0.017	0.015	0.006	-0.006	-0.015	-0.023	-0.024	-0.026	-0.003	0.004	0.001	-0.001	-0.001	0.000	0.007	0.004	-0.001		
2	0.009	0.021	0.027	0.028	0.023	0.006	-0.008	-0.029	-0.042	-0.046	-0.004	0.004	0.006	0.001	-0.002	0.001	0.004	0.006	0.007	-0.006	
3	0.002	0.013	0.018	0.024	0.023	0.020	0.008	-0.010	-0.038	-0.054	-0.004	0.001	0.008	0.006	0.003	-0.003	0.004	0.006	0.006	0.002	-0.001
4	-0.001	0.006	0.006	0.018	0.020	0.021	0.016	0.002	-0.020	-0.050	-0.004	0.005	0.004	0.005	0.001	0.003	0.003	0.009	0.003	-0.003	-0.003
5	-0.003	0.001	0.001	0.009	0.010	0.014	0.011	0.006	-0.004	-0.024	-0.001	0.000	0.004	0.002	0.000	0.003	0.003	0.004	0.005	0.005	-0.001
6	-0.004	-0.005	0.004	0.001	0.001	0.007	0.007	0.009	0.005	-0.001	0.000	0.001	0.002	0.001	0.002	0.003	0.004	0.002	0.000	0.000	0.002
7	-0.003	-0.003	-0.001	-0.005	-0.003	-0.001	-0.002	0.007	0.014	0.016	0.005	-0.001	0.003	-0.002	-0.000	0.003	0.003	0.000	-0.001	0.001	0.001
8	0.001	-0.006	-0.007	-0.012	-0.011	-0.010	-0.001	0.007	0.023	0.034	0.001	0.001	-0.002	0.002	0.004	0.001	-0.002	-0.005	0.002	0.002	0.006
9	0.004	-0.006	-0.011	-0.017	-0.019	-0.018	-0.009	0.000	0.019	0.046	0.003	-0.002	-0.005	-0.001	-0.003	-0.002	-0.004	-0.006	-0.002	0.002	
10	0.004	-0.004	-0.015	-0.020	-0.023	-0.024	-0.017	-0.004	0.010	0.030	-0.002	-0.007	-0.009	-0.009	-0.005	-0.004	-0.008	-0.008	-0.008	-0.005	-0.005
11	-0.003	0.000	0.005	0.008	0.008	0.007	0.000	-0.001	-0.006	-0.011	0.005	0.004	0.002	-0.003	-0.006	-0.006	-0.003	0.003	0.005	0.006	0.006
12	0.005	0.003	0.002	0.002	-0.000	0.001	-0.000	-0.002	-0.004	-0.005	0.003	0.003	0.002	-0.000	-0.005	-0.003	0.000	0.001	0.003	0.002	
13	0.012	0.006	-0.001	-0.005	-0.007	-0.009	-0.007	-0.005	-0.002	-0.001	0.000	0.003	0.002	-0.004	-0.005	-0.006	-0.002	0.001	0.003	0.000	
14	0.019	0.007	-0.004	-0.010	-0.017	-0.015	-0.012	-0.005	0.001	0.011	0.001	-0.000	0.001	-0.001	-0.004	-0.006	-0.005	0.001	-0.000	-0.000	-0.000
15	0.017	0.006	-0.004	-0.012	-0.016	-0.019	-0.013	-0.005	0.009	0.015	-0.002	-0.002	-0.001	-0.002	-0.004	-0.001	-0.000	0.002	-0.000	-0.000	-0.004
16	0.015	0.004	-0.004	-0.012	-0.013	-0.013	-0.009	-0.001	0.008	0.015	-0.002	-0.000	0.003	-0.001	-0.002	-0.000	-0.000	0.002	-0.000	-0.000	-0.003
17	0.007	0.002	-0.001	-0.003	-0.008	-0.008	-0.004	-0.002	0.001	0.006	-0.003	-0.002	-0.001	0.001	0.001	0.002	0.002	-0.001	-0.003	-0.003	-0.003
18	-0.004	-0.001	-0.001	0.001	0.005	0.004	0.004	0.006	0.001	0.001	-0.004	-0.002	0.000	0.003	0.006	0.006	0.004	-0.002	0.001	0.001	0.001
19	-0.026	-0.007	0.004	0.015	0.021	0.020	0.015	0.006	-0.006	-0.013	-0.003	-0.002	-0.001	0.003	0.008	0.008	0.005	0.001	-0.005	0.001	0.001
20	-0.057	-0.019	0.013	0.035	0.046	0.051	0.031	0.010	-0.015	-0.040	0.006	-0.001	-0.002	0.003	0.009	0.011	0.003	-0.005	-0.002	0.004	0.004

Table A.13: Statistical uncertainty correlation matrix for the electron mode [6].

Bin	1	2	3	4	5	6	7	8	9	10	11	12	13	14	15	16	17	18	19	20
21	0.022	0.009	0.002	-0.001	-0.003	-0.004	0.001	0.004	0.004	-0.003	0.005	0.012	0.019	0.017	0.015	0.007	-0.004	-0.026	-0.057	
22	0.019	0.021	0.013	0.006	0.001	-0.005	-0.003	-0.006	-0.006	-0.004	0.000	0.003	0.006	0.007	0.006	0.004	0.002	-0.001	-0.007	-0.019
23	0.017	0.027	0.018	0.006	0.001	0.004	-0.001	-0.007	-0.011	-0.015	0.005	0.002	-0.001	-0.004	-0.004	-0.004	-0.001	-0.001	0.004	0.013
24	0.015	0.028	0.024	0.018	0.009	0.001	-0.005	-0.012	-0.017	-0.020	0.008	0.002	-0.005	-0.010	-0.012	-0.012	-0.003	0.001	0.015	0.035
25	0.006	0.023	0.023	0.020	0.010	0.001	-0.003	-0.011	-0.019	-0.023	0.008	-0.000	-0.007	-0.017	-0.016	-0.013	-0.008	0.005	0.005	0.046
26	-0.006	0.006	0.020	0.021	0.014	0.007	-0.001	-0.010	-0.018	-0.024	0.007	0.001	-0.009	-0.015	-0.019	-0.013	-0.008	0.004	0.020	0.051
27	-0.015	-0.008	0.008	0.016	0.011	0.007	-0.002	-0.001	-0.009	-0.017	0.000	-0.000	-0.007	-0.012	-0.013	-0.009	-0.004	0.004	0.015	0.031
28	-0.023	-0.029	-0.010	0.002	0.006	0.009	0.007	0.007	0.000	-0.004	-0.001	-0.002	-0.005	-0.005	-0.005	-0.005	-0.002	0.006	0.006	0.010
29	-0.024	-0.042	-0.038	-0.020	-0.004	0.005	0.014	0.023	0.019	0.010	-0.006	-0.004	-0.002	0.001	0.009	0.008	0.001	0.001	-0.006	-0.015
30	-0.026	-0.046	-0.054	-0.050	-0.024	-0.001	0.016	0.034	0.046	0.030	-0.011	-0.005	-0.001	0.011	0.015	0.015	0.006	0.001	-0.013	-0.040
31	-0.003	-0.004	-0.004	-0.001	0.000	0.005	0.001	0.003	0.003	-0.002	0.006	0.000	0.003	0.000	0.001	-0.002	-0.003	-0.004	-0.003	0.006
32	0.001	0.004	0.001	0.005	0.000	0.001	-0.001	0.001	-0.002	-0.007	0.003	0.003	-0.000	-0.000	-0.002	-0.002	-0.002	-0.002	-0.001	-0.001
33	0.004	0.006	0.008	0.004	0.004	0.002	0.003	-0.002	-0.005	-0.009	0.002	0.001	0.002	0.001	-0.001	0.003	-0.001	0.000	-0.001	-0.002
34	0.003	0.001	0.006	0.005	0.002	0.001	-0.002	0.002	-0.001	-0.009	-0.003	-0.000	-0.004	-0.001	-0.002	-0.001	0.001	0.003	0.003	0.003
35	-0.001	-0.002	0.003	0.001	0.000	0.002	-0.000	0.004	-0.003	-0.005	-0.006	-0.005	-0.004	-0.003	-0.002	0.001	0.006	0.008	0.009	0.009
36	-0.001	0.001	-0.003	0.003	0.003	0.003	0.003	0.003	0.001	-0.002	-0.004	-0.006	-0.003	-0.006	-0.001	-0.000	0.002	0.006	0.008	0.011
37	0.000	0.004	0.004	0.003	0.003	0.004	0.003	0.003	-0.002	-0.008	-0.003	0.000	-0.002	-0.005	-0.000	-0.000	0.002	0.004	0.005	0.003
38	0.007	0.006	0.006	0.009	0.004	0.002	0.000	-0.005	-0.004	-0.008	0.003	0.001	0.001	0.002	0.002	-0.001	-0.002	0.001	-0.005	-0.005
39	0.004	0.007	0.002	0.003	0.005	0.000	-0.001	0.002	-0.006	-0.008	0.005	0.003	0.003	-0.001	-0.000	-0.003	0.001	-0.004	-0.002	-0.002
40	-0.001	-0.006	-0.001	-0.003	-0.001	0.002	0.001	0.006	0.002	-0.005	0.006	0.002	0.000	-0.000	-0.004	-0.003	0.001	0.001	0.005	0.005

Table A.14: Statistical uncertainty correlation matrix for the electron mode [6].

Bin	21	22	23	24	25	26	27	28	29	30	31	32	33	34	35	36	37	38	39	40
21	1.000	0.000	0.000	0.000	0.000	0.000	0.000	0.000	0.000	-0.002	-0.009	-0.007	0.005	0.016	0.018	0.009	-0.006	-0.006	-0.004	
22	0.000	1.000	0.000	0.000	0.000	0.000	0.000	0.000	0.000	-0.014	-0.009	0.001	0.008	0.020	0.019	0.009	-0.001	-0.010	-0.016	
23	0.000	0.000	1.000	0.000	0.000	0.000	0.000	0.000	0.000	-0.019	-0.010	0.001	0.010	0.016	0.017	0.011	0.004	-0.009	-0.018	
24	0.000	0.000	0.000	1.000	0.000	0.000	0.000	0.000	0.000	-0.016	-0.005	0.005	0.011	0.006	0.009	0.006	0.005	-0.005	-0.015	
25	0.000	0.000	0.000	0.000	1.000	0.000	0.000	0.000	0.000	-0.009	0.003	0.004	0.002	-0.006	-0.003	0.003	0.007	-0.001	-0.008	
26	0.000	0.000	0.000	0.000	0.000	1.000	0.000	0.000	0.000	0.002	0.005	0.007	-0.005	-0.011	-0.014	-0.005	0.003	0.006	0.001	
27	0.000	0.000	0.000	0.000	0.000	0.000	1.000	0.000	0.000	0.011	0.008	0.003	-0.009	-0.019	-0.019	-0.009	0.002	0.009	0.013	
28	0.000	0.000	0.000	0.000	0.000	0.000	0.000	1.000	0.000	0.000	0.019	0.010	-0.001	-0.014	-0.021	-0.020	-0.012	0.002	0.012	
29	0.000	0.000	0.000	0.000	0.000	0.000	0.000	0.000	1.000	0.000	0.021	0.011	-0.002	-0.012	-0.017	-0.018	-0.013	-0.004	0.009	
30	0.000	0.000	0.000	0.000	0.000	0.000	0.000	0.000	0.000	1.000	0.019	0.005	-0.005	-0.008	-0.009	-0.009	-0.008	-0.007	0.006	
31	-0.002	-0.014	-0.019	-0.016	-0.009	0.002	0.011	0.019	0.021	0.019	1.000	0.000	0.000	0.000	0.000	0.000	0.000	0.000	0.018	
32	-0.009	-0.009	-0.010	-0.005	0.003	0.005	0.008	0.010	0.011	0.005	0.000	1.000	0.000	0.000	0.000	0.000	0.000	0.000	0.000	
33	-0.007	0.001	0.001	0.005	0.004	0.007	0.003	-0.001	-0.002	-0.005	0.000	0.000	1.000	0.000	0.000	0.000	0.000	0.000	0.000	
34	0.005	0.008	0.010	0.011	0.002	-0.005	-0.009	-0.014	-0.012	-0.008	0.000	0.000	0.000	1.000	0.000	0.000	0.000	0.000	0.000	
35	0.016	0.020	0.016	0.006	-0.006	-0.011	-0.019	-0.021	-0.017	-0.009	0.000	0.000	0.000	1.000	0.000	0.000	0.000	0.000	0.000	
36	0.018	0.019	0.017	0.009	-0.003	-0.014	-0.019	-0.020	-0.018	-0.009	0.000	0.000	0.000	0.000	1.000	0.000	0.000	0.000	0.000	
37	0.009	0.009	0.011	0.006	0.003	-0.005	-0.009	-0.012	-0.013	-0.008	0.000	0.000	0.000	0.000	1.000	0.000	0.000	0.000	0.000	
38	-0.006	-0.001	0.004	0.005	0.007	0.003	0.002	0.002	-0.004	-0.007	0.000	0.000	0.000	0.000	1.000	0.000	0.000	0.000	0.000	
39	-0.006	-0.010	-0.009	-0.005	-0.001	0.006	0.009	0.012	0.009	0.006	0.000	0.000	0.000	0.000	0.000	1.000	0.000	0.000	0.000	
40	-0.004	-0.016	-0.018	-0.015	-0.008	0.001	0.013	0.022	0.023	0.018	0.000	0.000	0.000	0.000	0.000	0.000	0.000	0.000	1.000	

Table A.15: Statistical uncertainty correlation matrix for the muon mode [6].

Bin	1	2	3	4	5	6	7	8	9	10	11	12	13	14	15	16	17	18	19	20
1	1.000	0.000	0.000	0.000	0.000	0.000	0.000	0.000	0.000	0.020	0.014	0.005	0.002	-0.003	-0.006	-0.004	-0.001	0.006		
2	0.000	1.000	0.000	0.000	0.000	0.000	0.000	0.000	0.000	0.034	0.022	0.009	-0.005	-0.007	-0.009	-0.003	-0.000	0.018		
3	0.000	0.000	1.000	0.000	0.000	0.000	0.000	0.000	0.000	0.029	0.019	0.009	-0.004	-0.010	-0.010	-0.007	-0.001	0.007	0.022	
4	0.000	0.000	0.000	1.000	0.000	0.000	0.000	0.000	0.000	0.026	0.016	0.004	-0.003	-0.010	-0.008	-0.005	-0.003	0.009	0.027	
5	0.000	0.000	0.000	0.000	1.000	0.000	0.000	0.000	0.000	0.014	0.012	0.002	-0.004	-0.007	-0.005	-0.001	0.001	0.009	0.023	
6	0.000	0.000	0.000	0.000	0.000	1.000	0.000	0.000	0.000	0.010	0.009	0.001	-0.001	-0.003	-0.001	0.000	0.007	0.005	0.013	
7	0.000	0.000	0.000	0.000	0.000	0.000	1.000	0.000	0.000	0.020	-0.004	0.004	-0.000	0.001	0.003	0.007	0.007	0.000		
8	0.000	0.000	0.000	0.000	0.000	0.000	0.000	1.000	0.000	0.000	-0.019	-0.018	-0.001	0.000	0.005	0.007	0.008	0.002	-0.008	
9	0.000	0.000	0.000	0.000	0.000	0.000	0.000	0.000	1.000	0.000	-0.016	-0.021	-0.010	0.002	0.005	0.007	0.006	0.007	-0.003	
10	0.000	0.000	0.000	0.000	0.000	0.000	0.000	0.000	0.000	1.000	-0.012	-0.014	-0.015	-0.005	-0.001	0.003	-0.001	-0.008	-0.022	
11	0.020	0.034	0.029	0.026	0.014	0.014	-0.010	-0.020	-0.019	-0.016	-0.012	1.000	0.000	0.000	0.000	0.000	0.000	0.000	0.000	
12	0.014	0.022	0.019	0.016	0.012	0.009	-0.004	-0.018	-0.018	-0.021	-0.014	0.000	1.000	0.000	0.000	0.000	0.000	0.000	0.000	
13	0.005	0.009	0.009	0.004	0.002	0.001	0.004	-0.001	-0.001	-0.010	-0.015	0.000	0.000	1.000	0.000	0.000	0.000	0.000	0.000	
14	0.002	-0.005	-0.005	-0.004	-0.003	-0.004	-0.001	-0.000	-0.000	-0.002	-0.005	0.000	0.000	1.000	0.000	0.000	0.000	0.000	0.000	
15	-0.003	-0.007	-0.010	-0.007	-0.003	0.001	0.005	0.005	-0.001	0.000	0.000	0.000	0.000	1.000	0.000	0.000	0.000	0.000	0.000	
16	-0.003	-0.009	-0.010	-0.008	-0.005	-0.001	0.003	0.007	0.007	0.003	0.000	0.000	0.000	1.000	0.000	0.000	0.000	0.000	0.000	
17	-0.006	-0.009	-0.007	-0.005	-0.001	0.000	0.003	0.008	0.006	0.003	0.000	0.000	0.000	1.000	0.000	0.000	0.000	0.000	0.000	
18	-0.004	-0.003	-0.001	-0.003	0.001	0.007	0.007	0.006	0.007	-0.001	0.000	0.000	0.000	0.000	1.000	0.000	0.000	0.000	0.000	
19	-0.001	-0.000	0.007	0.009	0.005	0.005	0.007	0.002	-0.003	-0.008	0.000	0.000	0.000	0.000	1.000	0.000	0.000	0.000	0.000	
20	0.006	0.018	0.022	0.027	0.023	0.013	0.000	-0.008	-0.022	-0.022	0.000	0.000	0.000	0.000	0.000	1.000	0.000	0.000	0.000	

Table A.16: Statistical uncertainty correlation matrix for the muon mode [6].

Bin	21	22	23	24	25	26	27	28	29	30	31	32	33	34	35	36	37	38	39	40
1	0.019	0.023	0.015	0.012	0.009	-0.006	-0.017	-0.020	-0.023	-0.024	-0.002	0.006	0.002	-0.002	-0.002	0.005	0.005	0.002	-0.003	
2	0.012	0.019	0.022	0.026	0.020	0.011	-0.009	-0.024	-0.039	-0.043	-0.004	0.001	0.005	0.004	0.004	0.006	0.006	-0.006	-0.003	
3	0.002	0.013	0.018	0.023	0.021	0.021	0.006	-0.013	-0.035	-0.050	-0.003	0.001	0.006	0.004	0.006	0.007	0.006	0.002	-0.005	
4	-0.001	0.004	0.013	0.018	0.018	0.017	0.012	0.001	-0.018	-0.042	-0.002	0.002	0.006	0.009	0.003	0.001	0.005	0.007	-0.000	-0.004
5	-0.004	0.000	0.003	0.009	0.010	0.014	0.014	0.007	-0.004	-0.020	-0.001	0.002	0.006	0.004	0.001	0.002	0.003	0.004	0.003	-0.000
6	-0.005	-0.002	0.000	0.001	0.006	0.008	0.008	0.007	-0.003	0.004	0.004	0.004	0.001	0.002	0.002	0.002	0.002	-0.001	0.001	
7	0.000	-0.004	-0.005	-0.005	-0.005	-0.003	0.001	0.007	0.014	0.017	0.003	0.001	0.002	0.001	-0.001	-0.002	0.000	0.001	0.002	0.003
8	0.001	-0.006	-0.007	-0.012	-0.011	-0.011	-0.003	0.005	0.020	0.033	0.002	-0.001	-0.004	-0.002	-0.001	0.003	-0.002	0.002	-0.000	0.003
9	0.003	-0.004	-0.012	-0.018	-0.020	-0.017	-0.011	0.000	0.017	0.039	-0.000	-0.004	-0.004	-0.007	-0.001	-0.004	-0.005	-0.003	0.002	
10	0.001	-0.004	-0.012	-0.022	-0.022	-0.014	-0.007	0.010	0.032	-0.006	-0.005	-0.007	-0.008	-0.005	-0.005	-0.008	-0.009	-0.006	-0.003	
11	-0.004	0.003	0.004	0.005	0.007	0.004	0.000	-0.004	-0.005	-0.011	0.000	0.001	0.001	0.000	0.000	-0.001	-0.002	0.001	0.001	
12	0.005	0.001	0.003	0.004	0.003	0.000	-0.001	-0.003	-0.004	-0.009	0.001	0.002	0.001	0.002	-0.004	-0.004	-0.000	0.002	0.003	
13	0.012	0.005	-0.001	-0.005	-0.008	-0.007	-0.007	-0.004	-0.002	-0.003	-0.002	0.001	0.001	-0.004	-0.006	-0.002	0.003	0.000	0.001	
14	0.014	0.004	-0.004	-0.011	-0.014	-0.014	-0.009	-0.005	-0.000	0.006	-0.002	-0.002	-0.000	-0.003	-0.007	-0.006	-0.002	-0.001	-0.001	
15	0.014	0.006	-0.005	-0.014	-0.016	-0.018	-0.011	-0.003	0.004	0.013	-0.003	-0.001	0.001	-0.003	-0.006	-0.007	-0.003	-0.000	0.001	
16	0.013	0.005	-0.003	-0.010	-0.015	-0.013	-0.009	-0.002	0.006	0.014	-0.002	0.002	0.002	0.001	-0.002	-0.003	0.001	-0.000	-0.004	
17	0.008	0.004	-0.002	-0.007	-0.009	-0.005	0.001	0.005	0.014	-0.003	0.001	0.001	0.003	0.001	0.003	0.001	0.001	-0.002	-0.001	
18	-0.001	-0.000	0.003	0.002	0.006	0.004	0.006	0.002	0.003	0.003	0.001	-0.001	0.000	0.002	0.000	0.005	0.005	0.002	0.004	
19	-0.024	-0.007	0.007	0.015	0.023	0.023	0.019	0.002	-0.006	-0.013	0.001	-0.002	0.002	0.000	0.014	0.009	0.003	0.003	-0.004	
20	-0.051	-0.019	0.013	0.041	0.043	0.051	0.029	0.008	-0.016	-0.037	0.008	-0.001	-0.006	0.003	0.010	0.014	0.006	-0.003	-0.003	

Table A.17: Statistical uncertainty correlation matrix for the muon mode [6].

Bin	1	2	3	4	5	6	7	8	9	10	11	12	13	14	15	16	17	18	19	20
21	0.019	0.012	0.002	-0.001	-0.004	-0.005	0.000	0.001	0.003	0.001	-0.004	0.005	0.012	0.014	0.013	0.008	-0.001	-0.024	-0.051	
22	0.023	0.019	0.013	0.004	0.000	-0.002	-0.004	-0.006	-0.004	-0.004	0.003	0.001	0.005	0.004	0.006	0.005	0.004	-0.000	-0.007	-0.019
23	0.015	0.022	0.018	0.013	0.003	0.000	-0.005	-0.007	-0.007	-0.012	-0.012	0.004	0.003	-0.001	-0.004	-0.005	-0.003	-0.002	0.003	0.013
24	0.012	0.026	0.023	0.018	0.009	0.000	-0.005	-0.012	-0.018	-0.022	-0.022	0.005	0.004	-0.005	-0.011	-0.014	-0.010	-0.007	0.002	0.015
25	0.009	0.020	0.021	0.018	0.010	0.001	-0.005	-0.011	-0.020	-0.022	-0.022	0.007	0.003	-0.008	-0.014	-0.016	-0.015	-0.009	0.006	0.023
26	-0.006	0.011	0.021	0.017	0.014	0.006	-0.003	-0.011	-0.017	-0.022	-0.022	0.004	0.000	-0.007	-0.014	-0.018	-0.013	-0.009	0.004	0.023
27	-0.017	-0.009	0.006	0.012	0.014	0.008	0.001	-0.003	-0.011	-0.014	-0.000	-0.001	-0.007	-0.009	-0.011	-0.009	-0.005	0.006	0.019	0.029
28	-0.020	-0.024	-0.013	0.001	0.007	0.008	0.007	0.005	0.000	-0.007	-0.004	-0.003	-0.003	-0.004	-0.005	-0.005	-0.003	-0.002	0.002	0.008
29	-0.023	-0.039	-0.035	-0.018	-0.004	0.007	0.014	0.020	0.017	0.010	-0.005	-0.004	-0.002	-0.000	-0.004	-0.006	0.005	0.003	-0.006	-0.016
30	-0.024	-0.043	-0.043	-0.050	-0.042	-0.020	-0.003	-0.020	-0.017	0.033	0.039	0.032	-0.011	-0.009	-0.003	0.006	0.013	0.014	0.014	-0.013
31	-0.002	-0.004	-0.003	-0.002	-0.001	0.004	0.003	0.002	-0.000	-0.006	0.009	0.000	-0.003	-0.003	-0.004	-0.003	-0.003	-0.001	0.001	0.008
32	0.002	0.001	0.001	0.002	0.002	0.004	0.001	-0.001	-0.004	-0.005	-0.000	0.010	-0.001	-0.003	-0.002	0.001	0.000	-0.000	-0.002	-0.001
33	0.006	0.004	0.006	0.006	0.006	0.001	0.002	-0.004	-0.004	-0.007	-0.000	0.000	0.006	-0.001	0.000	0.001	0.002	0.002	-0.006	-0.006
34	0.002	0.005	0.004	0.009	0.004	0.001	0.001	-0.002	-0.007	-0.008	-0.002	0.001	-0.002	-0.003	0.001	0.003	-0.001	0.000	0.000	0.003
35	-0.002	0.001	0.006	0.003	0.001	0.002	-0.001	-0.001	-0.002	-0.005	-0.001	-0.005	-0.005	-0.008	-0.002	-0.003	0.000	0.005	0.013	0.010
36	-0.002	0.000	-0.000	0.001	0.001	0.002	0.002	-0.002	0.003	-0.001	-0.005	-0.003	-0.005	-0.007	-0.007	0.001	0.002	0.005	0.009	0.013
37	0.005	0.006	0.007	0.005	0.005	0.003	0.002	0.000	-0.002	-0.004	-0.008	-0.003	-0.002	-0.003	-0.003	0.001	0.006	0.004	0.002	0.005
38	0.005	0.004	0.006	0.007	0.004	0.002	0.001	0.002	-0.005	-0.009	-0.001	0.001	0.002	-0.002	-0.001	-0.001	0.000	0.008	0.002	-0.003
39	0.002	0.006	0.002	-0.000	0.003	-0.001	0.001	0.002	-0.000	-0.003	-0.006	-0.000	0.002	-0.001	-0.000	-0.003	0.004	0.003	-0.003	-0.003
40	-0.003	-0.003	-0.005	-0.004	-0.000	0.001	0.003	0.003	0.002	-0.003	-0.001	0.001	0.001	-0.000	-0.003	-0.004	-0.002	0.000	-0.001	0.014

Table A.18: Statistical uncertainty correlation matrix for the muon mode [6].

Bin	21	22	23	24	25	26	27	28	29	30	31	32	33	34	35	36	37	38	39	40
21	1.000	0.000	0.000	0.000	0.000	0.000	0.000	0.000	0.000	-0.006	-0.007	-0.004	0.005	0.017	0.017	0.003	-0.005	-0.005	-0.001	
22	0.000	1.000	0.000	0.000	0.000	0.000	0.000	0.000	0.000	-0.014	-0.011	-0.000	0.010	0.018	0.021	0.012	0.001	-0.009	-0.016	
23	0.000	0.000	1.000	0.000	0.000	0.000	0.000	0.000	0.000	-0.018	-0.009	0.004	0.009	0.017	0.018	0.011	0.003	-0.011	-0.018	
24	0.000	0.000	0.000	1.000	0.000	0.000	0.000	0.000	0.000	-0.016	-0.006	0.006	0.009	0.004	0.005	0.009	0.004	-0.004	-0.016	
25	0.000	0.000	0.000	0.000	1.000	0.000	0.000	0.000	0.000	-0.010	-0.002	0.005	0.005	-0.004	-0.004	0.001	0.007	-0.001	-0.007	
26	0.000	0.000	0.000	0.000	0.000	1.000	0.000	0.000	0.000	0.005	0.005	0.007	0.007	-0.013	-0.015	-0.003	0.003	0.005	-0.000	
27	0.000	0.000	0.000	0.000	0.000	0.000	1.000	0.000	0.000	0.011	0.010	0.010	0.001	-0.008	-0.019	-0.007	0.004	0.010	0.011	
28	0.000	0.000	0.000	0.000	0.000	0.000	0.000	1.000	0.000	0.000	0.018	0.011	-0.000	-0.015	-0.018	-0.022	-0.013	-0.002	0.009	
29	0.000	0.000	0.000	0.000	0.000	0.000	0.000	0.000	1.000	0.000	0.022	0.014	-0.005	-0.015	-0.019	-0.015	-0.002	0.011	0.022	
30	0.000	0.000	0.000	0.000	0.000	0.000	0.000	0.000	0.000	1.000	0.017	0.006	-0.004	-0.009	-0.008	-0.012	-0.008	-0.005	0.005	
31	-0.006	-0.014	-0.018	-0.016	-0.010	0.005	0.011	0.018	0.022	0.018	1.000	0.000	0.000	0.000	0.000	0.000	0.000	0.000	0.018	
32	-0.008	-0.011	-0.009	-0.006	-0.002	0.007	0.010	0.011	0.015	0.006	0.000	1.000	0.000	0.000	0.000	0.000	0.000	0.000	0.000	
33	-0.004	-0.000	0.003	0.006	0.005	0.007	0.001	0.000	-0.005	-0.004	0.000	0.000	1.000	0.000	0.000	0.000	0.000	0.000	0.000	
34	0.005	0.010	0.009	0.009	0.005	-0.003	-0.008	-0.015	-0.014	-0.008	0.000	0.000	0.000	1.000	0.000	0.000	0.000	0.000	0.000	
35	0.017	0.018	0.017	0.004	-0.003	-0.012	-0.019	-0.018	-0.019	-0.008	0.000	0.000	0.000	1.000	0.000	0.000	0.000	0.000	0.000	
36	0.017	0.021	0.018	0.005	-0.004	-0.015	-0.019	-0.021	-0.019	-0.011	0.000	0.000	0.000	0.000	1.000	0.000	0.000	0.000	0.000	
37	0.003	0.012	0.011	0.009	0.001	-0.002	-0.007	-0.013	-0.014	-0.008	0.000	0.000	0.000	0.000	1.000	0.000	0.000	0.000	0.000	
38	-0.005	0.000	0.003	0.004	0.007	0.003	0.004	-0.004	-0.002	-0.005	0.000	0.000	0.000	0.000	1.000	0.000	0.000	0.000	0.000	
39	-0.005	-0.009	-0.011	-0.004	-0.000	0.005	0.010	0.009	0.011	0.005	0.000	0.000	0.000	0.000	0.000	1.000	0.000	0.000	0.000	
40	-0.002	-0.016	-0.018	-0.016	-0.007	-0.000	0.012	0.020	0.022	0.018	0.000	0.000	0.000	0.000	0.000	0.000	0.000	0.000	1.000	

Table A.19: Systematic uncertainty correlation matrix [6].

Bin	1	2	3	4	5	6	7	8	9	10	11	12	13	14	15	16	17	18	19	20
1	1.000	0.872	0.755	0.682	0.656	0.612	0.555	0.500	0.487	0.409	0.786	0.699	0.633	0.621	0.623	0.628	0.630	0.640	0.653	0.662
2	0.872	1.000	0.955	0.899	0.878	0.850	0.819	0.779	0.763	0.680	0.934	0.891	0.855	0.857	0.865	0.872	0.872	0.879	0.889	0.896
3	0.755	0.955	1.000	0.978	0.957	0.936	0.917	0.891	0.885	0.819	0.952	0.946	0.933	0.943	0.951	0.957	0.957	0.963	0.969	0.974
4	0.682	0.899	0.978	1.000	0.985	0.967	0.952	0.943	0.931	0.854	0.934	0.950	0.952	0.959	0.968	0.977	0.979	0.984	0.986	0.990
5	0.656	0.878	0.957	0.985	1.000	0.992	0.978	0.950	0.941	0.875	0.925	0.957	0.968	0.980	0.986	0.987	0.989	0.990	0.993	0.992
6	0.612	0.850	0.936	0.967	0.992	1.000	0.994	0.963	0.948	0.879	0.906	0.950	0.970	0.982	0.987	0.986	0.988	0.987	0.989	0.985
7	0.555	0.819	0.917	0.952	0.978	0.994	1.000	0.979	0.967	0.902	0.884	0.938	0.967	0.982	0.987	0.986	0.982	0.983	0.976	
8	0.500	0.779	0.891	0.943	0.950	0.963	0.979	1.000	0.991	0.922	0.858	0.918	0.951	0.963	0.969	0.973	0.971	0.968	0.963	0.956
9	0.487	0.763	0.885	0.931	0.941	0.948	0.967	0.991	1.000	0.961	0.838	0.904	0.941	0.965	0.971	0.973	0.969	0.965	0.958	0.951
10	0.409	0.680	0.819	0.854	0.875	0.879	0.902	0.922	0.961	1.000	0.755	0.840	0.885	0.928	0.929	0.922	0.912	0.905	0.896	0.887
11	0.786	0.934	0.952	0.934	0.925	0.906	0.884	0.858	0.838	0.755	1.000	0.983	0.952	0.927	0.915	0.906	0.902	0.907	0.918	0.919
12	0.699	0.891	0.946	0.950	0.957	0.950	0.938	0.918	0.904	0.840	0.983	1.000	0.991	0.972	0.959	0.947	0.941	0.941	0.950	0.945
13	0.633	0.855	0.933	0.952	0.968	0.970	0.967	0.951	0.941	0.885	0.952	0.991	1.000	0.989	0.978	0.966	0.961	0.958	0.964	0.956
14	0.621	0.857	0.943	0.959	0.980	0.982	0.982	0.963	0.965	0.928	0.927	0.972	0.989	1.000	0.997	0.989	0.984	0.981	0.983	0.977
15	0.623	0.865	0.951	0.968	0.986	0.987	0.987	0.969	0.971	0.929	0.915	0.959	0.978	0.997	1.000	0.997	0.994	0.992	0.993	0.988
16	0.628	0.872	0.957	0.977	0.987	0.986	0.986	0.973	0.973	0.922	0.906	0.947	0.966	0.989	0.997	1.000	0.999	0.998	0.997	0.995
17	0.630	0.872	0.957	0.979	0.989	0.988	0.986	0.971	0.969	0.912	0.902	0.941	0.961	0.984	0.994	0.999	1.000	0.999	0.999	0.996
18	0.640	0.879	0.963	0.984	0.990	0.987	0.982	0.968	0.965	0.905	0.907	0.941	0.958	0.981	0.992	0.998	0.999	1.000	0.999	0.998
19	0.653	0.889	0.969	0.986	0.993	0.989	0.983	0.963	0.958	0.896	0.918	0.950	0.964	0.983	0.993	0.997	0.999	1.000	0.999	0.999
20	0.662	0.896	0.974	0.990	0.992	0.985	0.976	0.956	0.951	0.887	0.919	0.945	0.956	0.977	0.988	0.995	0.996	0.998	0.999	1.000

Table A.20: Systematic uncertainty correlation matrix [6].

Bin	21	22	23	24	25	26	27	28	29	30	31	32	33	34	35	36	37	38	39	40
1	0.508	0.524	0.558	0.591	0.638	0.686	0.731	0.756	0.781	0.840	0.666	0.668	0.651	0.633	0.608	0.609	0.634	0.657	0.670	0.665
2	0.763	0.783	0.814	0.842	0.880	0.911	0.938	0.952	0.965	0.993	0.900	0.900	0.886	0.869	0.849	0.851	0.871	0.890	0.902	0.899
3	0.877	0.895	0.921	0.942	0.967	0.984	0.993	0.997	0.996	0.976	0.974	0.975	0.965	0.955	0.942	0.944	0.957	0.969	0.975	0.974
4	0.919	0.938	0.963	0.982	0.992	0.996	0.991	0.979	0.968	0.925	0.989	0.989	0.981	0.975	0.968	0.970	0.978	0.985	0.985	0.989
5	0.954	0.967	0.983	0.991	0.990	0.988	0.982	0.968	0.956	0.912	0.991	0.992	0.993	0.990	0.987	0.987	0.992	0.990	0.990	0.990
6	0.970	0.981	0.990	0.991	0.981	0.973	0.964	0.947	0.936	0.887	0.984	0.985	0.991	0.990	0.990	0.991	0.992	0.986	0.984	0.984
7	0.983	0.991	0.994	0.989	0.973	0.960	0.946	0.928	0.915	0.861	0.977	0.978	0.986	0.988	0.991	0.991	0.992	0.989	0.981	0.977
8	0.975	0.982	0.986	0.980	0.965	0.945	0.922	0.898	0.879	0.816	0.962	0.962	0.965	0.971	0.974	0.977	0.969	0.968	0.960	0.963
9	0.981	0.983	0.981	0.969	0.958	0.938	0.916	0.897	0.873	0.806	0.955	0.957	0.961	0.970	0.975	0.976	0.966	0.964	0.957	0.956
10	0.951	0.942	0.926	0.901	0.896	0.873	0.848	0.840	0.806	0.739	0.891	0.897	0.904	0.919	0.926	0.924	0.911	0.908	0.903	0.892
11	0.851	0.866	0.886	0.902	0.918	0.934	0.944	0.949	0.954	0.947	0.926	0.931	0.928	0.922	0.906	0.908	0.917	0.930	0.935	0.926
12	0.920	0.930	0.941	0.947	0.950	0.953	0.949	0.947	0.920	0.956	0.960	0.963	0.962	0.951	0.952	0.955	0.962	0.964	0.956	
13	0.958	0.964	0.968	0.961	0.957	0.950	0.941	0.934	0.894	0.968	0.971	0.978	0.978	0.972	0.973	0.972	0.974	0.974	0.969	
14	0.980	0.984	0.985	0.980	0.977	0.971	0.963	0.956	0.943	0.900	0.982	0.986	0.992	0.995	0.993	0.992	0.991	0.990	0.990	0.983
15	0.981	0.987	0.991	0.987	0.985	0.979	0.972	0.963	0.949	0.905	0.991	0.993	0.997	0.999	0.998	0.998	0.997	0.995	0.995	0.991
16	0.974	0.983	0.991	0.991	0.992	0.986	0.978	0.967	0.952	0.907	0.995	0.996	0.997	0.998	0.997	0.997	0.998	0.998	0.996	0.995
17	0.970	0.980	0.991	0.993	0.993	0.988	0.980	0.967	0.953	0.907	0.996	0.996	0.997	0.996	0.995	0.996	0.998	0.997	0.995	0.996
18	0.964	0.976	0.988	0.992	0.995	0.991	0.984	0.972	0.957	0.912	0.997	0.997	0.996	0.995	0.994	0.994	0.997	0.997	0.996	0.996
19	0.961	0.973	0.987	0.992	0.995	0.993	0.987	0.976	0.964	0.922	0.998	0.999	0.998	0.995	0.993	0.994	0.998	0.998	0.997	0.998
20	0.950	0.964	0.981	0.990	0.996	0.991	0.981	0.968	0.927	0.997	0.998	0.995	0.992	0.989	0.990	0.995	0.996	0.996	0.996	

Table A.21: Systematic uncertainty correlation matrix [6].

Bin	1	2	3	4	5	6	7	8	9	10	11	12	13	14	15	16	17	18	19	20
21	0.508	0.763	0.877	0.919	0.954	0.970	0.983	0.975	0.981	0.951	0.851	0.920	0.958	0.980	0.981	0.974	0.970	0.964	0.961	0.950
22	0.524	0.783	0.895	0.938	0.967	0.981	0.991	0.982	0.983	0.942	0.866	0.930	0.964	0.984	0.987	0.983	0.980	0.976	0.973	0.964
23	0.558	0.814	0.921	0.963	0.983	0.990	0.994	0.986	0.981	0.926	0.886	0.941	0.968	0.985	0.991	0.991	0.991	0.988	0.987	0.981
24	0.591	0.842	0.942	0.982	0.991	0.991	0.989	0.980	0.969	0.901	0.902	0.947	0.968	0.980	0.987	0.991	0.993	0.992	0.990	
25	0.638	0.880	0.967	0.992	0.990	0.981	0.973	0.965	0.958	0.896	0.918	0.950	0.961	0.977	0.985	0.992	0.993	0.995	0.995	0.996
26	0.686	0.911	0.984	0.996	0.988	0.973	0.960	0.945	0.938	0.873	0.934	0.953	0.957	0.971	0.979	0.986	0.988	0.991	0.993	0.996
27	0.731	0.938	0.993	0.991	0.982	0.964	0.946	0.922	0.916	0.848	0.944	0.953	0.950	0.963	0.972	0.978	0.980	0.984	0.987	0.991
28	0.756	0.952	0.997	0.979	0.968	0.947	0.928	0.898	0.897	0.840	0.949	0.949	0.941	0.956	0.963	0.967	0.967	0.972	0.976	0.981
29	0.781	0.965	0.996	0.968	0.956	0.936	0.915	0.879	0.873	0.806	0.954	0.947	0.934	0.943	0.949	0.952	0.953	0.957	0.964	0.968
30	0.840	0.993	0.976	0.925	0.912	0.887	0.861	0.816	0.806	0.739	0.947	0.920	0.894	0.900	0.905	0.907	0.907	0.912	0.922	0.927
31	0.666	0.900	0.974	0.989	0.991	0.984	0.977	0.962	0.955	0.891	0.926	0.956	0.968	0.982	0.991	0.995	0.996	0.997	0.998	0.997
32	0.668	0.900	0.975	0.989	0.992	0.985	0.978	0.962	0.957	0.897	0.931	0.960	0.971	0.986	0.993	0.996	0.996	0.997	0.999	0.998
33	0.651	0.886	0.965	0.981	0.993	0.991	0.986	0.965	0.961	0.904	0.928	0.963	0.978	0.992	0.997	0.997	0.997	0.996	0.998	0.995
34	0.633	0.869	0.955	0.975	0.990	0.990	0.988	0.971	0.970	0.919	0.922	0.962	0.978	0.995	0.999	0.998	0.996	0.995	0.995	0.992
35	0.608	0.849	0.942	0.968	0.987	0.990	0.991	0.974	0.975	0.926	0.906	0.951	0.972	0.993	0.998	0.997	0.995	0.994	0.993	0.989
36	0.609	0.851	0.944	0.970	0.987	0.991	0.992	0.977	0.976	0.924	0.908	0.952	0.973	0.992	0.998	0.997	0.996	0.994	0.994	0.990
37	0.634	0.871	0.957	0.978	0.992	0.992	0.989	0.969	0.966	0.911	0.917	0.955	0.972	0.991	0.997	0.998	0.998	0.997	0.998	0.995
38	0.657	0.890	0.969	0.985	0.990	0.986	0.981	0.968	0.964	0.908	0.930	0.962	0.974	0.990	0.995	0.998	0.997	0.998	0.998	0.996
39	0.670	0.902	0.975	0.985	0.990	0.984	0.977	0.960	0.957	0.903	0.935	0.964	0.974	0.990	0.995	0.996	0.996	0.997	0.997	0.996
40	0.665	0.899	0.974	0.989	0.990	0.984	0.977	0.963	0.956	0.892	0.926	0.956	0.969	0.983	0.991	0.995	0.996	0.996	0.998	0.996

Table A.22: Systematic uncertainty correlation matrix [6].

Bin	21	22	23	24	25	26	27	28	29	30	31	32	33	34	35	36	37	38	39	40
21	1.000	0.998	0.987	0.968	0.949	0.929	0.911	0.894	0.873	0.813	0.953	0.957	0.969	0.978	0.985	0.984	0.975	0.964	0.959	0.954
22	0.998	1.000	0.995	0.981	0.964	0.946	0.928	0.910	0.890	0.830	0.966	0.969	0.979	0.986	0.991	0.991	0.985	0.975	0.970	0.966
23	0.987	0.995	1.000	0.995	0.983	0.968	0.952	0.933	0.914	0.855	0.981	0.983	0.989	0.993	0.995	0.996	0.992	0.987	0.982	0.981
24	0.968	0.981	0.995	1.000	0.994	0.984	0.970	0.950	0.934	0.878	0.990	0.990	0.991	0.991	0.991	0.992	0.992	0.991	0.988	0.990
25	0.949	0.964	0.983	0.994	1.000	0.996	0.987	0.974	0.959	0.912	0.995	0.995	0.992	0.990	0.986	0.987	0.990	0.995	0.994	0.995
26	0.929	0.946	0.968	0.984	0.996	1.000	0.997	0.988	0.978	0.939	0.995	0.995	0.989	0.984	0.977	0.978	0.986	0.993	0.994	0.995
27	0.911	0.928	0.952	0.970	0.987	0.997	1.000	0.996	0.991	0.962	0.991	0.991	0.983	0.976	0.967	0.968	0.978	0.986	0.990	0.991
28	0.894	0.910	0.933	0.950	0.974	0.988	0.996	1.000	0.996	0.976	0.980	0.981	0.974	0.966	0.955	0.955	0.967	0.977	0.982	0.980
29	0.873	0.890	0.914	0.934	0.959	0.978	0.991	0.996	1.000	0.986	0.971	0.971	0.963	0.952	0.939	0.939	0.953	0.964	0.972	0.971
30	0.813	0.830	0.855	0.878	0.912	0.939	0.962	0.976	0.986	1.000	0.931	0.931	0.921	0.907	0.889	0.890	0.908	0.923	0.934	0.931
31	0.953	0.966	0.981	0.990	0.995	0.991	0.980	0.971	0.931	1.000	0.999	0.997	0.993	0.988	0.989	0.994	0.997	0.998	1.000	
32	0.957	0.969	0.983	0.990	0.995	0.995	0.991	0.981	0.971	0.931	0.999	1.000	0.998	0.995	0.991	0.992	0.996	0.999	0.999	
33	0.969	0.979	0.989	0.991	0.992	0.989	0.983	0.974	0.963	0.921	0.997	0.998	1.000	0.999	0.996	0.996	0.999	0.998	0.998	0.997
34	0.978	0.986	0.993	0.991	0.990	0.984	0.976	0.966	0.952	0.907	0.993	0.995	0.999	1.000	0.999	0.999	0.999	0.997	0.996	0.993
35	0.985	0.991	0.995	0.991	0.986	0.977	0.967	0.955	0.939	0.889	0.988	0.991	0.996	0.999	1.000	1.000	0.998	0.994	0.992	0.988
36	0.984	0.991	0.996	0.992	0.987	0.978	0.968	0.955	0.939	0.890	0.989	0.992	0.996	0.999	1.000	1.000	0.998	0.995	0.993	0.989
37	0.975	0.985	0.992	0.992	0.990	0.986	0.978	0.967	0.953	0.908	0.994	0.996	0.999	0.999	0.998	0.998	1.000	0.997	0.996	0.994
38	0.964	0.975	0.987	0.991	0.995	0.993	0.986	0.977	0.964	0.923	0.997	0.999	0.998	0.997	0.994	0.995	0.997	1.000	0.999	0.997
39	0.959	0.970	0.982	0.988	0.994	0.994	0.990	0.982	0.972	0.934	0.998	0.999	0.998	0.996	0.992	0.993	0.996	0.999	1.000	0.998
40	0.954	0.966	0.981	0.990	0.995	0.995	0.991	0.980	0.971	0.931	1.000	0.999	0.997	0.993	0.988	0.989	0.994	0.997	0.998	1.000

Appendix B

Fit Results

B.1 40 bin Fit

	e-mode	μ -mode	full sample
ρ^2	1.178 ± 0.048	1.155 ± 0.052	1.167 ± 0.036
$R_1(1)$	1.092 ± 0.039	1.292 ± 0.044	1.195 ± 0.030
$R_2(1)$	0.844 ± 0.030	0.848 ± 0.033	0.845 ± 0.023
$\mathcal{F}(1) V_{cb} \eta_{EW} \times 10^3$	36.22 ± 0.66	35.45 ± 0.66	35.63 ± 0.46
$\chi^2/\text{n.d.f.}$	$30.0 / 36.0$	$40.3 / 36.0$	$93.2 / 76.0$

Table B.1: Fit result of the 40 bin Fit to the CLN parametrization. The first two columns show the results for the electron and muon modes and the third column shows the results for the full sample. The statistical uncertainties are stated.

	ρ^2	$R_1(1)$	$R_2(1)$	$\mathcal{F}(1) V_{cb} \eta_{EW}$
ρ^2	+1.000	+0.529	-0.816	+0.311
$R_1(1)$		+1.000	-0.691	-0.164
$R_2(1)$			+1.000	-0.034
$\mathcal{F}(1) V_{cb} \eta_{EW}$				+1.000

Table B.2: Statistical correlation matrix of the 40 bin Fit for the electron mode in the CLN parametrization.

	ρ^2	$R_1(1)$	$R_2(1)$	$\mathcal{F}(1) V_{cb} \eta_{EW}$
ρ^2	+1.000	+0.558	-0.821	+0.307
$R_1(1)$		+1.000	-0.723	-0.163
$R_2(1)$			+1.000	-0.029
$\mathcal{F}(1) V_{cb} \eta_{EW}$				+1.000

Table B.3: Statistical correlation matrix of the 40 bin Fit for the muon mode in the CLN parametrization.

	ρ^2	$R_1(1)$	$R_2(1)$	$\mathcal{F}(1) V_{cb} \eta_{EW}$
ρ^2	+1.000	+0.526	-0.815	+0.311
$R_1(1)$		+1.000	-0.687	-0.163
$R_2(1)$			+1.000	-0.035
$\mathcal{F}(1) V_{cb} \eta_{EW}$				+1.000

Table B.4: Statistical correlation matrix of the 40 bin Fit for the full sample in the CLN parametrization.

B.2 37 bin Fit

	e-mode	μ -mode	full sample
ρ^2	1.178 ± 0.049	1.156 ± 0.052	1.168 ± 0.036
$R_1(1)$	1.125 ± 0.049	1.334 ± 0.053	1.234 ± 0.037
$R_2(1)$	0.841 ± 0.032	0.850 ± 0.035	0.844 ± 0.024
$\mathcal{F}(1) V_{cb} \eta_{EW} \times 10^3$	36.12 ± 0.67	35.46 ± 0.67	35.65 ± 0.47
$\chi^2/\text{n.d.f.}$	28.5 / 33.0	37.3 / 33.0	80.3 / 70.0

Table B.5: Fit result of the 37 bin Fit to the CLN parametrization. The first two columns show the results for the electron and muon modes and the third column shows the results for the full sample. The statistical uncertainties are stated.

	ρ^2	$R_1(1)$	$R_2(1)$	$\mathcal{F}(1) V_{cb} \eta_{EW}$
ρ^2	+1.000	+0.424	-0.785	+0.296
$R_1(1)$		+1.000	-0.573	-0.215
$R_2(1)$			+1.000	+0.023
$\mathcal{F}(1) V_{cb} \eta_{EW}$				+1.000

Table B.6: Statistical correlation matrix of the 37 bin Fit for the electron mode in the CLN parametrization.

	ρ^2	$R_1(1)$	$R_2(1)$	$\mathcal{F}(1) V_{cb} \eta_{EW}$
ρ^2	+1.000	+0.498	-0.800	+0.284
$R_1(1)$		+1.000	-0.650	-0.210
$R_2(1)$			+1.000	+0.031
$\mathcal{F}(1) V_{cb} \eta_{EW}$				+1.000

Table B.7: Statistical correlation matrix of the 37 bin Fit for the muon mode in the CLN parametrization.

	ρ^2	$R_1(1)$	$R_2(1)$	$\mathcal{F}(1) V_{cb} \eta_{EW}$
ρ^2	+1.000	+0.463	-0.792	+0.290
$R_1(1)$		+1.000	-0.615	-0.214
$R_2(1)$			+1.000	+0.028
$\mathcal{F}(1) V_{cb} \eta_{EW}$				+1.000

Table B.8: Statistical correlation matrix of the 37 bin Fit for the full sample in the CLN parametrization.

B.3 40 Bin Fit using only the statistical uncertainties

	e-mode	μ -mode	full sample
ρ^2	1.065 ± 0.042	1.107 ± 0.052	1.087 ± 0.030
$R_1(1)$	1.088 ± 0.036	1.294 ± 0.044	1.190 ± 0.027
$R_2(1)$	0.867 ± 0.027	0.859 ± 0.033	0.863 ± 0.020
$\mathcal{F}(1) V_{cb} \eta_{EW} \times 10^3$	35.62 ± 0.21	35.48 ± 0.22	35.57 ± 0.15
$\chi^2/n.d.f.$	49.1 / 36.0	47.1 / 36.0	126.0 / 76.0

Table B.9: Fit result of the 40 Bin Fit using only the statistical uncertainties to the CLN parametrization. The first two columns show the results for the electron and muon modes and the third column shows the results for the full sample. The statistical uncertainties are stated.

	ρ^2	$R_1(1)$	$R_2(1)$	$\mathcal{F}(1) V_{cb} \eta_{\text{EW}}$
ρ^2	+1.000	+0.616	-0.876	+0.682
$R_1(1)$		+1.000	-0.717	-0.003
$R_2(1)$			+1.000	-0.283
$\mathcal{F}(1) V_{cb} \eta_{\text{EW}}$				+1.000

Table B.10: Statistical correlation matrix of the 40 Bin Fit using only the statistical uncertainties for the electron mode in the CLN parametrization.

	ρ^2	$R_1(1)$	$R_2(1)$	$\mathcal{F}(1) V_{cb} \eta_{\text{EW}}$
ρ^2	+1.000	+0.644	-0.880	+0.653
$R_1(1)$		+1.000	-0.748	-0.024
$R_2(1)$			+1.000	-0.254
$\mathcal{F}(1) V_{cb} \eta_{\text{EW}}$				+1.000

Table B.11: Statistical correlation matrix of the 40 Bin Fit using only the statistical uncertainties for the muon mode in the CLN parametrization.

	ρ^2	$R_1(1)$	$R_2(1)$	$\mathcal{F}(1) V_{cb} \eta_{\text{EW}}$
ρ^2	+1.000	+0.615	-0.874	+0.683
$R_1(1)$		+1.000	-0.716	-0.001
$R_2(1)$			+1.000	-0.282
$\mathcal{F}(1) V_{cb} \eta_{\text{EW}}$				+1.000

Table B.12: Statistical correlation matrix of the 40 Bin Fit using only the statistical uncertainties for the full sample in the CLN parametrization.

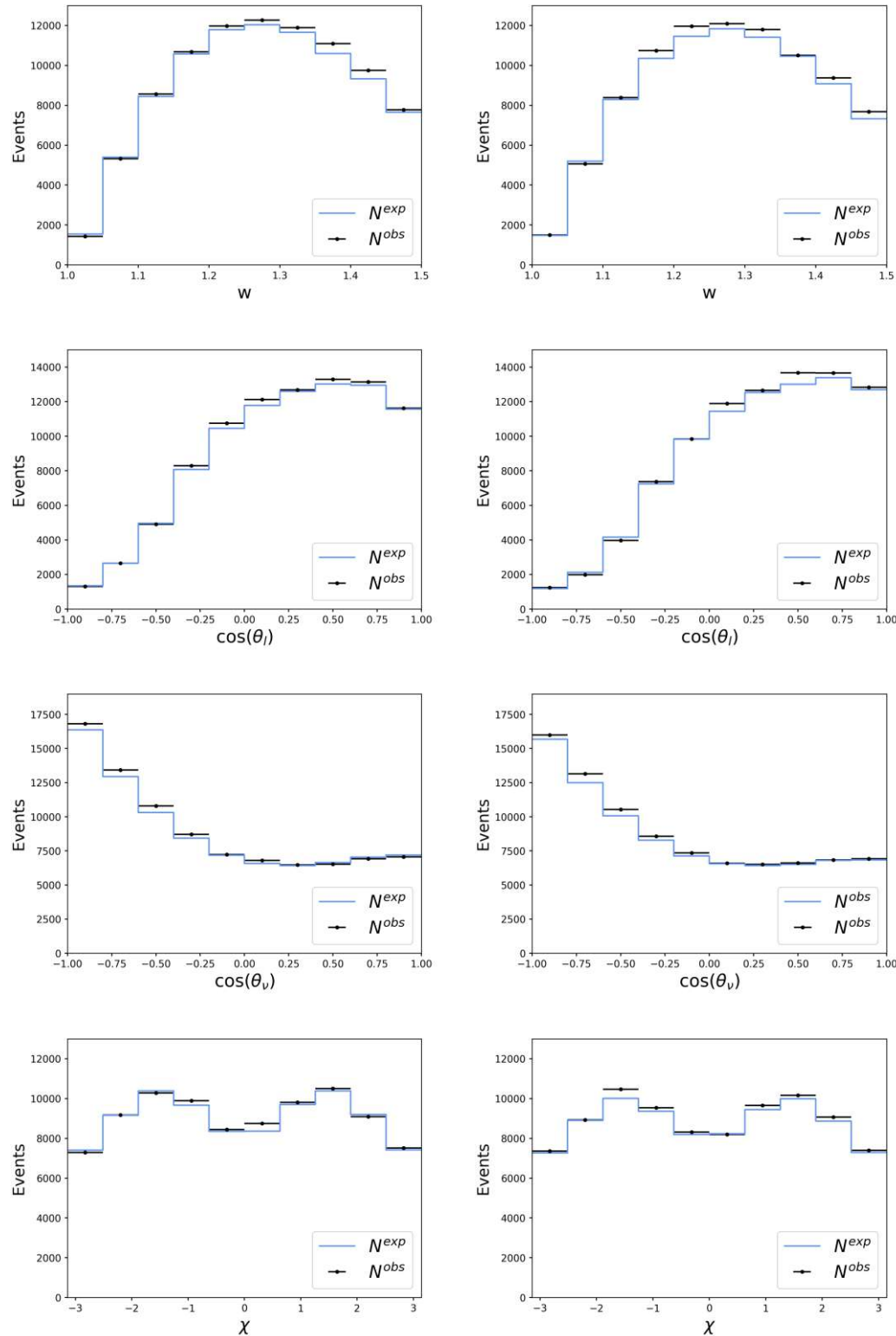


Figure B.1: Result of the 40 bin Fit to the CLN parametrization. The number of observed events N^{obs} and the number of expected events N^{exp} are plotted. The e mode is shown on the left and the μ mode on the right. The figures show the distributions in w , \cos_{θ_l} , \cos_{θ_v} and χ .

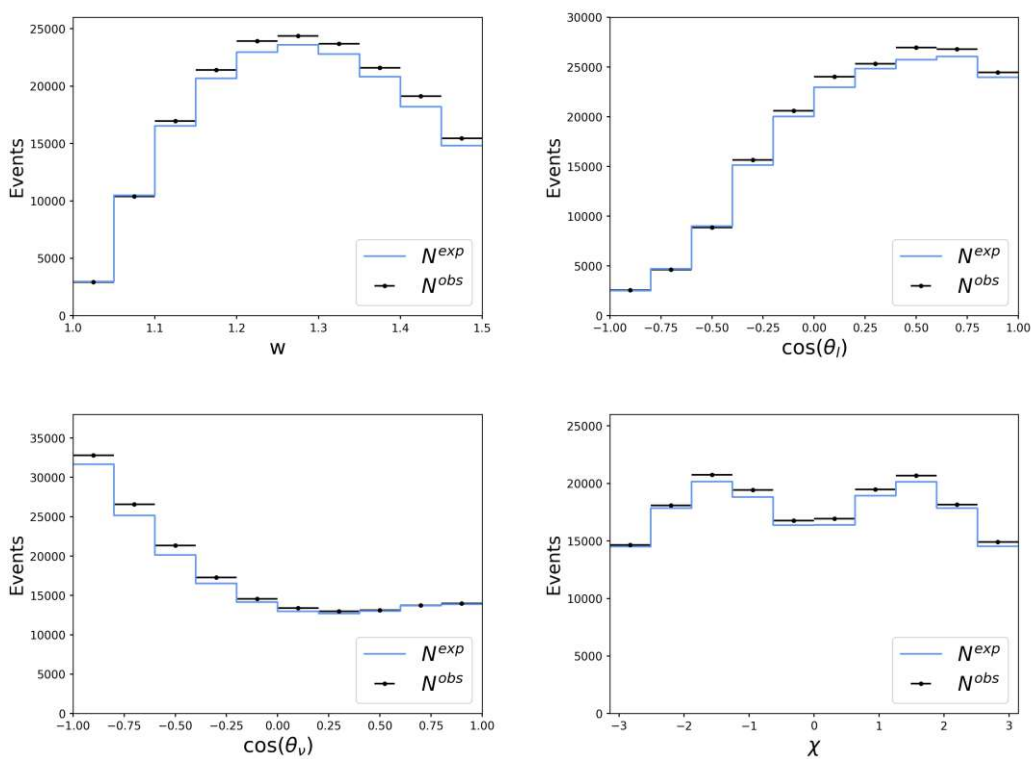


Figure B.2: Result of the 40 bin Fit to the CLN parametrization for the full sample. The figures show the distributions in w , $\cos\theta_l$, $\cos\theta_v$ and χ .

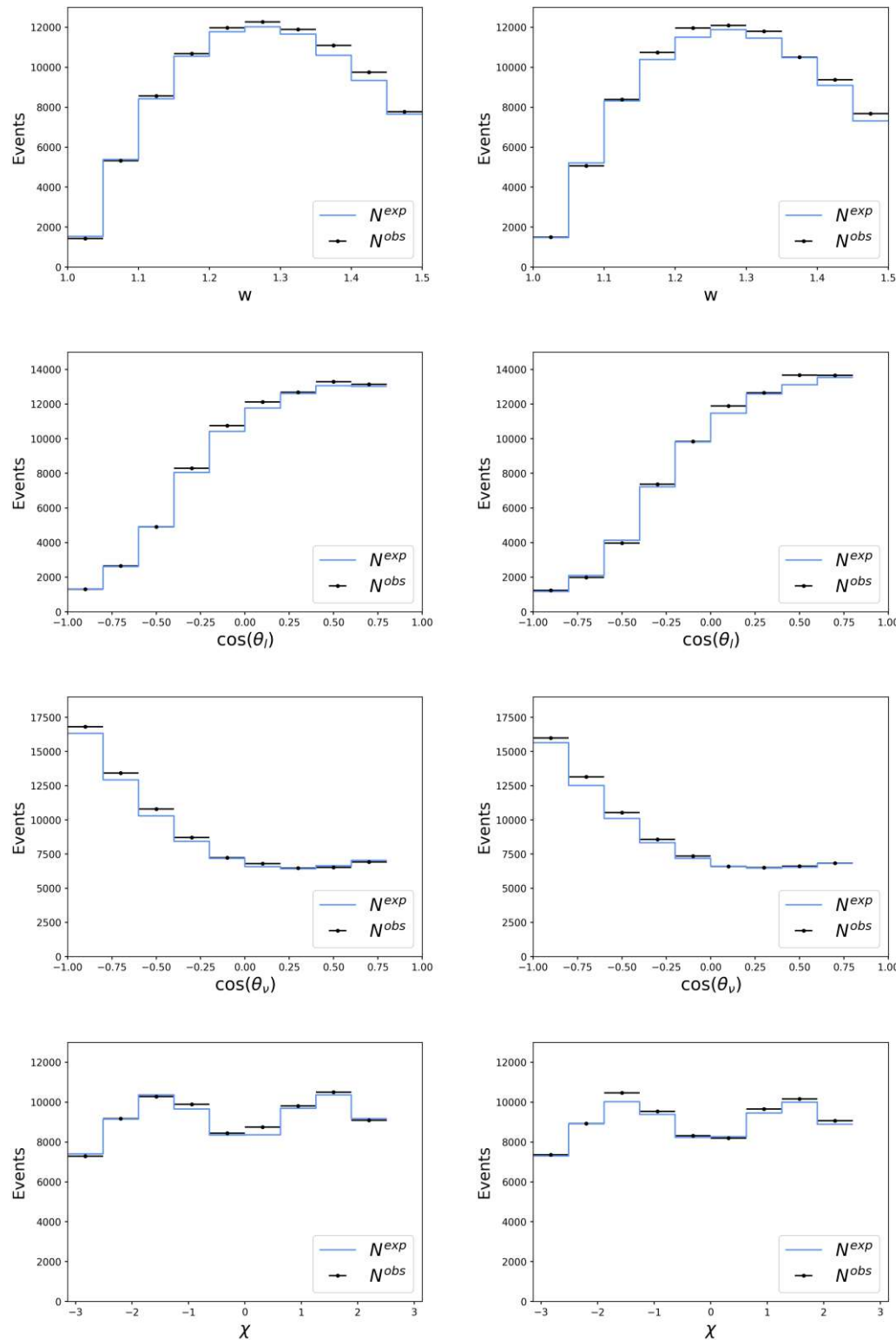


Figure B.3: Result of the 37 bin Fit to the CLN parametrization. The number of observed events N^{obs} and the number of expected events N^{exp} are plotted. The e mode is shown on the left and the μ mode on the right. The figures show the distributions in w , $\cos\theta_l$, $\cos\theta_v$ and χ .

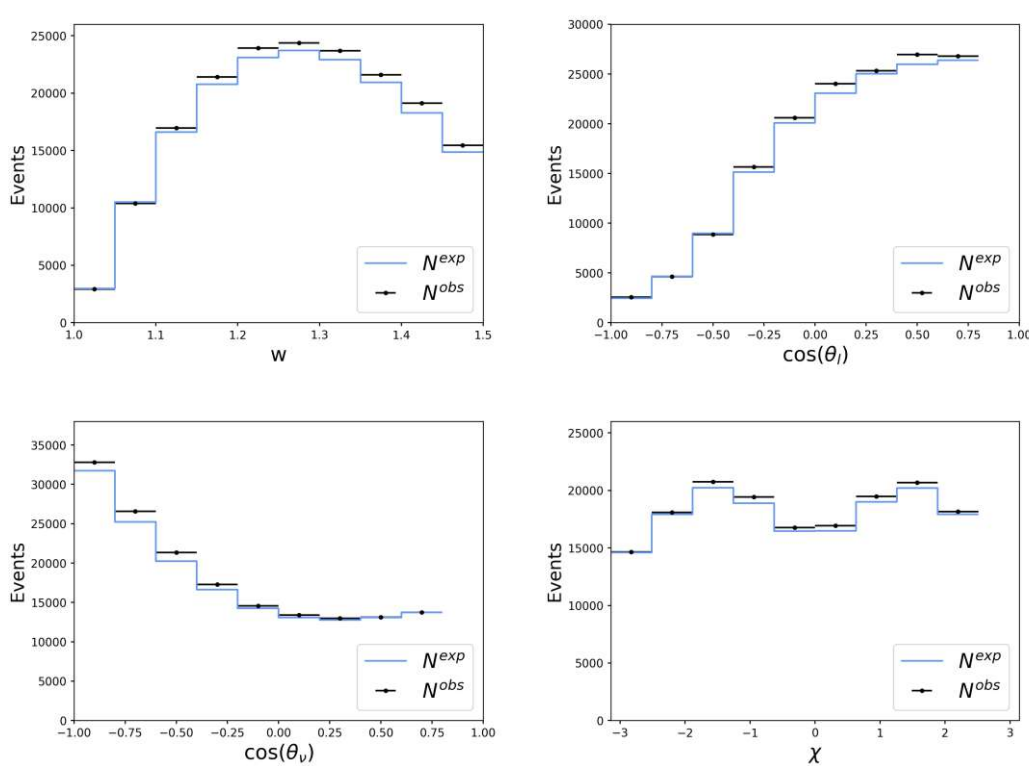


Figure B.4: Result of the 37 bin Fit to the CLN parametrization for the full sample. The figures show the distributions in w , $\cos\theta_l$, $\cos\theta_v$ and χ .

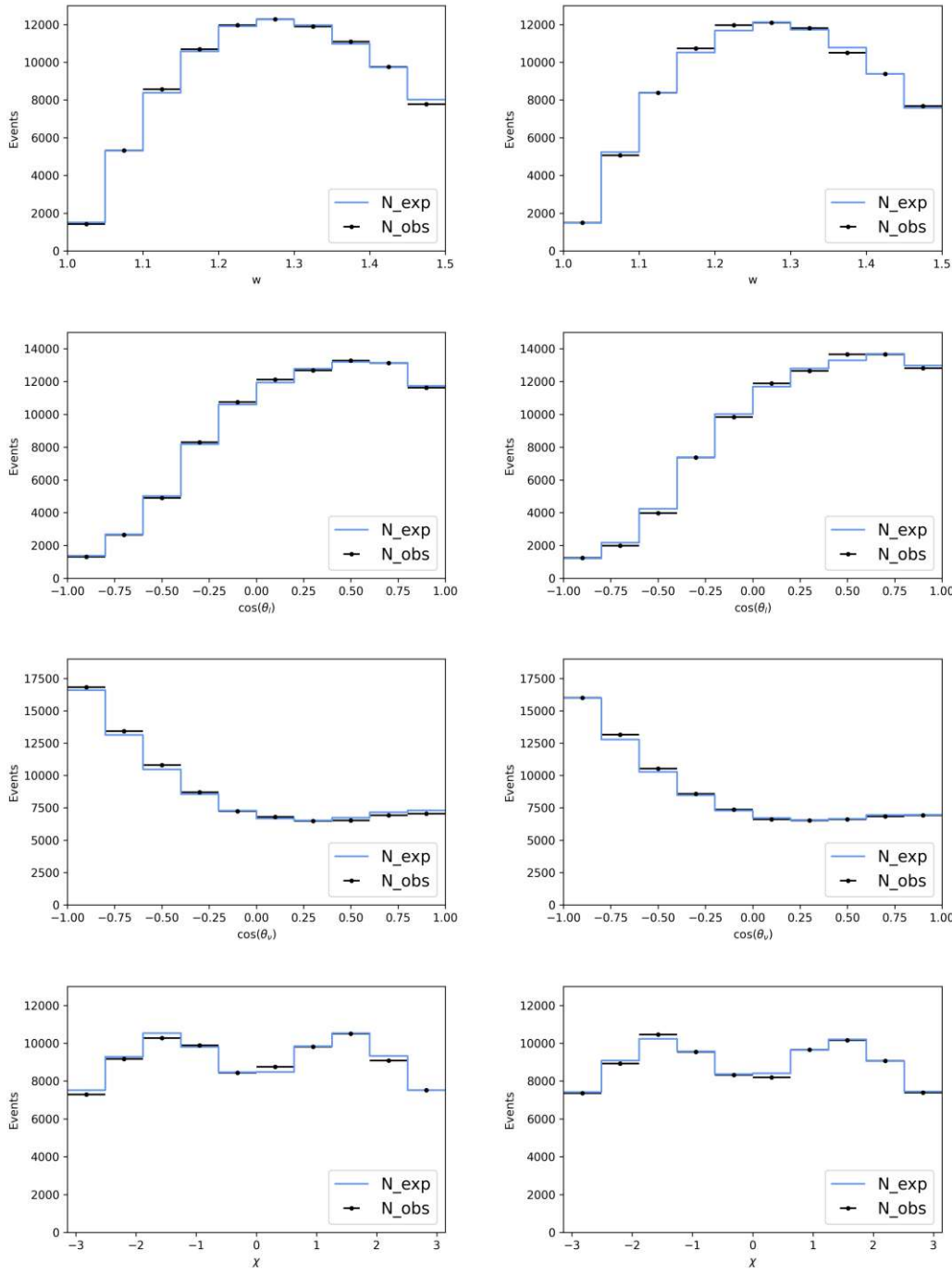


Figure B.5: Result of the 40 Bin Fit using only the statistical uncertainties to the CLN parametrization. The number of observed events N^{obs} and the number of expected events N^{exp} are plotted. The e mode is shown on the left and the μ mode on the right. The figures show the distributions in w , $\cos\theta_l$, $\cos\theta_v$, and χ .

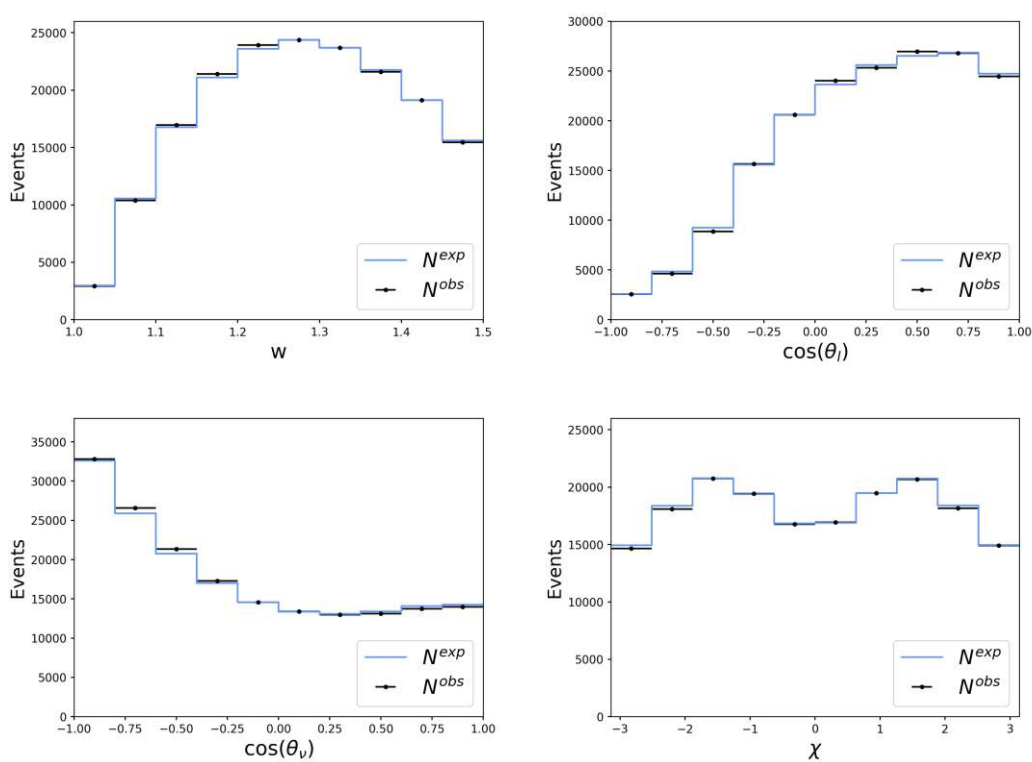


Figure B.6: Result of the 40 Bin Fit using only the statistical uncertainties to the CLN parametrization for the full sample. The figures show the distributions in w , $\cos\theta_l$, $\cos\theta_\nu$ and χ .

Bibliography

- [1] Mark Thomson, *Modern particle physics*, Cambridge University Press (2013).
- [2] A.J. Bevan, B. Golob, Th. Mannel et al., *The Physics of the B Factories*, The European Physical Journal C 74, 3026 (2014).
- [3] Antonio Pich, *The Standard Model of Electroweak Interactions*, arXiv:0705.4264 [hep-ph] (2007).
- [4] M. Battaglia et al., *The CKM Matrix and the Unitarity Triangle*, arXiv:hep-ph/0304132 (2003).
- [5] Christoph Schwanda, *Determination of the Cabibbo-Kobayashi-Maskawa Matrix Elements $|V_{cb}|$ and $|V_{ub}|$ at the Belle Experiment*, Wien, Techn. Univ., Habil.-Schr. (2013).
- [6] E. Waheed et al. (Belle Collaboration), *Measurement of the CKM matrix element $|V_{cb}|$* , Physical Review D 100, 052007 (2019).
- [7] Benjamin Grinstein and Andrew Kobach, *Model-Independent Extraction of $|V_{cb}|$ from $B \rightarrow D^* \ell \bar{\nu}$* , Phys.Lett. B771 (2017) 359-364.
- [8] Irinel Caprini, Laurent Lellouch, Matthias Neubert, *Dispersive bounds on the shape of $\bar{B} \rightarrow D^{(*)} \ell \bar{\nu}$ form factors*, Nuclear Physics B530 (1998) 153-181.
- [9] Heavy Flavor Averaging Group (HFLAV), *Averages of b-hadron, c-hadron, and τ -lepton properties as of 2021*, arXiv:2206.07501 [hep-ex] (2022).
- [10] J. A. Bailey et al. (Fermilab Lattice and MILC Collaborations), *Update of $|V_{cb}|$ from the $\bar{B} \rightarrow D^* \ell \bar{\nu}$ form factor at zero recoil with three-flavor lattice QCD*, Phys. Rev. D 89, 114504 (2014).
- [11] M. Okamoto et al., *Semileptonic $D \rightarrow \pi/K$ and $B \rightarrow \pi/D$ decays in 2+1 flavor lattice QCD*, Nuclear Physics B - Proceedings Supplements, 140 (2005) 461.

- [12] J. Brodzicka et. al. (Belle Collaboration), *Physics Achievements from the Belle Experiment*, Progress of Theoretical and Experimental Physics, Volume 2012, Issue 1 (2012) 04D001.
- [13] The Belle Collaboration, June 2022, <http://belle.kek.jp>.
- [14] Z. Natkaniec et al., *Status of the Belle silicon vertex detector*, Nuclear Instruments and Methods in Physics Research Section A 560, 1 (2006).
- [15] A. Abashian et al., *The Belle detector*, Nuclear Instruments and Methods in Physics Research Section A 479 (2002) 117-232.
- [16] The SciPy community, *SciPy documentation Version 1.8.0*, <https://docs.scipy.org/doc/scipy/reference/generated/scipy.integrate.quad.html>, February 2022.
- [17] Hans Dembinski and Piti Ongmongkolkul et al., *scikit-hep/iminuit*, <https://doi.org/10.5281/zenodo.3949207>, February 2022.
- [18] Christoph Bobeth, Marzia Bordone, Nico Gubernari, Martin Jung and Danny van Dyk, *Lepton-flavour non-universality of $\bar{B} \rightarrow D^{(*)}\ell\bar{\nu}$ angular distributions in and beyond the Standard Model*, European Physical Journal C 81, Article number: 984 (2021).
- [19] G. D'Agostini, *On the use of the covariance matrix to fit correlated data*, Nuclear Instruments and Methods in Physics Research Section A 346, 306 (1994).
- [20] Martin Jung and David M. Straub, *Constraining new physics in $b \rightarrow c\ell\nu$ transitions*, Journal of High Energy Physics Article number: 9 (2019).